

UC Berkeley
SEMM Reports Series

Title

The Analysis of Thin Shells By a Finite Element Procedure

Permalink

<https://escholarship.org/uc/item/80x6s861>

Author

Johnson, C. Phillip

Publication Date

1967-09-01

REPORT NO.
67-22

STRUCTURES AND MATERIALS RESEARCH
DEPARTMENT OF CIVIL ENGINEERING

THE ANALYSIS OF THIN SHELLS BY A FINITE ELEMENT PROCEDURE

by

C. PHILIP JOHNSON

Report to
National Science Foundation
NSF Grant GK-75

SEPTEMBER 1967

STRUCTURAL ENGINEERING LABORATORY
UNIVERSITY OF CALIFORNIA
BERKELEY CALIFORNIA

Structures and Materials Research
Department of Civil Engineering

Report No. 67-22

THE ANALYSIS OF THIN SHELLS
BY A FINITE ELEMENT PROCEDURE

by

C. Philip Johnson

Faculty Investigator: Ray W. Clough

Prepared under the sponsorship of
National Science Foundation
Grant GK-75

University of California
Berkeley, California

September 1967

TABLE OF CONTENTS

	Page
ABSTRACT	iv
ACKNOWLEDGMENTS	v
1. INTRODUCTION	1
1.1 Historical Background	1
1.2 The Finite Element Procedure	4
1.3 Purpose and Scope	7
2. THE FINITE ELEMENT IDEALIZATION	10
2.1 Geometric Discretization	10
2.2 Displacement Field Discretization for the Triangle	11
2.3 Displacement Field Discretization for the Quadrilateral	12
2.4 Advantages of the Discretized Displacement Field of the Quadrilateral Element	14
3. EVALUATION OF THE ELEMENT STIFFNESSES	23
3.1 Triangular Coordinates for Triangular Elements	23
3.2 Procedure for Evaluating Plane Stress Element Stiffnesses	25
3.3 Procedure for Evaluating Plate Bending Element Stiffness	28
3.4 Derivation of the Constant Strain Triangle (CST) Element Stiffness	30
3.5 Derivation of the Constrained Linear Strain Triangle Element Stiffness	31
3.6 Derivation of the Plate Bending Element Stiffness	34

	Page
4. THE ELEMENT ASSEMBLAGE	45
4.1 Coordinate Systems	45
4.2 Coordinate Transformation	46
4.3 Transformation and Assemblage of Triangular Elements	47
4.4 Transformation and Assemblage of Quadrilateral Elements	50
4.5 Condensation of the Internal Degrees of Freedom of the Quadrilateral	55
5. SOLUTION OF THE EQUILIBRIUM EQUATIONS	61
5.1 Direct Solution of the Equilibrium Equations	62
5.2 Practical Aspects of Computer Algorithms for the Finite Element Procedure	67
5.3 Computation of Consistent Loading and Element Stresses and Moments	68
6. RESULT OF ANALYSIS	76
6.1 Cantilever Beam (Example 1)	79
6.2 Spherical Dome (Examples 2 and 3)	80
6.3 Circular Cylinders with Free Edges (Example 4)	81
6.4 Typical Interior Cylinder (Example 5)	84
6.5 North Light Folded Plate Model (Example 6)	84
6.6 Translational Shells (Example 7)	85
6.7 Conoid (Example 8)	87
CONCLUSIONS	112
REFERENCES	116

ABSTRACT

A finite element procedure is presented for the analysis of thin shells of arbitrary geometry. The smoothly curved shell surface is discretized by an assemblage of flat triangular elements. The element stiffness properties are derived from assumed displacement functions in the form of truncated polynomials, and triangular coordinates are used for the derivation. Both triangular and non-planar quadrilaterals (an assemblage of four triangular elements) are utilized, and their stiffness properties are compared.

The stiffness properties of the complete assemblage are obtained by the direct stiffness procedure. The treatment of force and displacement boundary conditions is discussed and a direct procedure is used to solve the nodal point equilibrium equations of the assemblage. Practical aspects of a computer algorithm for the solution of large systems of equations which are banded, symmetric, positive definite and sparse is discussed; and typical solution times are recorded.

A five degree of freedom nodal point displacement system is used which permits substantial mesh refinement in treating shells with intricacies of geometric detail. The convergence properties with decreasing mesh size for both element types are studied, and the results of several analyses are compared with existing solutions.

ACKNOWLEDGMENTS

The research reported herein was carried out during the author's graduate study for the Ph. D degree in Civil Engineering at the University of California, Berkeley.

The author wishes to express his deep appreciation to Professor Ray W. Clough for his supervision and encouragement throughout the course of this research. He is also grateful to Professors E. L. Wilson and G. M. McCue, members of his thesis committee, for their helpful guidance. In addition, Professor A. C. Scordelis and Carlos A. Felippa deserve recognition for their assistance.

This work was sponsored by the National Science Foundation by Grant GK-75. The Berkeley Computer Center provided their facilities for the computer work.

Mrs. Gerry Myers typed the final copy.

CHAPTER 1. INTRODUCTION

1.1 Historical Background

The widespread use of thin shell structures has created a need for a systematic method of analysis which can adequately account for arbitrary geometric form and boundary conditions as well as arbitrary general types of loading. Classical thin shell theory yields differential equations of equilibrium or continuity whose complexity depends greatly on the shell geometry and whose solution is a function of the geometric position of the boundary and the type of force or displacement quantity which must be satisfied there. Therefore, classical solutions are available only for simple geometric forms whose boundaries coincide with the parametric curves that describe the shell surface. In this context, the sphere and the circular cylinder are amenable to classical solutions and have been studied extensively. However, the complications caused by geometry and boundary conditions together with variable thickness, variable material properties, discontinuities in the shell surface (cut-outs), and general loading disqualify the classical approach as a systematic method of analysis for most real problems.

With the aid of the digital computer various numerical procedures such as finite differences, numerical integration, variational methods (Galerkin and Kantorovich), have been presented for a certain class of problems based on shallow-shell theory. These solutions, however, have been limited to special geometric forms, such as shallow translational shells, which are subjected to particular loadings and boundary conditions.

A completely general approach for the solution of problems in continuum mechanics was introduced in the late fifties [1]* and later became

* The numbers in brackets refer to the references listed at the end.

known as the finite element method [2]. This method was first applied to the solution of plane stress problems [1, 2] and subsequently was extended to the analysis of axisymmetric solids and plate bending problems [3] and to axisymmetric shells [4]. This procedure also has been used previously in thin shell analysis to a limited extent [5, 6] and is presently being extended to general three-dimensional solids.

In the above references [5, 6] the analyses were based on the use of planar elements but were limited in application due to the lack of a suitable triangular plate bending element. More recently a general shell element has been presented [7] which utilizes the conventional constant strain triangular element [1] and the fully compatible plate bending triangular element [8] derived by Clough and Tocher. This analysis [7] utilized a 5 degree of freedom nodal point displacement system (three translations and two rotations) and thus provides for an efficient solution for a given idealization. The solutions provided by this analysis [7] for smoothly curved shells were considered adequate; however, for shells having complex membrane straining modes, extremely fine subdivisions were necessary to achieve the desired accuracy. Recently an element [9] has been presented which utilizes the same plate bending element [8] together with a "refined" membrane stiffness. This analysis resulted in a 9 degree of freedom nodal point displacement system for the assembled structure and therefore includes strains in addition to translations and rotations as degrees of freedom. The convergence properties of this element cited in Ref. [9] are good and this is attributed primarily to the improved membrane stiffness properties.

The solutions presented in Refs. [7] and [9] characterize the two alternate approaches of the finite element procedure. In the first

approach a relatively simple representation of the stiffness properties is utilized and the desired accuracy is achieved by mesh refinement (i.e., increasing the number of subdivisions), while in the second approach an improved representation of the element stiffness properties is utilized which generally requires a less refined mesh (i.e., a fewer number of subdivisions). In evaluating these two approaches for the analysis of doubly curved shells which have complex geometries, the geometric idealization resulting from the use of planar elements must be considered; and in this respect the solution of Ref. [7] offers distinct advantages, since the 5 degree of freedom nodal point system permits substantial mesh refinement as compared with the 9 degrees of freedom of Ref. [9]. In addition, the nodal point degrees of freedom [7] have an immediate and simple interpretation since they consist only of linear translations and rotations, and in this context it was possible to extend this solution procedure with only minor modifications for the analysis of tubular joints [10] in which the intersecting tubular members were treated simultaneously in the solution.

In this presentation the use of the solution procedure of Ref. [7] is retained, but is augmented by a quadrilateral element which consists of an assemblage of four triangular elements. Following the procedure of Wilson [11] and Felippa [12] the interior degrees of freedom are eliminated by static condensation using inverse Gaussian elimination. The subject quadrilateral element provides an improved membrane stiffness since it is able to represent more precisely plane stress beam type straining modes, and this improved membrane stiffness property has accounted for the slow convergence as mentioned above for certain solutions presented in Ref. [7]. It should be noted that this improvement

did not require utilizing additional types of nodal point degrees of freedom; therefore, the 5 degree of freedom nodal point displacement system is retained.

1.2 The Finite Element Procedure

The basic concept of the finite element method is the idealization of the continuum as an assemblage of discrete structural elements. The stiffness properties of each element are then evaluated and the stiffness properties of the complete structure are obtained by superposition of the individual element stiffnesses. This gives a system of linear equations in terms of nodal point loads and displacements whose solution yields the unknown nodal point displacements.

The idealization governs the type of element which must be used in the solution. If, for example, the idealization of the shell were obtained by merely subdividing the actual shell surface into a specified number of regions (elements), then for the most general case, one would have to deal with doubly curved elements in evaluating the stiffness properties of the individual elements. On the other hand, it is possible to use for the idealization an assemblage of planar elements which only approximate the shell surface. In this case, the element stiffnesses may be derived from the planar elements which are identical to those used for plane stress and plate bending problems. Although the use of planar elements simplifies the evaluation of the element stiffness properties, the resulting geometric discretization error must be recognized, since the behavior of the discretized shell can only approach that of the actual shell with decreasing mesh size.

Displacement models have in general proved to be superior to equilibrium models in evaluating stiffness properties of the individual

elements. In this procedure, the deformation of the element is constrained to consist of certain displacement patterns or shapes which may conveniently be established from truncated polynomials or interpolation functions. In either case, the displacement field in each element must be finally expressed as a function of nodal point displacements only; and this must be done in such a way as to maintain inter-element compatibility, since this condition is necessary to establish a bound on the strain energy. Therefore, the displacement patterns and the nodal point degrees of freedom must be chosen judiciously for each problem considered. In addition to the compatibility requirement, the displacement functions should include the following:

- 1) rigid body modes
- 2) constant strain and curvature states
- 3) invariance of the element stiffness

The inclusion of rigid body modes is necessary for equilibrium of the nodal forces and moments which correspond to the displacement nodal degrees of freedom of the element and for the satisfaction of global equilibrium. In order that the solution converge to the actual state of strain and curvature, the constant strain and curvature should be included. This requirement is obvious for structures subjected to constant strain and curvature states; while for arbitrary states of strain and curvature, reduction in mesh size will simplify the element strains and curvatures and in the limit element strains and curvatures approach a constant value. The invariance property is necessary to insure that the element stiffness properties remain the same for all coordinate systems which are used for their derivation.

While the above requirements are sufficient to guarantee convergence to the true solution with decreasing mesh size [3, 13, 14, 15], it has been demonstrated for the rectangular plate bending element (ACM element, Ref. [8]), in which a twelve term polynomial is used, that complete compatibility is not achieved and yet the convergence to the correct displacements is considered adequate. However, if complete compatibility is not achieved, there exists an uncertainty as to the bound on the strain energy of the system; and if the solution converges at all, it may do so from either above or below the true solution.

The use of planar elements, in which the membrane and plate bending stiffness are derived from displacement patterns of different forms, cannot insure complete compatibility of the assemblage. In this case, a geometric incompatibility results since the elements are not coplanar, and even on physical grounds it is expected that its effect would diminish with decreasing mesh size. For an analysis of this type, the most critical test is the performance in the limit (i.e., with decreasing mesh size); and if the performance is adequate in this respect, then the requirement on complete compatibility can be justifiably relaxed. In the present analysis, an extensive study of this phenomenon has been made, and it has been shown that the convergence to the true solution for a wide range of shell geometries is essentially monotonic with decreasing mesh size. A more limited study of folded plates in which there is no geometric discretization error, but in which the above incompatibility is present due to the large angle of intersection of the individual plates, has indicated that the present analysis can be used effectively even for this case.

The finite element method may be used only with the aid of high speed digital computers. The use of displacement models coupled with the direct

stiffness procedure have proved to be the most convenient and versatile means for the development of general computer programs. The direct stiffness procedure in its most useful form simply implies that the stiffness of the individual elements may be established in the base or common coordinate system on the element stiffness level which permits the stiffness of the complete assemblage to be obtained by direct superposition of the individual element stiffnesses. Direct solution procedures using Gaussian elimination (or special forms of this method such as triangular decomposition) together with automatic assembly subroutines make possible the general application of the finite element method, in which the essential modification for different problems is that of evaluating the element stiffness properties and transformations required for the direct assembly. Due to the wide applicability of the direct solution procedure and the overall ease and economy with which it can be performed, it is rapidly becoming the preferred method for the solution of one and two dimensional problems.

1.3 Purpose and Scope

The key factors in the finite element analysis are the geometric idealization and evaluation of the element stiffness properties. In the present analysis the shell is approximated by a system of flat triangular elements in which the nodes or corners of the triangles lie in the middle surface of the shell. The use of the triangle enables one to approximate arbitrary doubly curved shells with minimum error in the idealization.

Since shell behavior is characterized by both membrane action and bending action, it is essential to recognize both of these in evaluating the element stiffness properties. It is appropriate to represent the

membrane action by elements acting in the state of plane stress while the bending action can be represented by plate bending elements derived on the basis of the Kirchoff theory of thin plates. The above assumptions of plane stress and the Kirchoff theory are "equivalent" to the assumptions made in the classical theory of thin shells which degenerates thin shell problems from a three-dimensional problem in elasticity to a two-dimensional elasticity problem.

The plate bending element used in the analysis is the fully compatible element (HCT) after Hsieh, Clough and Tocher [8]; while two types of plane stress elements are employed--the first being the constant strain triangle [1] while the second type is a quadrilateral element constructed from four HCT elements and four linear strain triangles [12] with the boundaries constrained to deform linearly. This constraint eliminates the exterior mid-side nodes of the element, thereby reducing the connectivity (band width) which must be considered in the direct solution of the nodal point equilibrium equations.

The purpose of this thesis is to investigate the convergence properties of the triangular and quadrilateral elements as related to the static analysis of thin shell structures. Of particular interest in this study are the evaluation of the effect of the geometric idealization, the improved stiffness properties of the quadrilateral element, and the 5 degree of freedom nodal point displacement system. The criteria utilized to determine the accuracy of the solution is a direct comparison of the finite element solution with existing solutions obtained by classical shell theory. Direct evaluation, however, of the stiffness properties of the triangular element versus the quadrilateral element is

possible since identical geometric idealizations may be obtained with either element in which the effect of the 5 degrees of freedom is essentially the same.

CHAPTER 2. THE FINITE ELEMENT IDEALIZATION

The finite element idealization in the analysis of thin shells consists of the geometric discretization and the displacement field discretization. The geometric discretization is due to the use of planar triangular elements, since an assemblage of this type of element can only approximate the actual smoothly curved surface. In addition, since the boundaries of these elements are straight, curved shell boundaries are also represented approximately.

The displacement field discretization is caused by evaluating the stiffness properties of the individual elements from an assumed set of displacement shapes. Since the assumed set of displacement shapes must be relatively simple for efficient evaluation of the element stiffness properties, they only approximate the actual deformation of the shell. However, since the displacement shapes are piece-wise continuous, the actual deformation of the shell can be obtained by decreasing mesh size provided compatibility is maintained along the element interfaces. This phenomenon, which is referred to as convergence, is fundamental to any finite element solution since the comparison of solutions with decreasing mesh size gives a quantitative measure of the "exactness" of the finite element solution for a particular shell problem.

2.1 Geometric Discretization

The geometric discretization of a typical shell surface together with a typical triangular element and a typical quadrilateral element are shown in Fig. 2.1. The size and shape of the triangles are defined by the coordinates of the nodal points which lie in the middle surface of the shell.

The quadrilateral element is constructed from four triangular elements in which the exterior nodes (i, j, k, l) lie in the middle surface of the shell, while the coordinates of the central interior node "m" are taken as the average of the coordinates of the nodes i, j, k, l. In general, either type of element may be used in the analysis; and, if desirable, a combination of these two element types may be utilized. In this respect, the quadrilateral due to its superior stiffness properties should be used in regions subjected to complex straining modes while the triangle may be used effectively in regions of fairly constant strain states. In addition, the triangle is useful in grading the mesh. The geometric discretization is often referred to herein as the mesh.

2.2 Displacement Field Discretization for the Triangle

Typical membrane and plate bending elements are shown in Fig. 2.2 together with the displacement functions assumed in evaluating their stiffness matrices. These displacement functions are given first in Cartesian Coordinates to facilitate an immediate physical interpretation while the evaluation of the stiffness matrices is more conveniently carried out in the triangular coordinates (Chapter 3).

The membrane element has two degrees of freedom at each nodal point, and the displacements are assumed to vary linearly between nodal points [1]. This results in constant values of the three strain components over the entire element and this element is referred to as the constant strain element (CST).

The plate bending element has three degrees of freedom at each nodal point [8] (two rotations and the normal translation), thus a total of nine independent displacement functions should be specified. In this case,

however, in order to develop displacement functions which maintain full compatibility along the edges for the plate problem, it was necessary to divide the plate into three sub-elements and assume nine displacement functions in each sub-element. The resulting 27 displacement shapes were then reduced to the required nine independent patterns by applying internal compatibility constraints between the sub-elements. This discretized displacement field permits the transverse displacement, W , to vary as cubic functions within the element; and therefore, the three components of curvature vary linearly over each sub-element. The equivalent displacement field (in triangular coordinates), including the internal compatibility constraints, expressed directly in terms of the nine degrees of freedom at the three nodal points is given in Section 3.6, Eqn. 3.44.

2.3 Displacement Field Discretization for the Quadrilateral

A typical planar quadrilateral element together with the four triangles from which it is constructed is shown in Fig. 2.3. Also shown in Fig. 2.3 are the combined membrane and bending degrees of freedom. Each of the exterior nodes (1, 2, 3, 4) and the interior central node (pt. 5) have the usual five degrees of freedom which consist of two in-plane displacements, a transverse displacement and two in-plane rotations. The interior mid-side nodes (6, 7, 8, 9) possess only two degrees of freedom which are the two in-plane displacements associated with the membrane displacement functions.

Each of the four triangles (Fig. 2.3) is assigned independent membrane and bending displacement functions. The bending stiffness for each triangle is derived as described in Section 2.2 above, while the membrane stiffness for each triangle is derived from quadratic displacement

functions in which the in-plane displacements of the external interfaces (1-2, 2-3, 3-4, 4-5), Fig. 2.3, are constrained to vary linearly.

The quadratic membrane displacement functions for Triangle 1 together with the nodal point degrees of freedom are shown in Fig. 2.4. The use of the complete quadratic for $u(x,y)$, $v(x,y)$ requires twelve independent generalized coordinates ($\bar{\alpha}_1 \dots \bar{\alpha}_{12}$); and therefore, this element must have twelve degrees of freedom (two degrees of freedom at each corner node and at each mid-side node). This element, therefore, has a linear variation of the three strain components over the entire triangle and is called the "Linear Strain Triangle" (LST) [12]. The displacement functions for the subject triangular element (Fig. 2.5) is derived from the LST by setting $u_0 = (u_1 + u_2)/2$ and $v_0 = (v_1 + v_2)/2$, (Fig. 2.4). This eliminates the degrees of freedom at the mid-side nodes, (i.e., point 0), Fig. 2.4; and the resulting constrained LST with 10 degrees of freedom is shown in Fig. 2.5.

The stiffness of the subject quadrilateral element (Fig. 2.3) is then obtained by superposition of the bending elements (Fig. 2.2) and the constrained LST (Fig. 2.5). Since the connectivity of the interior points (5, 6, 7, 8, 9) of the quadrilateral as related to the direct stiffness procedure, are local to the quadrilateral element, they may be eliminated by static condensation (inverse Gaussian elimination), and the resulting condensed planar quadrilateral element has twenty degrees of freedom (five at each exterior node).

For simplicity, the above discussion was restricted to planar quadrilaterals. However, for doubly curved shells, the quadrilateral, in general, cannot be planar and modifications of the above procedure are necessary. The development of a general quadrilateral for the analysis of

doubly curved shells is accomplished by considering this element as a sub-structure and is carried out in Section 4.4.

2.4 Advantage of the Discretized Displacement Field of the Quadrilateral Element

Valuable information has been obtained through the study of the eigenvalues of quadrilateral elements formed from various types and arrangements of triangular elements in evaluating their desirability for practical application [12]. This is possible since the eigenvalues correspond to the strain energy of the element as it deforms through the corresponding eigenvectors. Additional information may be obtained by considering the strain energy required to excite certain prescribed straining modes; and in comparing the stiffness properties of different elements, it is desirable to use identical modes in the elements being evaluated. In evaluating the subject elements only the membrane stiffness is considered since only one type of displacement function is used for the bending stiffness.

In comparing the constant stress element to the constrained quadrilateral element, identical geometries are utilized as shown in Figs. 2.6 and 2.7, and this requires forming a quadrilateral from two constant stress triangles, Fig. 2.7. The straining modes which are of interest are those of extension, shear, and bending, Figs. 2.6, 2.7 (a, b, c). These modes are easily established by specifying nodal point displacements at the four corners of the quadrilateral; and in the case of the constrained quadrilateral, Fig. 2.6, the interior nodal point degrees of freedom are permitted to displace freely. To this end, the interior degrees of freedom are eliminated by condensation and the strain energy due to arbitrary displacements of the nodal point system r_i is:

$$\lambda_i^{(1)} = r_i^T k_m^{(1)} r_i \quad (2.1)$$

$$\lambda_i^{(2)} = r_i^T k_m^{(2)} r_i \quad (2.2)$$

where $\lambda_i^{(1)}$ = strain energy of constrained quadrilateral element due to the i th straining mode.

$\lambda_i^{(2)}$ = strain energy of quadrilateral composed of two constant strain triangles due to the i th straining mode.

r_i = nodal point displacements which result in the i th straining mode.

$k_m^{(1)}$, $k_m^{(2)}$ = membrane stiffness of constrained quadrilateral (condensed) and the quadrilateral composed of constant strain triangles, respectively.

The nodal point displacements for the extension, shear and bending modes respectively are (see Fig. 2.3 and Figs. 2.6 and 2.7):

$$\begin{aligned} r_1^T &: u_2 = u_3 = .1'' \quad , \quad u_1 = u_4 = 0 \quad , \quad v_i = 0 \quad , \quad i = 1,2,3,4 \\ r_2^T &: u_3 = u_4 = .1'' \quad , \quad u_1 = u_2 = 0 \quad , \quad \dots \quad \dots \\ r_3^T &: u_1 = u_3 = -u_2 = -u_4 = .1'' \quad , \quad \dots \quad \dots \end{aligned} \quad (2.3)$$

Utilizing Eqns. 2.1, 2.2, and 2.3, the values for $\lambda_i^{(1)}$ and $\lambda_i^{(2)}$ are computed and shown on the corresponding diagrams in Figs. 2.6 and 2.7.

The strain energy for extension and shear are identical for the two elements indicating that both elements have identical stiffness properties for these particular deformation modes. This is as expected since σ_x

and σ_y are constant for the extension mode and τ_{xy} is constant for the shear mode, and the constant strain element can represent these states exactly. The difference in the stiffness properties of the two elements is reflected in the bending or beam type straining mode. The strain energy, $\lambda_3^{(2)}$, required to produce the bending mode in Fig. 2.7.c is approximately 3.5 times greater than $\lambda_3^{(1)}$, Fig. 2.6.c. This means that for identical geometric idealizations in structures subjected to this straining mode, the use of the two elements will result in different values of nodal point displacements (the values given by the two CST being the lower values). This phenomenon has been reported by Felippa [12] in the analysis of a cantilever beam loaded at the free end in which idealizations by the constant strain triangles were compared to idealizations by linear strain triangles. The results for the tip deflection for only two sub-divisions over the depth of the beam using the linear strain triangle were almost perfect while four and eight sub-divisions over the depth with the constant strain elements yielded tip deflections which were approximately 15% and 4% respectively in error. This clearly indicates that the constant strain element is deficient in representing the beam-type straining mode, and its use in structures subjected predominantly to this mode will generally require considerable mesh refinement to achieve convergence.

This beam-type straining mode is of particular importance in certain shell structures; for example, folded plates or cylinders idealized as folded plates, since the individual plates are subjected to longitudinal bending modes in transmitting the loads to the end diaphragms; and in these cases (see Examples 4 and 6) the use of the subject quadrilateral element gives significantly better results than the constant stress element.

In addition to the superior stiffness properties of the quadrilateral, it also results in a better representation of stresses and again this is related to the bending modes. For example, the bending mode gives a linear variation of (σ_x) for the element in Fig. 2.6, while the same mode yields constant compression (σ_x) in the lower triangle, Fig. 2.7, while the upper triangle is subjected to a constant tension (σ_x) . In this respect, the lower triangle gives a good value for σ_x along side 1-2 while the upper triangle gives a good value for σ_x along side 3-4. This procedure for interpreting the "best" stresses resulting from the use of the constant stress triangle may be used quite effectively for rectangular regions; however, this procedure is generally not easily applied to triangles of arbitrary shape.

COORDINATE DEFINITIONS:

- X, Y, Z = GLOBAL COORDINATES
- ξ_1, ξ_2, ξ_3 = SURFACE COORDINATES
- $\bar{X}, \bar{Y}, \bar{Z}$ = ELEMENT COORDINATES
- η_1, η_2, η_3 = η -COORDINATES

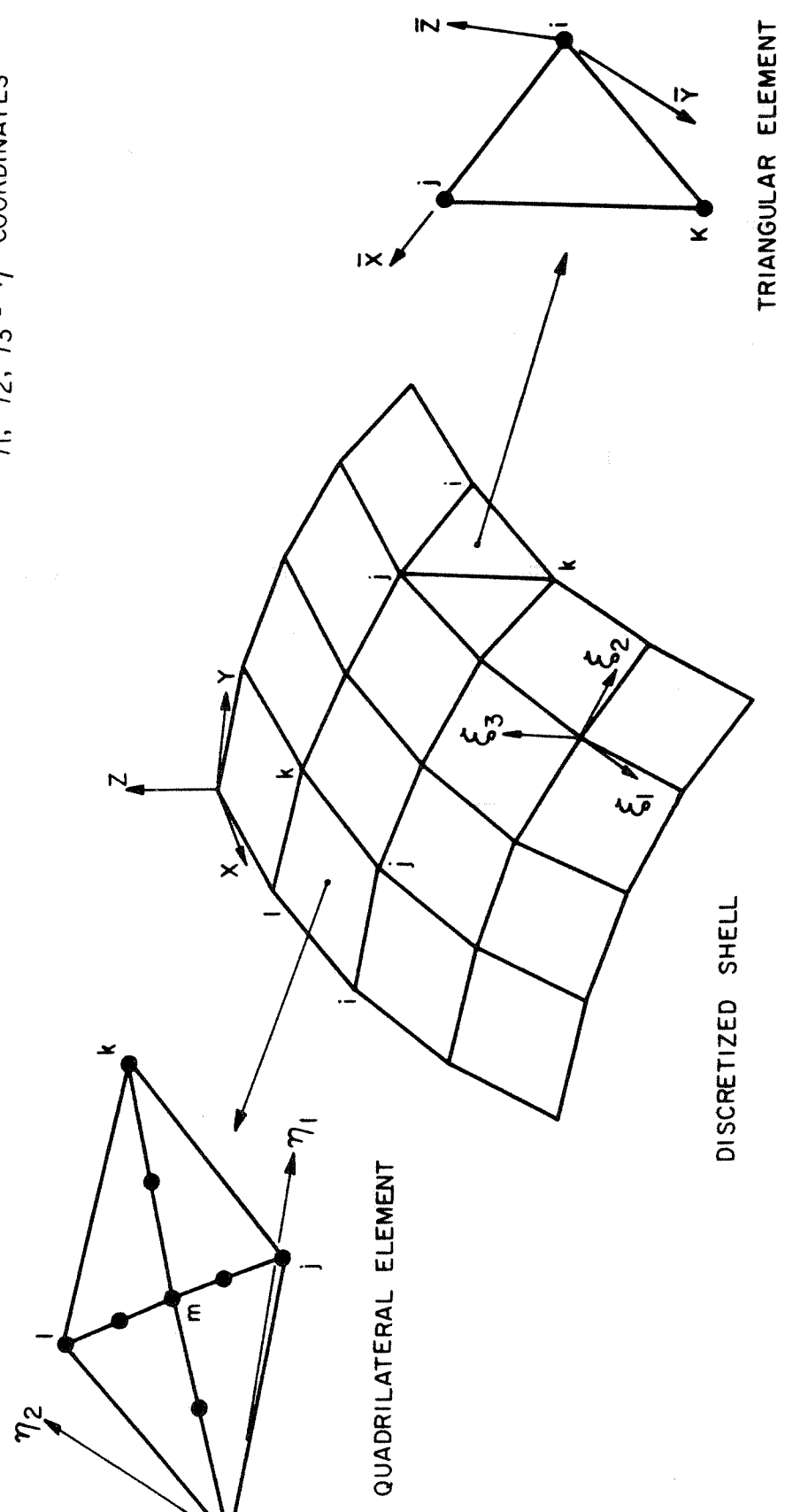
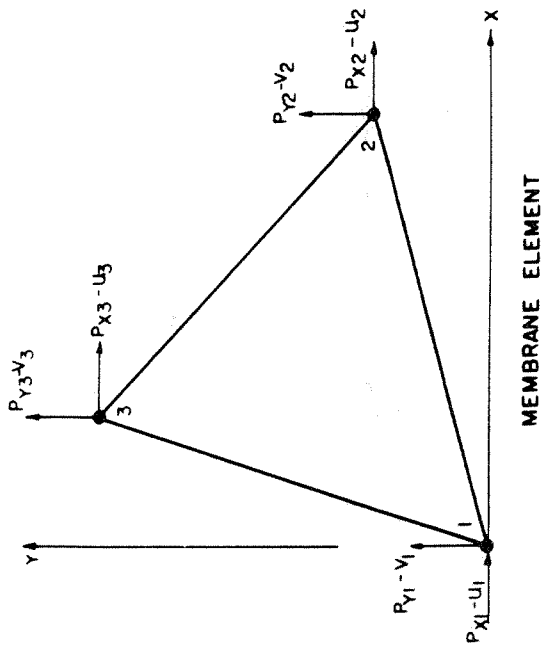


FIG. 2.1 DISCRETIZED SHELL WITH TYPICAL TRIANGULAR AND QUADRILATERAL ELEMENTS AND COORDINATE SYSTEMS



MEMBRANE ELEMENT

$$u = \begin{Bmatrix} \alpha_1 \\ \alpha_2 \\ \alpha_3 \end{Bmatrix}$$

$$v = \begin{Bmatrix} \alpha_4 \\ \alpha_5 \\ \alpha_6 \end{Bmatrix}$$

MEMBRANE DISPLACEMENT FUNCTIONS

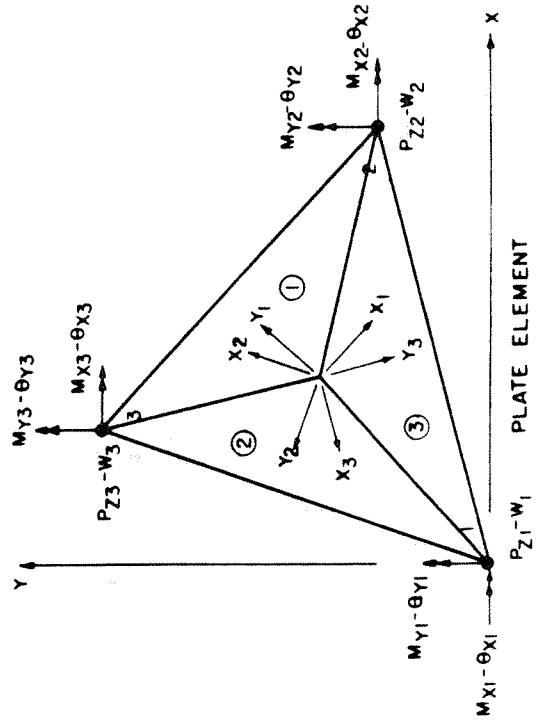


PLATE ELEMENT

$$w^{\alpha} = \begin{Bmatrix} \bar{\alpha}_1 \\ \vdots \\ \bar{\alpha}_9 \end{Bmatrix}$$

$$w^{(1)} = \begin{Bmatrix} \bar{\alpha}_{10} \\ \vdots \\ \bar{\alpha}_{18} \end{Bmatrix}$$

$$w^{(2)} = \begin{Bmatrix} \bar{\alpha}_{19} \\ \vdots \\ \bar{\alpha}_{27} \end{Bmatrix}$$

PLATE DISPLACEMENT FUNCTIONS

FIG. 2.2 DISPLACEMENT FUNCTIONS AND NODAL POINT SYSTEMS FOR TRIANGULAR MEMBRANE AND PLATE ELEMENTS

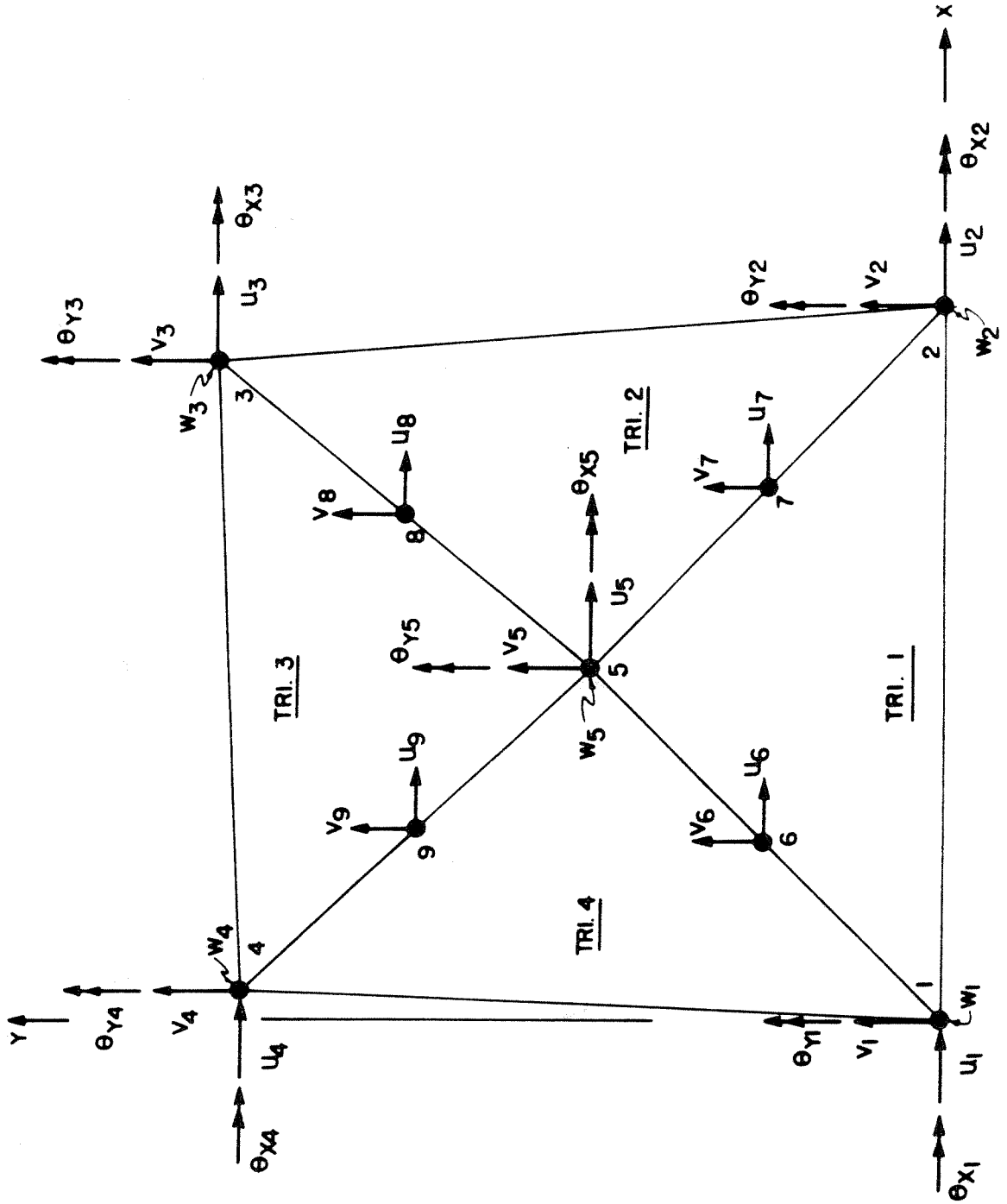


FIG. 2.3 PLANAR QUADRILATERAL WITH 33 DEGREES OF FREEDOM

$$u(x,y) = \{1, x, y, x^2, xy, y^2\} \begin{Bmatrix} \bar{a}_1 \\ \vdots \\ \bar{a}_6 \end{Bmatrix}$$

$$v(x,y) = \{1, x, y, x^2, xy, y^2\} \begin{Bmatrix} \bar{a}_7 \\ \vdots \\ \bar{a}_{12} \end{Bmatrix}$$

DISPLACEMENT FUNCTIONS FOR LST.
IN CARTESIAN COORDINATES

DISPLACEMENT FUNCTIONS SIMILAR
TO LST WITH:

$$u_0 = (u_1 + u_2)/2$$

$$v_0 = (v_1 + v_2)/2$$

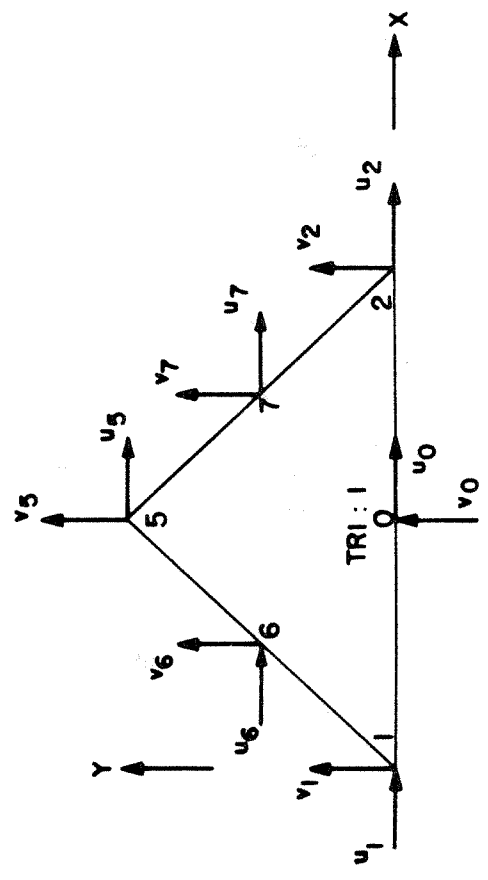


FIG. 2.4 LINEAR STRAIN TRIANGLE WITH 12 DEGREES OF FREEDOM

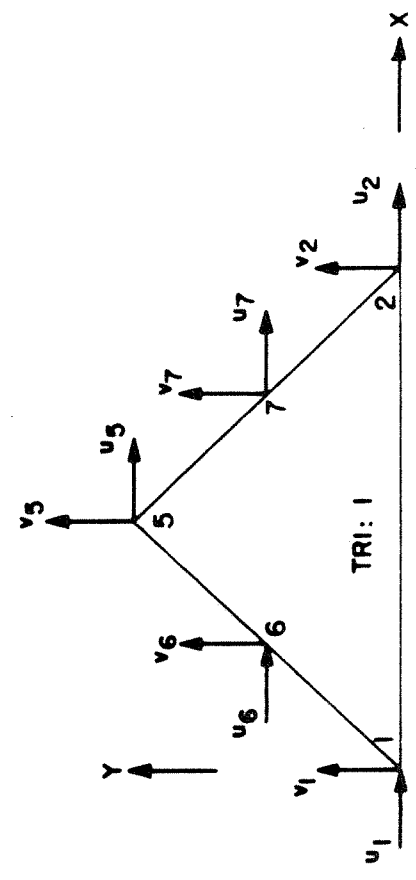


FIG. 2.5 CONSTRAINED LINEAR STRAIN TRIANGLE WITH 10 DEGREES OF FREEDOM

$E = 112.5 \text{ psi}$; $t = 1''$; $\nu = 0.25$

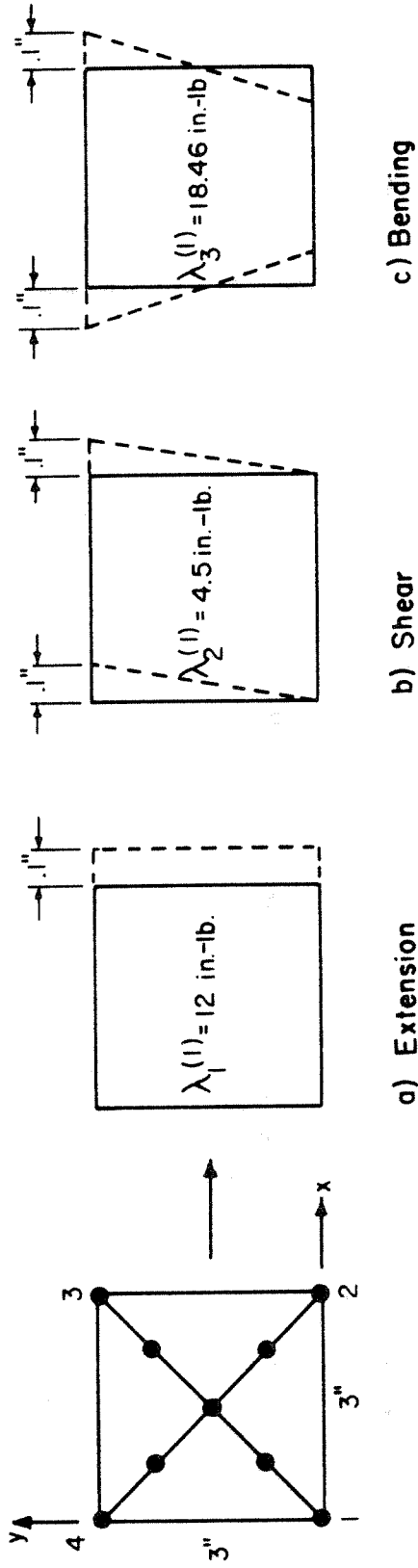


FIG. 2.6 CONSTRAINED QUADRILATERAL AND TYPICAL MEMBRANE STRAINING MODES

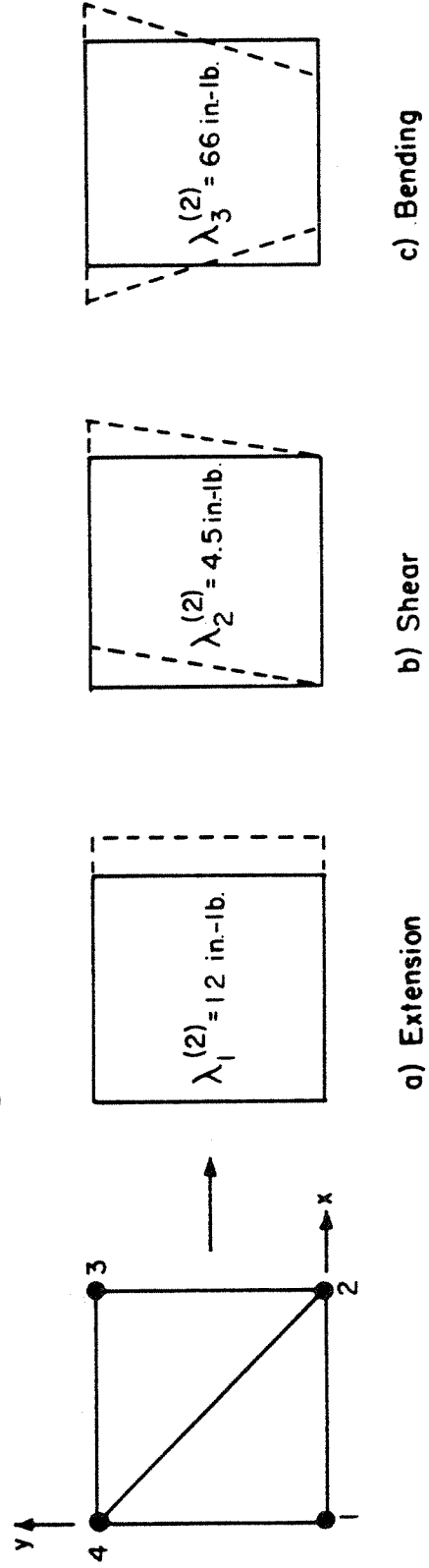


FIG. 2.7 QUADRILATERAL OF TWO CONSTANT STRESS TRIANGLES AND TYPICAL MEMBRANE STRAINING MODES

CHAPTER 3. EVALUATION OF THE ELEMENT STIFFNESSES

A general procedure for evaluating triangular element stiffnesses has been presented by Felippa [12] in which triangular coordinates (a natural coordinate system for triangular regions) are utilized. The displacement functions are expressed directly in terms of the nodal point system through the use of interpolation functions, thereby eliminating the conversion from generalized coordinates to the nodal point system. In addition, a valuable contribution of this presentation results from expressing the variation of strain, material properties, and thickness in terms of nodal point values through the use of appropriate interpolation functions. This greatly simplifies the integration which must be performed as the integration of the interpolation functions and their products are straightforward and are presented in Ref. [12]. In the present analysis, each element has a constant thickness and the material properties are linear, isotropic and are considered constant over the entire element. The following development is based on the procedure of Ref. [12] and is specialized for the above properties.

3.1 Triangular Coordinates for Triangular Elements

The geometry, the triangular coordinates $(\zeta_1, \zeta_2, \zeta_3)$, and Cartesian coordinates (x, y, z) of a typical triangle are shown in Figs. 3.1 and 3.2. The position of an arbitrary point "P" (Fig. 3.2) is established by the ratios of the areas bounded by the dashed lines and the sides of the triangle to the total area of the triangle. Only two triangular coordinates are necessary; however, all three are used since this simplifies the analysis. The triangular coordinates of the arbitrary point "P" are given in Fig. 3.2. Also the triangular coordinates of the corner points

are indicated on this figure together with the homogeneous (zero) coordinates along the sides of the triangle.

Experience has shown that it is more convenient to reference physical displacements, strains, and stresses to the Cartesian system (x, y, z) . Since these quantities are first expressed in triangular coordinates, the following transformations are required:

a) Transformation from triangular to Cartesian coordinates

$$\begin{Bmatrix} 1 \\ x \\ y \end{Bmatrix} = \begin{bmatrix} 1 & 1 & 1 \\ x_1 & x_2 & x_3 \\ y_1 & y_2 & y_3 \end{bmatrix} \begin{Bmatrix} \zeta_1 \\ \zeta_2 \\ \zeta_3 \end{Bmatrix} \quad (3.1)$$

b) Transformation from Cartesian to triangular coordinates

$$\begin{Bmatrix} \zeta_1 \\ \zeta_2 \\ \zeta_3 \end{Bmatrix} = \frac{1}{2A} \begin{bmatrix} x_2 y_3 - x_3 y_2 & y_2 - y_3 & x_3 - x_2 \\ x_3 y_1 - x_1 y_3 & y_3 - y_1 & x_1 - x_3 \\ x_1 y_2 - x_2 y_1 & y_1 - y_2 & x_2 - x_1 \end{bmatrix} \begin{Bmatrix} 1 \\ x \\ y \end{Bmatrix} \quad (3.2)$$

or:

$$\begin{Bmatrix} \zeta_1 \\ \zeta_2 \\ \zeta_3 \end{Bmatrix} = \frac{1}{2A} \begin{bmatrix} 2A_{23} & b_1 & a_1 \\ 2A_{31} & b_2 & a_2 \\ 2A_{12} & b_3 & a_3 \end{bmatrix} \begin{Bmatrix} 1 \\ x \\ y \end{Bmatrix} \quad (3.3)$$

where A_{ij} is the area subtended by corners i, j and the origin of the Cartesian coordinates.

c) Derivatives of triangular coordinates with respect to the Cartesian coordinates.

$$\begin{aligned} \frac{\partial \zeta_1}{\partial x} &= b_1/2A & \frac{\partial \zeta_1}{\partial y} &= a_1/2A \\ \frac{\partial \zeta_2}{\partial x} &= b_2/2A & \frac{\partial \zeta_2}{\partial y} &= a_2/2A \\ \frac{\partial \zeta_3}{\partial x} &= b_3/2A & \frac{\partial \zeta_3}{\partial y} &= a_3/2A \end{aligned} \quad (3.4)$$

In the above, Eqn. 3.2 is obtained by inverting Eqn. 3.1 and the derivatives given by expression 3.4 are obtained from Eqn. 3.3. The derivatives of products of the triangular coordinates may be obtained by the chain rule of differentiation and expression 3.4.

3.2 Procedure for Evaluating Plane Stress Element Stiffnesses

The strain energy due to straining the element is:

$$U = \frac{1}{2} \int_A (\epsilon_x \sigma_x + \epsilon_y \sigma_y + \gamma_{xy} \tau_{xy}) dA \quad (3.5)$$

or in matrix form:

$$U = \frac{1}{2} \int_A \begin{bmatrix} \epsilon_x & \epsilon_y & \gamma_{xy} \end{bmatrix} \begin{Bmatrix} \sigma_x \\ \sigma_y \\ \tau_{xy} \end{Bmatrix} dA \quad (3.6)$$

where the stress components $(\sigma_x, \sigma_y, \tau_{xy})$ are shown in Fig. 3.3 and

$\epsilon_x, \epsilon_y, \gamma_{xy}$ are the corresponding strain components. For the state of plane stress, the stress components are related to the strain components as:

$$\begin{Bmatrix} \sigma_x \\ \sigma_y \\ \tau_{xy} \end{Bmatrix} = \frac{E}{1-\nu^2} \begin{bmatrix} 1 & \nu & . \\ \nu & 1 & . \\ . & . & \frac{(1-\nu)}{2} \end{bmatrix} \begin{Bmatrix} \epsilon_x \\ \epsilon_y \\ \gamma_{xy} \end{Bmatrix} \quad (3.7)$$

by writing Eqn. 3.7 in the following form:

$$\sigma = D \epsilon \quad (3.8)$$

and by using Eqns. 3.6 and 3.8, we have for the strain energy of the element:

$$U = \frac{1}{2} \int_A \epsilon^T D \epsilon \, dA \quad (3.9)$$

From the discretized displacement field, the strains may be expressed in terms of the nodal point displacement vector r_i as:

$$\epsilon_x = \frac{\partial u}{\partial x} \quad ; \quad \epsilon_y = \frac{\partial v}{\partial y} \quad ; \quad \gamma_{xy} = \frac{\partial u}{\partial y} + \frac{\partial v}{\partial x} \quad (3.10)$$

or in matrix form:

$$\begin{Bmatrix} \epsilon_x \\ \epsilon_y \\ \gamma_{xy} \end{Bmatrix} = [B] \begin{Bmatrix} u_i \\ v_i \end{Bmatrix} \quad (3.11)$$

or:

$$\epsilon = B r_i \quad (3.12)$$

where: u is the discretized displacement field in the x- direction,
 v is the discretized displacement field in the y- direction,
 u_i is the nodal point system for displacement in the x- direction,
 v_i is the nodal point system for displacement in the y- direction,
 r_i is the total nodal point displacement system.

Using Eqns. 3.9 and 3.12 we obtain the following expression for U in terms of the nodal point displacement system r_i

$$U = \frac{1}{2} r_i^T \left[\int B^T DB \, dA \right] r_i \quad (3.13)$$

The element stiffness relating nodal point forces to nodal point displacements may be obtained from Eqn. 3.13 by Castigliano's first theorem as:

$$\beta_i = \frac{\partial U}{\partial r_i} \quad (3.14)$$

$$\beta_i = \left[\int_A B^T DB \, dA \right] r_i \quad (3.15)$$

where β_i are the nodal point forces corresponding to r_i and the element stiffness is:

$$k = \int_A B^T DB \, dA \quad (3.16)$$

So the evaluation of the plane stress element stiffness k reduces to the integration of Eqn. 3.16.

3.3 Procedure for Evaluating Plate Bending Element Stiffness

The strain energy due to straining (bending) of the element is:

$$U = \frac{1}{2} \int_A (X_x M_x + X_y M_y + 2X_{xy} M_{xy}) dA \quad (3.17)$$

or in matrix form:

$$U = \frac{1}{2} \int_A (X_x + X_y + 2X_{xy}) \begin{Bmatrix} M_x \\ M_y \\ M_{xy} \end{Bmatrix} = \frac{1}{2} \int_A X^T M dA \quad (3.18)$$

where the moments, M_x , M_y , M_{xy} , are given in Fig. 3.4 and X_x , X_y and X_{xy} are the corresponding curvatures, i.e.,

$$X_x = \frac{\partial^2 W}{\partial X^2} \quad ; \quad X_y = \frac{\partial^2 W}{\partial Y^2} \quad ; \quad X_{xy} = \frac{\partial^2 W}{\partial X \partial Y} \quad (3.19)$$

where W is the transverse displacement of the plate element. The conventional relationship between curvatures and moments is:

$$\begin{Bmatrix} M_x \\ M_y \\ M_{xy} \end{Bmatrix} = \frac{Et^3}{12(1-\nu^2)} \begin{bmatrix} 1 & \nu & 0 \\ \nu & 1 & 0 \\ 0 & 0 & \frac{(1-\nu)}{2} \end{bmatrix} \begin{Bmatrix} X_x \\ X_y \\ 2X_{xy} \end{Bmatrix} \quad (3.20)$$

or:

$$M = \bar{D}X \quad (3.21)$$

Using Eqns. 3.18 and 3.21 the strain energy in bending of the plate element is:

$$U = \frac{1}{2} \int_A X^T DX \, dA \quad (3.22)$$

Eqn. 3.22 is similar in form to Eqn. 3.9 and the evaluation of the plate bending stiffness follows from the procedure described in Section 3.2. However, since independent displacement functions are assigned to the three sub-elements, Fig. 2.2, the integration of Eqn. 3.22 must be performed separately for each sub-element. In addition, the determination of the curvature matrix X for each sub-triangle in terms of the nodal point displacement system is complicated due to the internal compatibility conditions described in Section 2.2. However, curvatures in triangular coordinates can be obtained for each sub-element directly in terms of the nodal point displacements r_i (Eqn. 3.45) so the element stiffness computation is given in symbolic form below:

$$k = \int_{A^{(1)}} X^{(1)T} DX^{(1)} \, dA + \int_{A^{(2)}} X^{(2)T} DX^{(2)} \, dA + \int_{A^{(3)}} X^{(3)T} DX^{(3)} \, dA \quad (3.23)$$

where $X^{(i)}$ is the curvature matrix in sub-element "i," (see Fig. 3.5), and $\int_{A^{(i)}}$ implies that the integration is to be performed only over sub-element "i."

3.4 Derivation of the Constant Strain Triangle (CST) Element Stiffness

The displacement functions for this element expressed in triangular coordinates are:

$$u = \begin{pmatrix} \zeta_1 & \zeta_2 & \zeta_3 \end{pmatrix} \begin{Bmatrix} u_1 \\ u_2 \\ u_3 \end{Bmatrix} \equiv \Phi_{(1)}^T u_i \quad (3.24)$$

$$v = \begin{pmatrix} \zeta_1 & \zeta_2 & \zeta_3 \end{pmatrix} \begin{Bmatrix} v_1 \\ v_2 \\ v_3 \end{Bmatrix} \equiv \Phi_{(1)}^T v_i \quad (3.25)$$

The element strains (Eqns. 3.11, 3.12) are obtained by appropriate differentiation of Eqns. 3.24 and 3.25 and with the use of expression 3.4 is given by

$$\begin{Bmatrix} \epsilon_x \\ \epsilon_y \\ \gamma_{xy} \end{Bmatrix} = \frac{1}{2A} \begin{bmatrix} b_1 & b_2 & b_3 & \cdot & \cdot & \cdot \\ \cdot & \cdot & \cdot & a_1 & a_2 & a_3 \\ a_1 & a_2 & a_3 & b_1 & b_2 & b_3 \end{bmatrix} \begin{Bmatrix} r_i \end{Bmatrix} \quad (3.26)$$

or: $\epsilon = B r_i$

where

$$r_i = \{u_1 \quad u_2 \quad u_3 \quad v_1 \quad v_2 \quad v_3\}^T \quad (3.27)$$

Thus:

$$k = \int_A B^T D B dA \quad (3.28)$$

The integration of Eqn. 3.28 is particularly simple since the element strains are constant, and by using Eqns. 3.26 and 3.28 the constant strain element stiffness is given by:

$$k = \frac{Et}{4A(1-\nu^2)} \begin{bmatrix} b_1 & \cdot & a_1 \\ b_2 & \cdot & a_2 \\ b_3 & \cdot & a_3 \\ \cdot & a_1 & b_1 \\ \cdot & a_2 & b_2 \\ \cdot & a_3 & b_3 \end{bmatrix} \begin{bmatrix} 1 & \nu & \cdot \\ \nu & 1 & \cdot \\ \cdot & \cdot & \frac{1-\nu}{2} \end{bmatrix} \begin{bmatrix} b_1 & b_2 & b_3 & \cdot & \cdot & \cdot \\ \cdot & \cdot & \cdot & a_1 & a_2 & a_3 \\ a_1 & a_2 & a_3 & b_1 & b_2 & b_3 \end{bmatrix} \quad (3.29)$$

3.5 Derivation of the Constrained Linear Strain Triangle Element Stiffness

This element stiffness is most conveniently derived by first establishing the strain displacement matrix B for the linear strain triangle (Fig. 2.4), and subsequently applying the constraints $u_0 = (u_1 + u_2)/2$ and $v_0 = (v_1 + v_2)/2$ (see Fig. 2.5) on the matrix B. The displacement functions for the linear strain triangle in triangular coordinates are:

$$u = \begin{Bmatrix} \zeta_1(2\zeta_1-1) \\ \zeta_2(2\zeta_2-1) \\ \zeta_3(2\zeta_3-1) \\ 4\zeta_1\zeta_2 \\ 4\zeta_2\zeta_3 \\ 4\zeta_3\zeta_1 \end{Bmatrix}^T \{u_i\} \quad \text{and} \quad v = \begin{Bmatrix} \zeta_1(2\zeta_1-1) \\ \zeta_2(2\zeta_2-1) \\ \zeta_3(2\zeta_3-1) \\ 4\zeta_1\zeta_2 \\ 4\zeta_2\zeta_3 \\ 4\zeta_3\zeta_1 \end{Bmatrix}^T \{v_i\} \quad (3.30)$$

or:

$$u = \phi_{(2)}^T u_i \quad v = \phi_{(2)}^T v_i \quad (3.31)$$

In performing the integration implied in Eqn. 3.16, it is convenient to express the strains (ϵ) in terms of nodal point strains together with the appropriate interpolation function. For constant thickness, the stresses and strains vary linearly and the three strain components everywhere in the element may be expressed as follows:

$$\begin{Bmatrix} \epsilon_x \\ \epsilon_y \\ \gamma_{xy} \end{Bmatrix} = \begin{bmatrix} \zeta_1 & \zeta_2 & \zeta_3 & \cdot & \cdot & \cdot & \cdot & \cdot & \cdot \\ \cdot & \cdot & \cdot & \zeta_1 & \zeta_2 & \zeta_3 & \cdot & \cdot & \cdot \\ \cdot & \cdot & \cdot & \cdot & \cdot & \cdot & \zeta_1 & \zeta_2 & \zeta_3 \end{bmatrix} \begin{Bmatrix} \epsilon_{xi} \\ \epsilon_{yi} \\ \gamma_{xyi} \end{Bmatrix} \left\{ r_i \right\} \quad (3.32)$$

or:
$$\epsilon = \Phi_\epsilon \epsilon_i r_i \equiv B r_i$$

where

$$\epsilon_{xi} = \begin{bmatrix} \epsilon_{x1} \\ \epsilon_{x2} \\ \epsilon_{x5} \end{bmatrix} \quad \epsilon_{yi} = \begin{bmatrix} \epsilon_{y1} \\ \epsilon_{y2} \\ \epsilon_{y5} \end{bmatrix} \quad \gamma_{xyi} = \begin{bmatrix} \gamma_{xy1} \\ \gamma_{xy2} \\ \gamma_{xy5} \end{bmatrix}$$

are evaluated at the three corners of the triangle and the nodal point displacement vector (Fig. 2.5) is:

$$r_i = \{u_1, u_2, u_5, u_0, u_7, u_6, v_1, v_2, v_5, v_0, v_7, v_6\}^T$$

Therefore from Eqn. 3.16:

$$k = \int_A B^T D B dA = \int_A \epsilon_i^T \Phi_\epsilon^T D \Phi_\epsilon \epsilon_i dA \quad (3.33)$$

Since ϵ_i is a matrix of constants, the above integration is reduced to evaluating $\int_A \Phi_\epsilon^T D \Phi_\epsilon$. This has been evaluated in Ref. [12] for a general

constitutive law and for this analysis results in the inner matrix (N), of Eqn. 3.34. Evaluation of the three stress components at the three corners of the triangle yields the following LST stiffness matrix:

$$k = \begin{bmatrix} B_{11}^T & \cdot & B_{21}^T \\ \cdot & B_{21}^T & B_{11}^T \\ B_{11}^T & \cdot & B_{21}^T \end{bmatrix} \begin{bmatrix} N_{11} & N_{12} & \cdot \\ N_{12} & N_{11} & \cdot \\ \cdot & \cdot & N_{33} \end{bmatrix} \begin{bmatrix} B_{11} & \cdot \\ \cdot & B_{21} \\ B_{21} & B_{11} \end{bmatrix} \quad (3.34)$$

$B^T \qquad \qquad \qquad N \qquad \qquad \qquad B$

where:

$$B_{11} = \frac{1}{2A} \begin{bmatrix} 3b_1 & -b_2 & -b_3 & 4b_2 & \cdot & 4b_3 \\ -b_1 & 3b_2 & -b_3 & 4b_1 & 4b_3 & \cdot \\ -b_1 & -b_2 & 3b_3 & \cdot & 4b_2 & 4b_1 \end{bmatrix} \quad (3.35)$$

$$B_{21} = \frac{1}{2A} \begin{bmatrix} 3a_1 & -a_2 & -a_3 & 4a_2 & \cdot & 4a_3 \\ -a_1 & 3a_2 & -a_3 & 4a_1 & 4a_3 & \cdot \\ -a_1 & -a_2 & 3a_3 & \cdot & 4a_2 & 4a_1 \end{bmatrix}$$

$$N_{11} = \frac{EtA}{12(1-\nu^2)} \begin{bmatrix} 2 & 1 & 1 \\ 1 & 2 & 1 \\ 1 & 1 & 2 \end{bmatrix}; \quad N_{12} = \frac{EtA\nu}{12(1-\nu^2)} \begin{bmatrix} 2 & 1 & 1 \\ 1 & 2 & 1 \\ 1 & 1 & 2 \end{bmatrix}; \quad N_{33} = \frac{EtA}{24(1+\nu)} \begin{bmatrix} 2 & 1 & 1 \\ 1 & 2 & 1 \\ 1 & 1 & 2 \end{bmatrix} \quad (3.36)$$

The element stiffness for the constrained LST is now obtained by modifying the B matrix by adding one half of column 4 to columns 1 and 2 and by adding one half of column 10 to columns 7 and 8. The resulting stiffness matrix is as follows:

$$k = \begin{bmatrix} \bar{B}_{11}^T & \cdot & \bar{B}_{21}^T \\ \cdot & \bar{B}_{21}^T & \bar{B}_{11}^T \\ \bar{B}_{11}^T & \cdot & \bar{B}_{21}^T \end{bmatrix} [N] \begin{bmatrix} \bar{B}_{11} & \cdot \\ \cdot & \bar{B}_{21} \\ \bar{B}_{21} & \bar{B}_{11} \end{bmatrix} \quad (3.37)$$

where:

$$\bar{B}_{11} = \frac{1}{2A} \begin{bmatrix} b_1 - 2b_3 & b_2 & -b_3 & \cdot & 4b_3 \\ b_1 & b_2 - 2b_3 & -b_3 & 4b_3 & \cdot \\ -b_1 & -b_2 & 3b_3 & 4b_2 & 4b_1 \end{bmatrix} \quad (3.38)$$

$$B_{21} = \frac{1}{2A} \begin{bmatrix} a_1 - 2a_3 & a_2 & -a_3 & \cdot & 4a_3 \\ a_1 & a_2 - 2a_3 & -a_3 & 4a_3 & \cdot \\ -a_1 & -a_2 & 3a_3 & 4a_2 & 4a_1 \end{bmatrix}$$

3.6 Derivation of the Plate Bending Element Stiffness

The evaluation of the subject plate bending element stiffness utilizing Cartesian coordinates has been presented in Ref. [8] and using triangular coordinates in Ref. [9] based on the work of Felippa [12]. Although the use of Cartesian coordinates proved useful in establishing displacement functions which insure a fully compatible element, the development of computer algorithms based on this coordinate system which result in minimal computational time, requires considerable effort. This difficulty is due to the fact that the displacement functions are first expressed in terms of 27 generalized coordinates; and not only must 18 of these generalized coordinates be eliminated by imposing internal compatibility conditions, but the remaining 9 independent generalized coordinates must be related to the nodal point displacement system (Fig. 2.2). Much of this difficulty is overcome by the use of triangular coordinates since the displacement functions are expressed directly in terms of the nodal point displacement system; however, the internal compatibility requirements are not considered directly in the displacement functions for each sub-element (Ref. [9]).

More recently Felippa has developed the displacement functions in triangular coordinates which account for the internal compatibility conditions. This development has considerably simplified the evaluation of the subject element stiffness and is presented in the following.

A typical plate bending element is shown in Fig. 3.5, in which the common interior point of the three sub-triangles has the triangular coordinates $\frac{1}{3}, \frac{1}{3}, \frac{1}{3}$. The displacement functions (valid only for region 3), Fig. 3.6, are given by Eqn. 3.44 where the constants $c_{1...9}, d_{1...9}, e_{1...9}, f_{1...9}$ in this equation are listed in Table 1. The superscripts for the coefficients of $\varphi^{(3)}$ in Eqn. 3.44, and for the coefficients in Table 1 have been eliminated for the sake of convenience, but it is understood that they correspond to those for Region 3, Fig. 3.5. Displacement functions which are valid in Regions 1 and 2 are obtained by placing the superscripts 1 and 2 on all quantities in Eqn. 3.44 and the quantities listed in Table 1 and by replacing these quantities by the values shown in Figs. 3.7 and 3.8 respectively. This is conveniently accomplished from Eqn. 3.44 by cyclic permutation on the quantities a_i and b_i , since, for example, for the quantities a_i we have:

$$\begin{aligned} a_i^{(1)} &= a_j^{(3)} & j &= 2,3,1 \\ & & \text{for } i &= 1,2,3; \text{ and} \\ a_i^{(2)} &= a_k^{(3)} & k &= 3,1,2 \end{aligned} \quad (3.39)$$

It should be noted that the displacement nodal point system given in Eqn. 3.44 is rotated when considering Region 1 and 2 as shown in Figs. 3.7 and 3.8. For example, $W_1^{(3)}, \theta_{x1}^{(3)}, \theta_{y1}^{(3)}$ are located at point 1 (Fig. 3.5), while $W_1^{(1)}, \theta_{x1}^{(1)}, \theta_{y1}^{(1)}$ and $W_1^{(2)}, \theta_{x1}^{(2)}, \theta_{y1}^{(2)}$ are located at

points 2 and 3 (Fig. 3.5) respectively. Having established displacement functions valid for the three regions of the plate bending element, the contribution of each region (see Eqn. 3.23) is easily evaluated and is subsequently illustrated for Region 3 (Fig. 3.6).

As in the case of the Linear Strain Triangle, it is convenient to express the curvatures, X , Eqn. 3.22, in terms of nodal point curvatures. Since the curvature varies linearly over each sub-region, it is appropriate to use Φ_ϵ from Eqn. 3.32 where the ζ_i in Φ_ϵ are understood to be the triangular coordinates of the particular region being considered. Therefore for Region 3, we have:

$$\begin{Bmatrix} X_x^{(3)} \\ X_y^{(3)} \\ 2X_{xy}^{(3)} \end{Bmatrix} = \begin{bmatrix} \Phi_\epsilon \end{bmatrix} \begin{bmatrix} X_{xi}^{(3)} \\ X_{yi}^{(3)} \\ 2X_{xyi}^{(3)} \end{bmatrix} \begin{bmatrix} r_i \end{bmatrix} = \Phi_\epsilon X_i^{(3)} r_i = X^{(3)} r_i \quad (3.40)$$

where:

$$X_{xi}^{(3)} = \begin{bmatrix} X_{x1} \\ X_{x2} \\ X_{x0} \end{bmatrix} ; \quad X_{yi}^{(3)} = \begin{bmatrix} X_{y1} \\ X_{y2} \\ X_{y0} \end{bmatrix} ; \quad X_{xyi}^{(3)} = \begin{bmatrix} X_{xy1} \\ X_{xy2} \\ X_{xy0} \end{bmatrix} \quad (3.41)$$

To evaluate the nodal point curvatures $X_{xi}^{(3)}$, $X_{yi}^{(3)}$, $X_{xyi}^{(3)}$, Eqn. 3.44 must be differentiated appropriately. This is accomplished by the chain rule and by using expression 3.4. The values for X_x are given by Eqn. 3.45 where the quantities b_{ij} are equal to $b_i b_j$. The purpose of using the designation b_{ij} is for establishing X_y , X_{xy} since they may be obtained from Eqn. 3.45 as follows:

replace b_{ij} by $a_i a_j$ for X_y

(3.42)

and

replace b_{ij} by $(a_i b_j + a_j b_i)/2$ for X_{xy}

Thus from Eqn. 3.45 and by the use of expression 3.42, $X^{(3)}$ is evaluated and the contribution to the total stiffness from Region 3 is:

$$k^{(3)} = \int_A X_i^{(3)T} \Phi_\epsilon^T \bar{D} \Phi_\epsilon X_i^{(3)} dA = X^{(3)T} \bar{N}X^{(3)} \quad (3.43)$$

By cyclic permutation of the quantities a_i and b_i for Regions 1 and 2 and by noting that the nodal point system for these regions is as shown in Figs. 3.7 and 3.8, the evaluation of Eqn. 3.23 is easily completed.

In the above derivation the nodal point system of displacements, r_i , is as shown in Fig. 2.2 except that the three transverse displacement components are considered positive when directed downward. A right-handed coordinate system of nodal point displacement may be established by changing the signs of the rows and columns associated with the three displacement components in the final element stiffness matrix. Alternately the right-handed system may be obtained by changing the signs of all rotations, i.e., $\phi_i^{(j)}$ ($j = 1, 2, 3$; $i = 2, 3, 5, 6, 8, 9$) in Eqn. 3.44.

$$\begin{aligned}
w_p^{(3)}(\zeta_1^{(3)}, \zeta_2^{(3)}, \zeta_3^{(3)}) &= \left[\begin{array}{l} c_1 \zeta_1 \zeta_2 \zeta_3 + \zeta_3^2(d_1 \zeta_1 + e_1 \zeta_2 + f_1 \zeta_3) + \zeta_1^2(3 - 2\zeta_1) \\ c_2 \zeta_1 \zeta_2 \zeta_3 + \zeta_3^2(d_2 \zeta_1 + e_2 \zeta_2 + f_2 \zeta_3) + \zeta_1^2(b_3 \zeta_2 - b_2 \zeta_3) \\ c_3 \zeta_1 \zeta_2 \zeta_3 + \zeta_3^2(d_3 \zeta_1 + e_3 \zeta_2 + f_3 \zeta_3) + \zeta_1^2(a_3 \zeta_2 - a_2 \zeta_3) \\ c_4 \zeta_1 \zeta_2 \zeta_3 + \zeta_3^2(d_4 \zeta_1 + e_4 \zeta_2 + f_4 \zeta_3) + \zeta_2^2(3 - 2\zeta_2) \\ c_5 \zeta_1 \zeta_2 \zeta_3 + \zeta_3^2(d_5 \zeta_1 + e_5 \zeta_2 + f_5 \zeta_3) + \zeta_2^2(b_1 \zeta_3 - b_3 \zeta_1) \\ c_6 \zeta_1 \zeta_2 \zeta_3 + \zeta_3^2(d_6 \zeta_1 + e_6 \zeta_2 + f_6 \zeta_3) + \zeta_2^2(a_1 \zeta_3 - a_3 \zeta_1) \\ c_7 \zeta_1 \zeta_2 \zeta_3 + \zeta_3^2(d_7 \zeta_1 + e_7 \zeta_2 + f_7 \zeta_3) \\ c_8 \zeta_1 \zeta_2 \zeta_3 + \zeta_3^2(d_8 \zeta_1 + e_8 \zeta_2 + f_8 \zeta_3) \\ c_9 \zeta_1 \zeta_2 \zeta_3 + \zeta_3^2(d_9 \zeta_1 + e_9 \zeta_2 + f_9 \zeta_3) \end{array} \right]^T \\
&= \left\{ \begin{array}{l} w_1^{(3)} \\ \theta_{x1}^{(3)} \\ \theta_{y1}^{(3)} \\ w_2^{(3)} \\ \theta_{x2}^{(3)} \\ \theta_{y2}^{(3)} \\ w_3^{(3)} \\ \theta_{x3}^{(3)} \\ \theta_{y3}^{(3)} \end{array} \right\} = \left[\begin{array}{l} \varphi_1^{(3)} \\ \varphi_2^{(3)} \\ \varphi_3^{(3)} \\ \varphi_4^{(3)} \\ \varphi_5^{(3)} \\ \varphi_6^{(3)} \\ \varphi_7^{(3)} \\ \varphi_8^{(3)} \\ \varphi_9^{(3)} \end{array} \right] \\
v_p^{(3)} &= \varphi^{(3)} v_p^{(3)}
\end{aligned}$$

(3.44)

Displacement Functions for Region 3 of Plate Bending Element

$$\begin{aligned}
\varphi_{1,xx}^{(3)} &= \frac{1}{4A^2} \left\{ \begin{array}{l} 2b_{23}c_1 + 2b_{33}d_1 - 6b_{11} \\ 2b_{13}c_1 + 2b_{33}e_1 + 6b_{11} \\ 2b_{12}c_1 + 4b_{13}d_1 + 4b_{23}e_1 + 6b_{33}f_1 + 6b_{11} \end{array} \right\}^T \left\{ \begin{array}{l} \zeta_1 \\ \zeta_2 \\ \zeta_3 \end{array} \right\} \\
\varphi_{2,xx}^{(3)} &= \frac{1}{4A^2} \left\{ \begin{array}{l} 2b_{23}c_2 + 2b_{33}d_2 + 4b_{12}b_3 - 4b_{13}b_2 \\ 2b_{13}c_2 + 2b_{33}e_2 + 2b_{11}b_3 \\ 2b_{12}c_2 + 4b_{13}d_2 + 4b_{23}e_2 + 6b_{33}f_2 - 2b_{11}b_2 \end{array} \right\}^T \left\{ \begin{array}{l} \zeta_1 \\ \zeta_2 \\ \zeta_3 \end{array} \right\} \\
\varphi_{3,xx}^{(3)} &= \frac{1}{4A^2} \left\{ \begin{array}{l} 2b_{23}c_3 + 2b_{33}d_3 + 4b_{12}a_3 - 4b_{13}a_2 \\ 2b_{13}c_3 + 2b_{33}e_3 + 2b_{11}a_3 \\ 2b_{12}c_3 + 4b_{13}d_3 + 4b_{23}e_3 + 6b_{33}f_3 - 2b_{11}a_2 \end{array} \right\}^T \left\{ \begin{array}{l} \zeta_1 \\ \zeta_2 \\ \zeta_3 \end{array} \right\} \\
\varphi_{4,xx}^{(3)} &= \frac{1}{4A^2} \left\{ \begin{array}{l} 2b_{23}c_4 + 2b_{33}d_4 - 6b_{22} \\ 2b_{13}c_4 + 2b_{33}e_4 + 6b_{22} \\ 2b_{12}c_4 + 4b_{13}d_4 + 4b_{23}e_4 + 6b_{33}f_4 + 6b_{22} \end{array} \right\}^T \left\{ \begin{array}{l} \zeta_1 \\ \zeta_2 \\ \zeta_3 \end{array} \right\} \\
\varphi_{5,xx}^{(3)} &= \frac{1}{4A^2} \left\{ \begin{array}{l} 2b_{23}c_5 + 2b_{33}d_5 - 2b_{22}b_3 \\ 2b_{13}c_5 + 2b_{33}e_5 + 4b_{23}b_1 - 4b_{12}b_3 \\ 2b_{12}c_5 + 4b_{13}d_5 + 4b_{23}e_5 + 6b_{33}f_5 + 2b_{22}b_1 \end{array} \right\}^T \left\{ \begin{array}{l} \zeta_1 \\ \zeta_2 \\ \zeta_3 \end{array} \right\} \\
\varphi_{6,xx}^{(3)} &= \frac{1}{4A^2} \left\{ \begin{array}{l} 2b_{23}c_6 + 2b_{33}d_6 - 2b_{22}a_3 \\ 2b_{13}c_6 + 2b_{33}e_6 + 4b_{23}a_1 - 4b_{12}a_3 \\ 2b_{12}c_6 + 4b_{13}d_6 + 4b_{23}e_6 + 6b_{33}f_6 + 2b_{22}a_1 \end{array} \right\}^T \left\{ \begin{array}{l} \zeta_1 \\ \zeta_2 \\ \zeta_3 \end{array} \right\} \\
\varphi_{7,xx}^{(3)} &= \frac{1}{4A^2} \left\{ \begin{array}{l} 2b_{23}c_7 + 2b_{33}d_7 \\ 2b_{13}c_7 + 2b_{33}e_7 \\ 2b_{12}c_7 + 4b_{13}d_7 + 4b_{23}e_7 + 6b_{33}f_7 \end{array} \right\}^T \left\{ \begin{array}{l} \zeta_1 \\ \zeta_2 \\ \zeta_3 \end{array} \right\} \\
\varphi_{8,xx}^{(3)} &= \frac{1}{4A^2} \left\{ \begin{array}{l} 2b_{23}c_8 + 2b_{33}d_8 \\ 2b_{13}c_8 + 2b_{33}e_8 \\ 2b_{12}c_8 + 4b_{13}d_8 + 4b_{23}e_8 + 6b_{33}f_8 \end{array} \right\}^T \left\{ \begin{array}{l} \zeta_1 \\ \zeta_2 \\ \zeta_3 \end{array} \right\} \\
\varphi_{9,xx}^{(33)} &= \frac{1}{4A^2} \left\{ \begin{array}{l} 2b_{23}c_9 + 2b_{33}d_9 \\ 2b_{13}c_9 + 2b_{33}e_9 \\ 2b_{12}c_9 + 4b_{13}d_9 + 4b_{23}e_9 + 6b_{33}f_9 \end{array} \right\}^T \left\{ \begin{array}{l} \zeta_1 \\ \zeta_2 \\ \zeta_3 \end{array} \right\}
\end{aligned} \tag{3.45}$$

Table 1

$$\begin{aligned}
c_1 &= 6\mu_3 \\
c_2 &= \mu_3 b_3 - b_1 + 4P_3 \\
c_3 &= \mu_3 a_3 - a_1 + 4R_3 \\
c_4 &= 6\lambda_3 \\
c_5 &= b_2 - \lambda_3 b_3 + 4P_3 \\
c_6 &= a_2 - \lambda_3 a_3 + 4R_3 \\
c_7 &= 0 \\
c_8 &= 0 \\
c_9 &= 0 \\
d_1 &= 3(\lambda_2 - \mu_3) \\
d_2 &= (9b_1 + 3\mu_2 b_2 + 3\lambda_3 b_3)/6 + 2P_2 - 2P_3 \\
d_3 &= (9a_1 + 3\mu_2 a_2 + 3\lambda_3 a_3)/6 + 2R_2 - 2R_3 \\
d_4 &= -3\lambda_3 \\
d_5 &= (3b_1 + 6b_3 - 3\mu_3 b_3)/6 - 2P_3 \\
d_6 &= (3a_1 + 6a_3 - 3\mu_3 a_3)/6 - 2R_3 \\
d_7 &= 3(1 + \mu_2) \\
d_8 &= (3b_1 + 12b_2 - 3\lambda_2 b_2)/6 + 2P_2 \\
d_9 &= (3a_1 + 12a_2 - 3\lambda_2 a_2)/6 + 2R_2 \\
e_1 &= -3\mu_3 \\
e_2 &= (-3b_2 - 6b_3 + 3\lambda_3 b_3)/6 - 2P_3 \\
e_3 &= (-3a_2 - 6a_3 + 3\lambda_3 a_3)/6 - 2R_3 \\
e_4 &= 3(\mu_1 - \lambda_3) \\
e_5 &= (-9b_2 - 3\lambda_1 b_1 - 3\mu_3 b_3)/6 + 2P_1 - 2P_3 \\
e_6 &= (-9a_2 - 3\lambda_1 a_1 - 3\mu_3 a_3)/6 + 2R_1 - 2R_3 \\
e_7 &= 3(1 + \lambda_1) \\
e_8 &= (-12b_1 - 3b_2 + 3\mu_1 b_1)/6 + 2P_1 \\
e_9 &= (-12a_1 - 3a_2 + 3\mu_1 a_1)/6 + 2R_1
\end{aligned}$$

Table 1 - continued

$$\begin{aligned}
f_1 &= 2\mu_3 - \lambda_2 \\
f_2 &= (4b_2 + 5b_3 - \mu_2 b_2 - 2\lambda_3 b_3)/6 + (4P_3 - 2P_2)/3 \\
f_3 &= (4a_2 + 5a_3 - \mu_2 a_2 - 2\lambda_3 a_3)/6 + (4R_3 - 2R_2)/3 \\
f_4 &= 2\lambda_3 - \mu_1 \\
f_5 &= (-4b_1 - 5b_3 + \lambda_1 b_1 + 2\mu_3 b_3)/6 + (4P_3 - 2P_1)/3 \\
f_6 &= (-4a_1 - 5a_3 + \lambda_1 a_1 + 2\mu_3 a_3)/6 + (4R_3 - 2R_1)/3 \\
f_7 &= 1 - \lambda_1 - \mu_2 \\
f_8 &= (\mu_1 b_1 - \lambda_2 b_2)/6 - (2P_1 + 2P_2)/3 \\
f_9 &= (\mu_1 a_1 - \lambda_2 a_2)/6 - (2R_1 + 2R_2)/3
\end{aligned}$$

where:

$$\begin{aligned}
l_1^2 &= a_1^2 + b_1^2 \\
l_2^2 &= a_2^2 + b_2^2 \\
l_3^2 &= a_3^2 + b_3^2 \\
\lambda_1 &= -(a_1 a_3 + b_1 b_3)/l_1^2 \\
\lambda_2 &= -(a_2 a_1 + b_2 b_1)/l_2^2 \\
\lambda_3 &= -(a_3 a_2 + b_3 b_2)/l_3^2 \\
\mu_1 &= 1 - \lambda_1 \\
\mu_2 &= 1 - \lambda_2 \\
\mu_3 &= 1 - \lambda_3 \\
P_1 &= -Aa_1/l_1^2 \\
P_2 &= -Aa_2/l_2^2 \\
P_3 &= -Aa_3/l_3^2 \\
R_1 &= Ab_1/l_1^2 \\
R_2 &= Ab_2/l_2^2 \\
R_3 &= Ab_3/l_3^2 \\
A &= (a_3 b_2 - a_2 b_3)/2
\end{aligned}$$

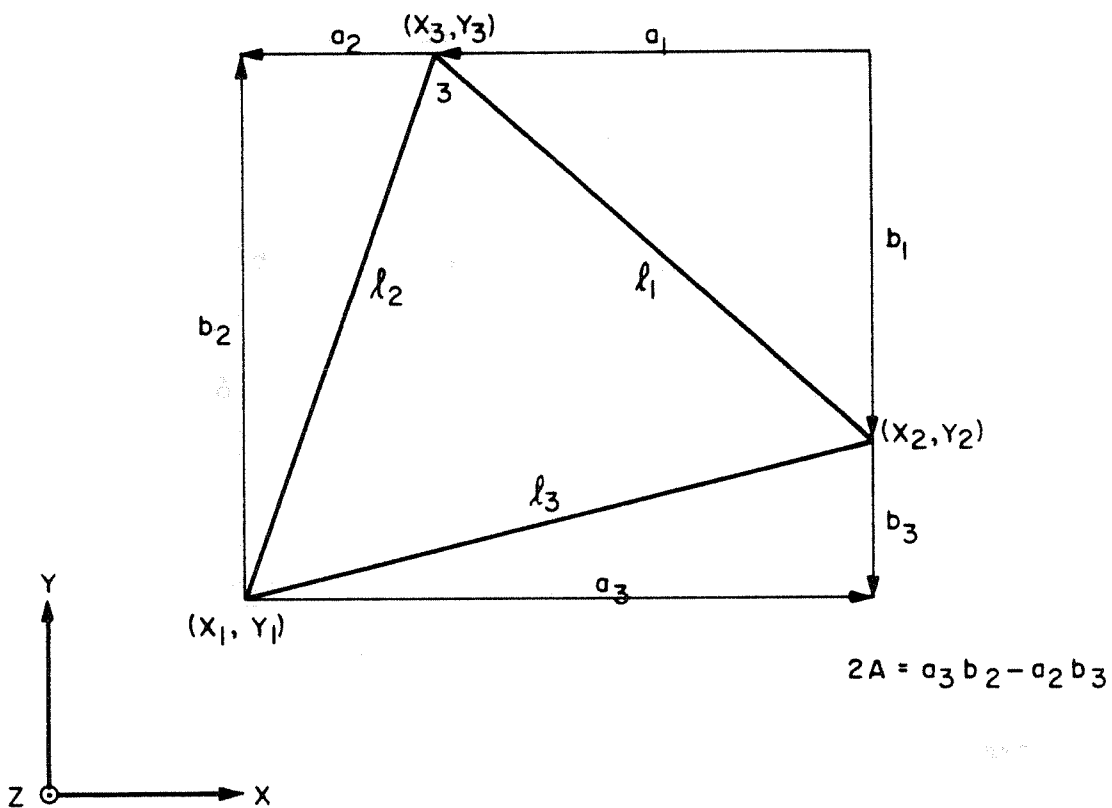


FIG. 3.1 GEOMETRY OF TRIANGLE

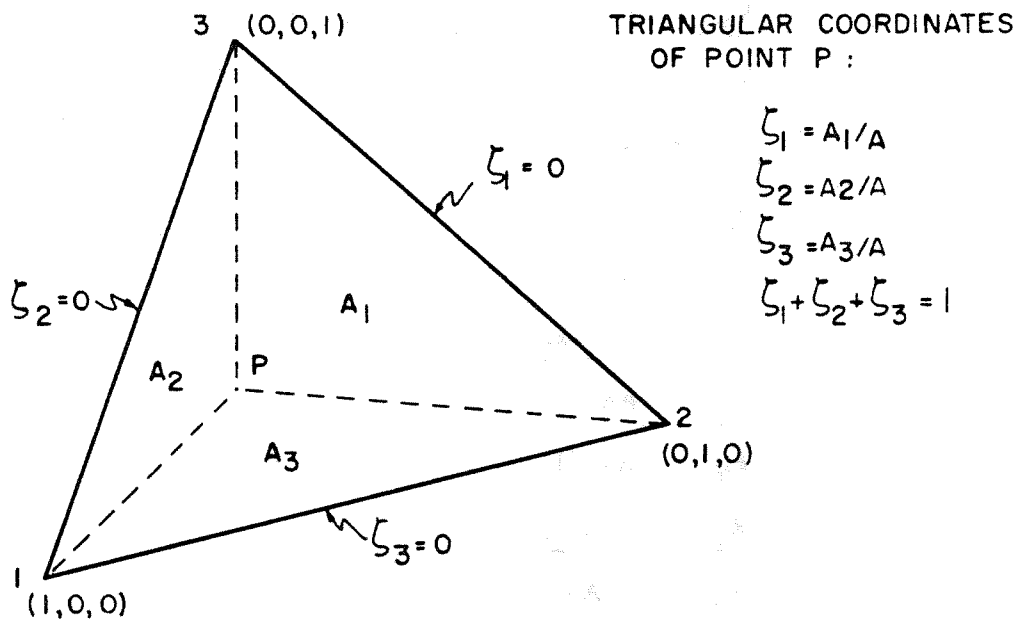


FIG. 3.2 TRIANGULAR COORDINATES

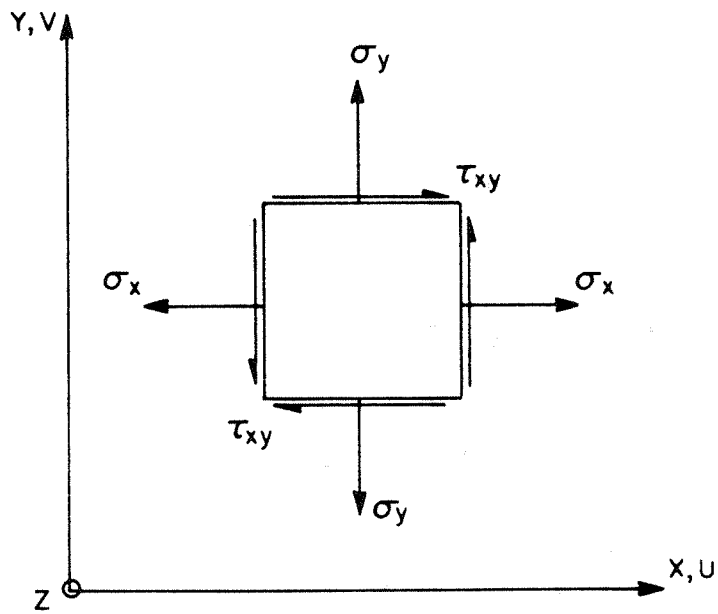


FIG. 3.3 CONVENTIONS FOR IN-PLANE STRESS COMPONENTS

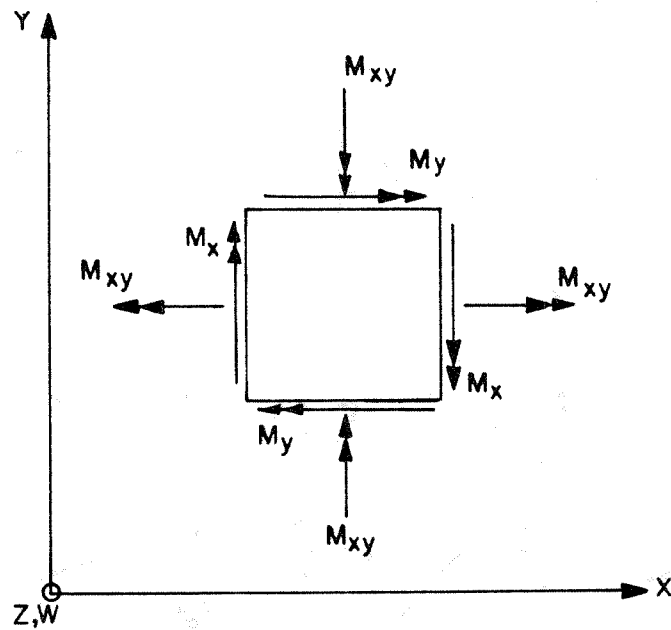


FIG. 3.4 CONVENTIONS FOR PLATE BENDING MOMENT COMPONENTS

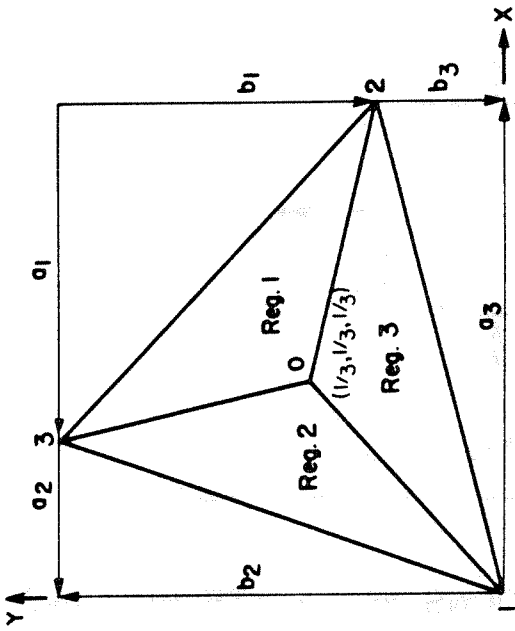


FIG. 3.5 POSITION OF REGIONS 1, 2, 3

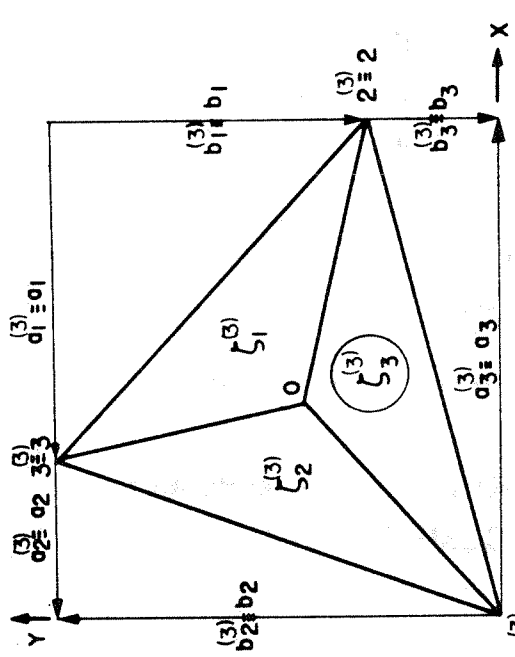


FIG. 3.6 CONVENTIONS FOR REGION 3

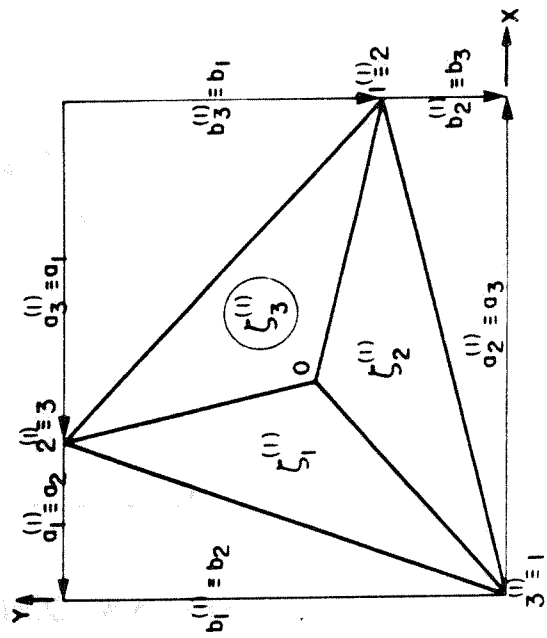


FIG. 3.7 CONVENTIONS FOR REGION 1

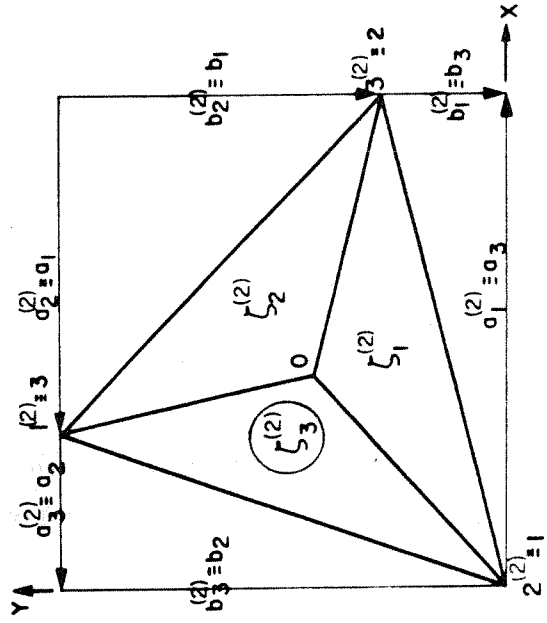


FIG. 3.8 CONVENTIONS FOR REGION 2

CHAPTER 4. THE ELEMENT ASSEMBLAGE

The stiffness matrix of the complete element assemblage is obtained most conveniently by the direct stiffness procedure. The two essential steps in this procedure are the coordinate transformations and the subsequent superposition of each element stiffness. The coordinate transformations are performed by rotating the element coordinates $(\bar{x}, \bar{y}, \bar{z})$ of each element stiffness so that the translational and rotational degrees of freedom of all elements which share a common nodal point are expressed in the same coordinates. This nodal point coordinate system in which the nodal forces and displacements of the complete assemblage are expressed is subsequently referred to as base coordinates. The superposition of each element stiffness is accomplished by adding its individual terms into the complete stiffness matrix according to the nodal point numbers of the element (see Fig. 4.1).

4.1 Coordinate Systems

In this analysis two types of nodal point coordinate systems are used. The first coordinate system (x, y, z) (Fig. 2.1) is referred to as global coordinates and is a fixed set of Cartesian coordinates, while the second coordinate system called surface coordinates (ξ_1, ξ_2, ξ_3) , Fig. 2.1 is an orthogonal coordinate system in which ξ_3 is taken normal to the shell surface at each nodal point. In addition, each triangle is given a separate coordinate system $(\bar{x}, \bar{y}, \bar{z})$ (Fig. 2.1), while each of the four sub-triangles of the quadrilateral have coordinates $(\bar{x}_i, \bar{y}_i, \bar{z}_i)$ (Fig. 4.3). These coordinates are called element coordinates.

For the quadrilateral element (Figs. 2.1 and 4.2), another coordinate system (η_1, η_2, η_3) referred to as the η -coordinates is utilized. The η_1 - η_2 plane is the plane which "best fits" the coordinates of the exterior nodes (1, 2, 3, 4), and is established by minimizing the sum of the squares of the normal distances from this plane to the exterior nodes. This plane is established automatically from the coordinates of the exterior nodes, and the η_1 axis is determined from a plane normal to the η_1 - η_2 plane which contains side 1-2 of the quadrilateral. All translational and rotational degrees of freedom of the interior nodes (5, 6, 7, 8, 9) are referred to this coordinate system.

4.2 Coordinate Transformation

In order to transform the triangular or quadrilateral element stiffnesses it is necessary to establish the direction cosine matrices which transform forces and displacements from the element, surface and η -coordinates. The transformation matrix for the element coordinates is determined from the coordinates of the three corners of the triangle, while the transformations from surface coordinates to global coordinates is established by specifying the direction cosines of any two lines lying in the tangent plane of the shell surface at each nodal point, from which the complete set of direction cosines is constructed for each nodal point. These two transformation matrices together with the direction cosines relating forces and displacement between the global and the η -coordinates constitute the complete set of transformation matrices required for the solution.

The above transformations from the element, the surface, and the η -coordinates to global coordinates may be expressed as:

$$\begin{Bmatrix} Q_x \\ Q_y \\ Q_z \end{Bmatrix} = \begin{bmatrix} \bar{T} \end{bmatrix} \begin{Bmatrix} \bar{P}_x \\ \bar{P}_y \\ \bar{P}_z \end{Bmatrix} ; \quad \begin{Bmatrix} Q_x \\ Q_y \\ Q_z \end{Bmatrix} = \begin{bmatrix} T_\xi \end{bmatrix} \begin{Bmatrix} P_{\xi 1} \\ P_{\xi 2} \\ P_{\xi 3} \end{Bmatrix} ; \quad \begin{Bmatrix} Q_x \\ Q_y \\ Q_z \end{Bmatrix} = \begin{bmatrix} T_\eta \end{bmatrix} \begin{Bmatrix} P_{\eta 1} \\ P_{\eta 2} \\ P_{\eta 3} \end{Bmatrix} \quad (4.1)$$

or:

$$Q = \bar{T} \bar{P} \qquad Q = T_\xi P_\xi \qquad Q = T_\eta P_\eta \quad (4.2)$$

where Q , \bar{P} , P_ξ , P_η represent similar force quantities expressed in global coordinates, element coordinates, surface coordinates and η -coordinates respectively; and \bar{T} , T_ξ , T_η represent the usual direction cosines.

4.3 Transformation and Assemblage of Triangular Elements

The transformation from element coordinates to surface coordinates is obtained by equating the first two expressions of Eqn. 4.2:

$$P_\xi = T_\xi^T \bar{T} \bar{P} \equiv \bar{T}_\xi \bar{P} \quad (4.3)$$

The matrices $(\bar{T}, T_\xi, \bar{T}_\xi)$ define all the necessary transformations for force and displacement quantities, provided no constraints are placed on these quantities. However, in the stiffness matrix defined for each element, only two rotational degrees of freedom are considered at each node. Accordingly, only two rotational degrees of freedom at each nodal point were utilized in the base system describing the assembled structure. These two rotational degrees of freedom at each nodal point are referenced to the surface coordinates ξ_1 and ξ_2 . The third rotation quantity, about ξ_3 , was neglected because for a good mesh representation each triangle associated with a given node will lie close to the tangent plane of the node, and hence, the plate bending type rotation about ξ_3 should not

appreciably affect the stiffness of the complete assemblage. The transformation described below (Eqn. 4.4) for the two rotational quantities is identical to assigning a zero stiffness to the rotation about \bar{z} for each element, transforming the element stiffness considering three degrees of freedom for rotation at each node both for the element and the assemblage and subsequently setting to zero the rotation about the ξ_3 axis in the assembled stiffness matrix. It was assumed that this treatment of the rotation about ξ_3 would be negligible in the analysis, and results from numerous examples have verified this assumption. The moment transformation of the two rotational degrees of freedom which are considered for a typical node "i" is:

$$\begin{Bmatrix} M_{\xi 1} \\ M_{\xi 2} \end{Bmatrix} = \begin{bmatrix} T_c \end{bmatrix} \begin{Bmatrix} M_x \\ M_y \end{Bmatrix} \quad (4.4)$$

where T_c is the upper left 2×2 block of \bar{T}_ξ , Eqn. 4.3.

The transformation of the element stiffness to base coordinates for a typical element is accomplished by combining the membrane stiffness (Eqn. 3.29) and the plate stiffness (Sec. 3.6) so that the five degrees of freedom at each corner are grouped together in Eqn. 4.5. In the following description, the nodal point displacement system is as given in Fig. 2.2, except these quantities are rotated to coincide with the element coordinates, Fig. 2.1.

$$\begin{Bmatrix} \bar{\beta}_1 \\ \bar{\beta}_2 \\ \bar{\beta}_3 \end{Bmatrix} = \begin{bmatrix} \bar{K} \end{bmatrix} \begin{Bmatrix} \bar{v}_1 \\ \bar{v}_2 \\ \bar{v}_3 \end{Bmatrix} \quad (4.5)$$

where forces and displacements are (see Fig. 2.2):

$$\bar{\beta}_i = \begin{Bmatrix} M_{xi} \\ M_{yi} \\ P_{xi} \\ P_{yi} \\ P_{zi} \end{Bmatrix} \quad \text{and} \quad \bar{V}_i = \begin{Bmatrix} \theta_{xi} \\ \theta_{yi} \\ \bar{u}_i \\ \bar{v}_i \\ \bar{w}_i \end{Bmatrix} ; \quad \text{for } i = 1, 2, 3 \quad (4.6)$$

If global coordinates are used for the three linear displacements, then the appropriate transformation matrix is:

$$T \equiv \begin{bmatrix} T_c^{(1)} & & & & & \\ & \bar{T} & & & & \\ & & T_c^{(2)} & & & \\ & & & \bar{T} & & \\ & & & & T_c^{(3)} & \\ & & & & & \bar{T} \end{bmatrix} \quad (4.7)$$

where $T_c^{(1)}$, $T_c^{(2)}$, $T_c^{(3)}$ are transformations of the type of Eqn. 4.4 defined at points 1, 2, and 3 respectively. Then the transformed element stiffness, k , expressed in base coordinates is given by:

$$k = T \bar{k} T^T \quad (4.8)$$

where \bar{k} represents the element stiffness expressed in its element coordinates, Eqn. 4.5. It is to be emphasized that the base coordinates defined here are global coordinates for the translational degrees of freedom, and that only two rotational degrees of freedom are included (rotation about the normal being neglected).

In the finite element analysis of any shell, the stiffness of each element in the idealization is transformed to the common base coordinate system as shown in Eqn. 4.8. The contribution of each element may then be added directly into the (base coordinate) stiffness matrix K of the complete structure as indicated in Fig. 4.1.

4.4 Transformation and Assemblage of Quadrilateral Elements

A typical non-planar quadrilateral representing a shell with negative Gaussian curvature is shown in Figs. 4.2 and 4.3. The non-planar property of the quadrilateral element for the discretization of doubly curved shells is accentuated in this particular case by the negative curvature and the orientation of element. For other orientations or in the case of positive curvature, the non-planar effect occurs to a lesser extent. However, with the exception of a limited class of geometries, this element is non-planar and must be treated accordingly.

Since this element may be viewed as a sub-structure formed from four individual triangles, the treatment of the four exterior nodes (1, 2, 3, 4) and the central interior node (5) is as described in Sec. 4.3. However, the interior mid-side nodes require special treatment, since only two degrees of freedom (membrane) are utilized in evaluating the stiffness properties of the four sub-triangles. Therefore, if the element is planar, only two degrees of freedom need be considered at nodes 6, 7, 8, 9. If, however, the four sub-triangles have a non-zero juncture angle, one has to consider three translational degrees of freedom at the interior mid-side nodes. A consistent approach for treating these nodes involves transforming the translational degrees of freedom to the η_1 - η_2 plane as shown in Fig. 4.2, and subsequently constraining the displacements in

the η_3 direction at the interior mid-side nodes to be the average of the central node and the corresponding exterior node, that is:

$$\begin{aligned}
 \delta_{\eta 36} &= \delta_{\eta 31} + \delta_{\eta 35} \\
 \delta_{\eta 37} &= \delta_{\eta 32} + \delta_{\eta 35} \\
 \delta_{\eta 38} &= \delta_{\eta 33} + \delta_{\eta 35} \\
 \delta_{\eta 39} &= \delta_{\eta 34} + \delta_{\eta 35}
 \end{aligned} \tag{4.9}$$

It should be noted that this type of constraint preserves the rigid body translation modes of the assembled quadrilateral stiffness. This procedure is illustrated by considering sub-element 1 (Figs. 4.2 and 4.3) in which the membrane and bending stiffnesses are again uncoupled in element coordinates. In order to transform this element stiffness, the membrane and plate stiffnesses are combined and arranged as follows:

$$\begin{Bmatrix} \bar{\beta}_1 \\ \bar{\beta}_2 \\ \bar{\beta}_5 \\ \bar{\beta}_7 \\ \bar{\beta}_6 \end{Bmatrix} = [\bar{k}] \begin{Bmatrix} \bar{v}_1 \\ \bar{v}_2 \\ \bar{v}_5 \\ \bar{v}_7 \\ \bar{v}_6 \end{Bmatrix} \tag{4.10}$$

where β_i and \bar{v}_i , $i = 1, 2, 5$ are of the type given by Eqn. 4.6 while β_i and \bar{v}_i , $i = 6, 7$ are given by:

$$\bar{\beta}_i = \begin{Bmatrix} P_{\bar{x}i} \\ P_{\bar{y}i} \\ 0 \end{Bmatrix} \quad \text{and} \quad \bar{v}_i = \begin{Bmatrix} \bar{u}_i \\ \bar{v}_i \\ \bar{w}_i \end{Bmatrix}; \quad \text{for } i = 6, 7 \tag{4.11}$$

A zero has been added to the last element of $\bar{\beta}_i$ in Eqn. 4.11 and a transverse displacement component, W_i has been added to \bar{V}_i to permit the two in-plane displacements at the mid-side nodes to transform into three displacement degrees of freedom. It should be emphasized again that the transversal component W_i in Eqn. 4.11 is associated with the bending element; thus the rows and columns of \bar{k} (Eqn. 4.10), corresponding to W_6 and W_7 , consist of zeroes since no bending type stiffness has been defined at the mid-side nodes.

In order to constrain the displacements $\delta_{\eta 3i}$ ($i = 6, 7, 8, 9$) in Eqn. 4.9 all displacement components in Eqn. 4.10 are transformed from element coordinates to the η -coordinates. This transformation using the first and last expressions of Eqn. 4.2 is:

$$P_{\eta} = T_{\eta}^T \bar{T} \bar{P} = \bar{T}_{\eta} \bar{P} \quad (4.12)$$

where it is understood that \bar{T} refers to the element being considered, i.e., sub-triangle 1. While performing this transformation, it is necessary to also transform the rotational degrees of freedom to the base coordinates, which are the surface coordinates for exterior corners (1, 2, 3, 4) and the η -coordinates for the mid-point 5. Thus the transformation of the translational components to the η -coordinates and the rotational components to base coordinates for sub-element 1 is written symbolically as:

$$k_{\eta}^{(1)} = T_Q^{(1)} k^{(1)} T_Q^{(1)T} \quad (4.13)$$

where:

and

$$\mathbf{r}_{\eta i} = \begin{Bmatrix} \delta_{\eta 1i} \\ \delta_{\eta 2i} \\ \delta_{\eta 3i} \end{Bmatrix} ; \quad \text{for } i = 6, 7, 8, 9 \quad (4.18)$$

and \mathbf{R}_{η} are the corresponding forces and moments. The constraints of expression 4.9 are now imposed on Eqn. 4.15 by adding:

- 1) one-half of col. 28 to cols. 5 and 25
- 2) one-half of col. 31 to cols. 10 and 25
- 3) one-half of col. 34 to cols. 15 and 25
- 4) one-half of col. 37 to cols. 20 and 25

and subsequently by adding:

- 1) one-half of row 28 to rows 5 and 25
- 2) one-half of row 31 to rows 10 and 25
- 3) one-half of row 34 to rows 15 and 25
- 4) one-half of row 37 to rows 20 and 25

This procedure annuls equations 28, 31, 34, 37 in Eqn. 4.15 and the modified stiffness is:

$$\bar{\mathbf{R}}_Q = \bar{\mathbf{K}}_Q \bar{\mathbf{r}}_Q \quad (4.21)$$

where:

$$\bar{\mathbf{r}}_Q = \{r_{\eta 1} \ r_{\eta 2} \ r_{\eta 3} \ r_{\eta 4} \ r_{\eta 5} \ \bar{r}_{\eta 6} \ \bar{r}_{\eta 7} \ \bar{r}_{\eta 8} \ \bar{r}_{\eta 9}\} \quad (4.22)$$

where $r_{\eta i} = (i = 1, 2, 3, 4, 5)$ are given by Eqn. 4.17 and

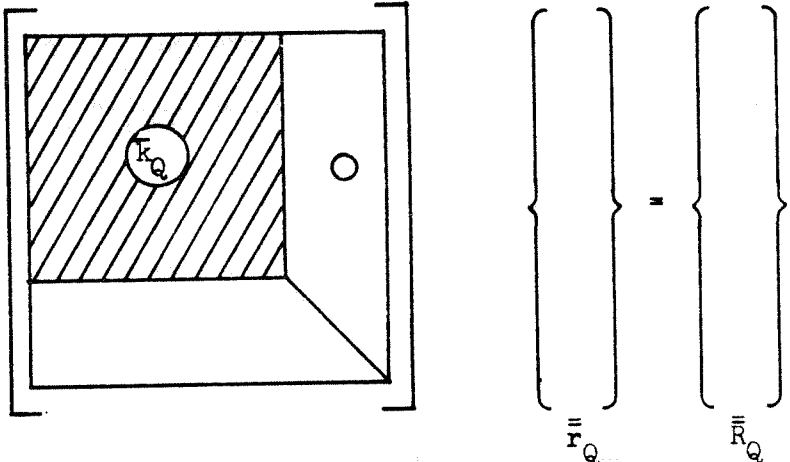
$$\bar{r}_{\eta i} = \begin{Bmatrix} \delta_{\eta 1i} \\ \delta_{\eta 2i} \end{Bmatrix} \quad \text{for } i = 6, 7, 8, 9 \quad (4.23)$$

4.5 Condensation of the Internal Degrees of Freedom of the Quadrilateral

Since the connectivity of the internal degrees of freedom are local to each quadrilateral element, they may be eliminated by superposition at the element stiffness level, and thus they do not appear in the equilibrium equations of the complete assemblage. This procedure is easily illustrated by partitioning Eqn. 4.21 as follows:

$$\bar{K}_Q = \bar{r}_Q = \bar{R}_Q \quad (4.24)$$

where the shaded area represents the coefficients of the internal degrees of freedom which are contained in the element equilibrium equations of the external nodes. To uncouple the influence of the internal degrees of freedom on the equilibrium equations of the external nodes it is necessary to reduce the coefficients in the shaded area to zero. This is conveniently done by inverse Gaussian elimination which gives the following equation:



$$\left[\begin{array}{c} \text{shaded quadrilateral} \\ \text{node } K_Q \end{array} \right] = \left[\begin{array}{c} \text{matrix} \\ \text{matrix} \end{array} \right] \quad (4.25)$$

in which the condensed quadrilateral stiffness which is used to assemble the equilibrium equations is the shaded upper left 20x20 block of Eqn. 4.25, i.e.,

$$\bar{K}_Q \bar{r}_Q = \bar{R}_Q \quad (4.26)$$

where:

$$\bar{r}_Q = (r_{n1} \ r_{n2} \ r_{n3} \ r_{n4})^T \quad (4.27)$$

where:

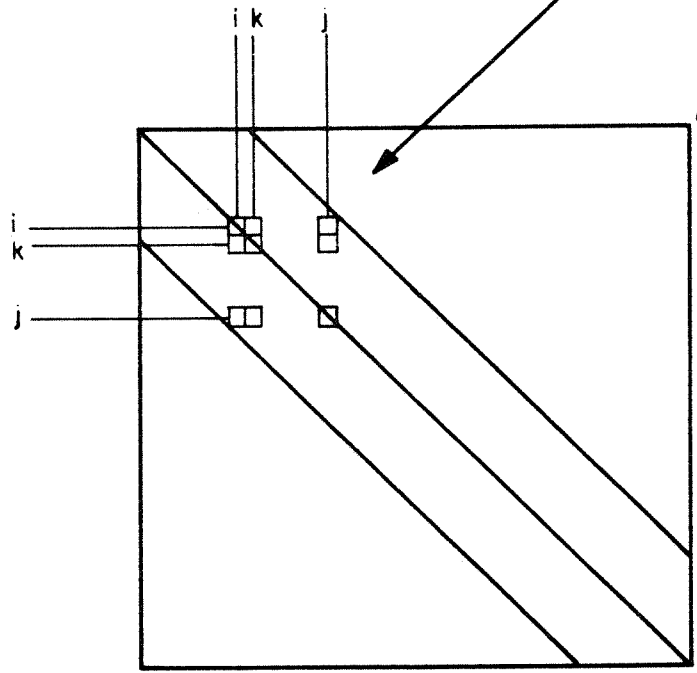
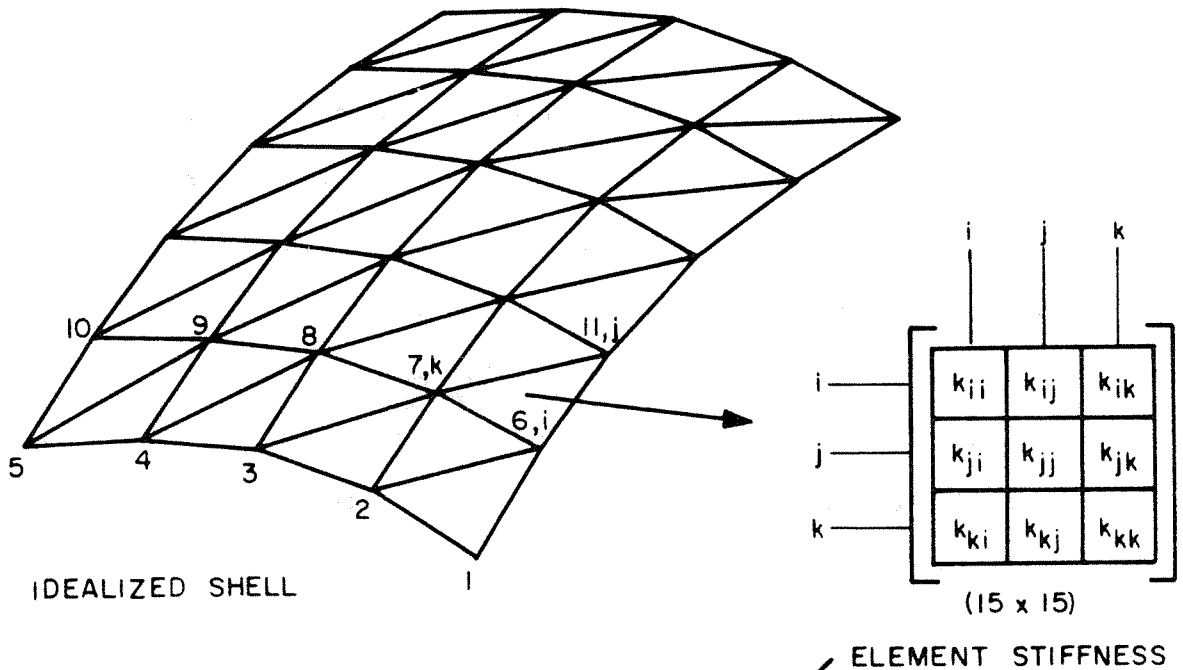
$$r_{ni} = \begin{Bmatrix} \theta_{\xi 1i} \\ \theta_{\xi 2i} \\ d_{\eta 1i} \\ d_{\eta 2i} \\ d_{\eta 3i} \end{Bmatrix} ; \quad \text{for } i = 1, 2, 3, 4 \quad (4.28)$$

It should be noted that in performing the above condensation the nodal forces and moments were taken as zero at all interior nodes, so the load vector \bar{R}_Q in Eqn. 4.25 remains unaltered during the condensation.

Since the translational degrees of freedom in Eqn. 4.26 for each element are referenced to the η -coordinates, they have to be transformed to the base coordinates before the element stiffness can be superposed into the complete assemblage. If global coordinates are used as base coordinates, the translational degrees of freedom in Eqn. 4.26 are transformed by T_η , Eqn. 4.2, or if surface coordinates are used, expressions of the form $P_\xi = T_\xi^T T_\eta P_\eta = T_{\xi\eta} P_\eta$ must be utilized. Performing this transformation, the quadrilateral stiffness in base coordinates is expressed as:

$$k_{QQ} r_Q = R_Q \quad (4.29)$$

which is the desired form for the assemblage.



CONTRIBUTION OF ONE ELEMENT TO TOTAL STIFFNESS

FIG. 4.1 DIRECT STIFFNESS FORMULATION OF THE STRUCTURE STIFFNESS MATRIX.

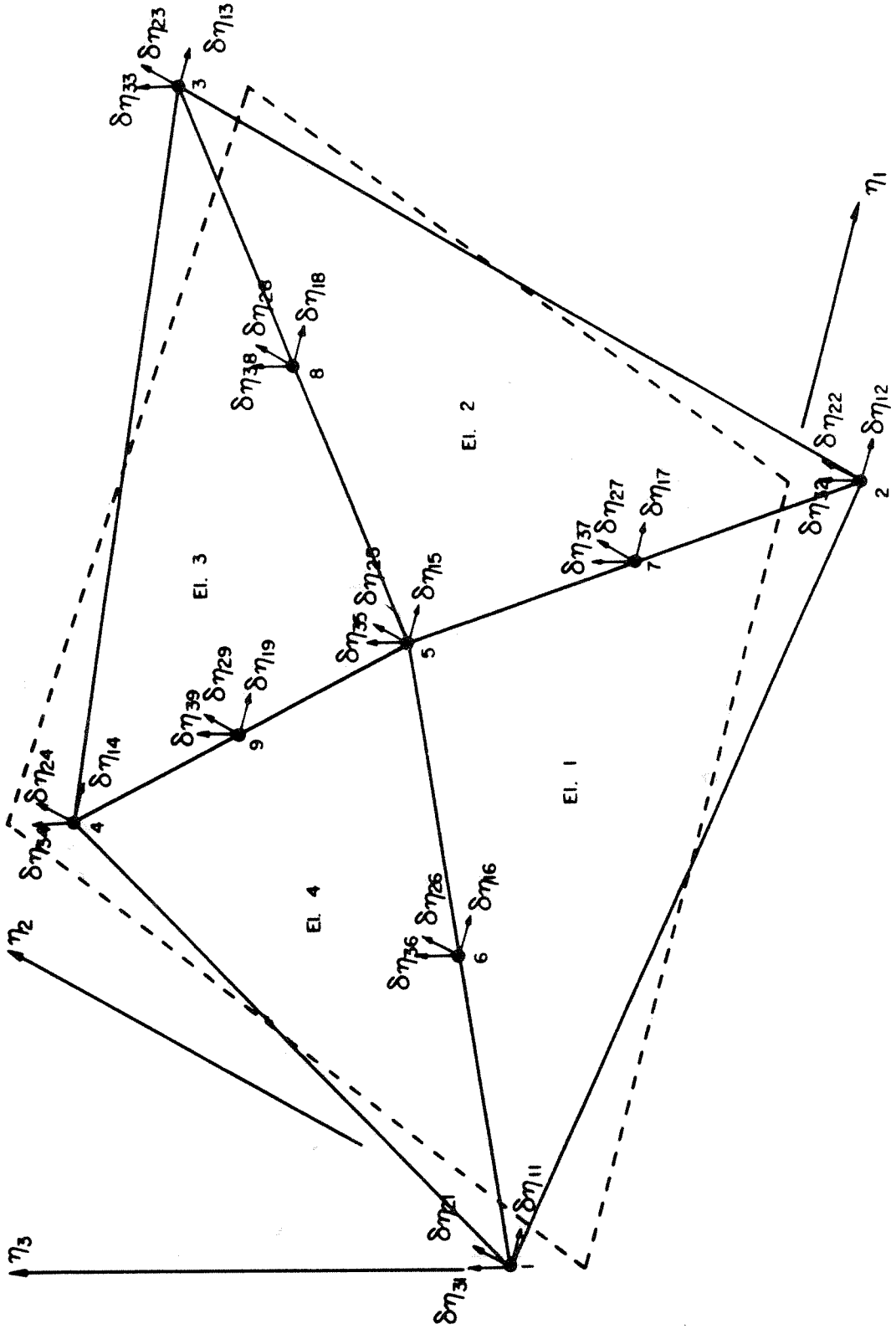


FIG. 4.2 TRANSLATIONAL DEGREES OF FREEDOM FOR QUADRILATERAL

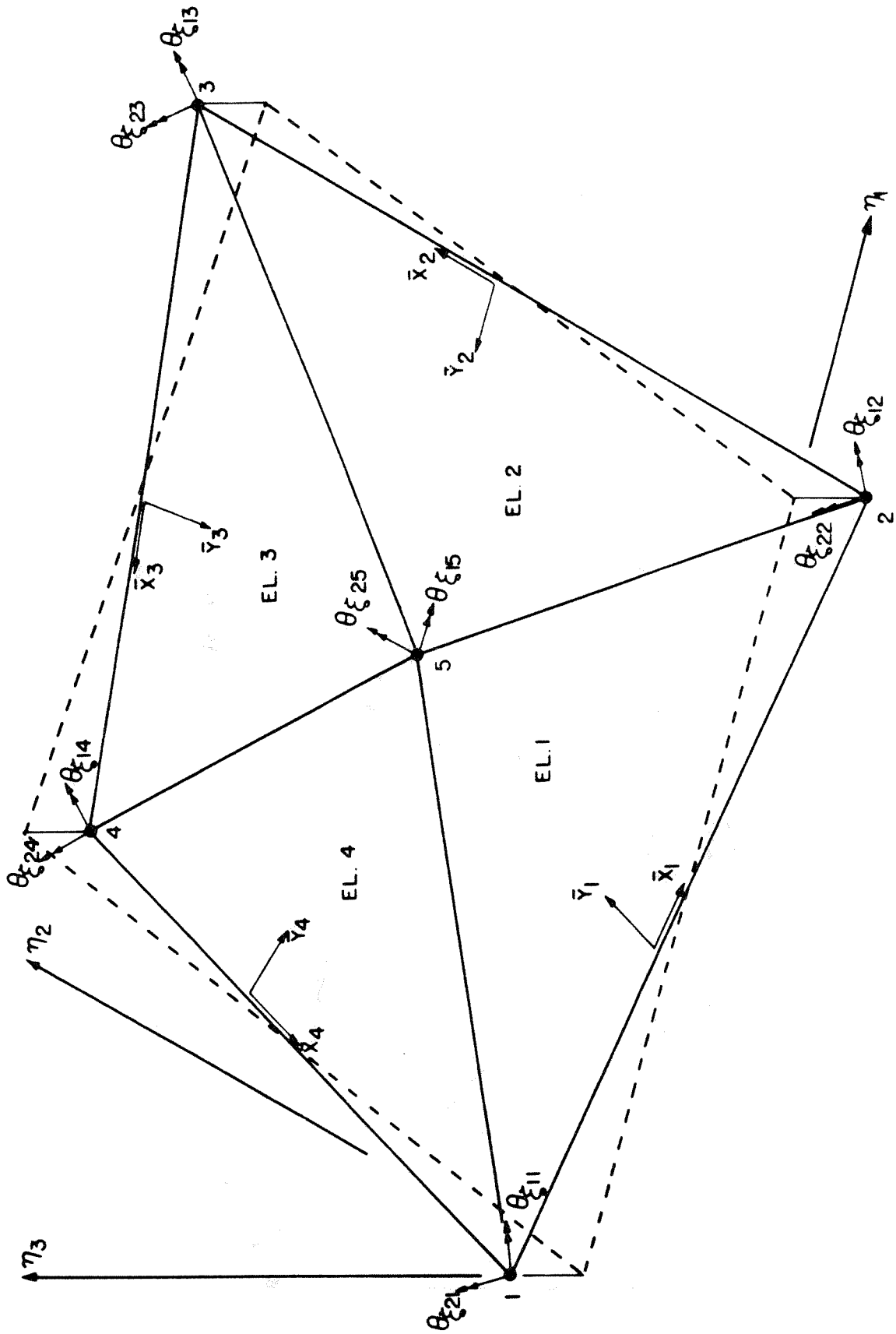


FIG. 4.3 ROTATIONAL DEGREES OF FREEDOM FOR QUADRILATERAL

CHAPTER 5. SOLUTION OF THE EQUILIBRIUM EQUATIONS

The stiffness matrix K of the complete assemblage relates the nodal loads R acting on the shell to the corresponding nodal displacements r :

$$Kr = R \quad (5.1)$$

The nodal point displacements r and forces R in Eqn. 5.1 are arbitrary since this equation was obtained by superposition of all the elements in the idealization. Therefore, Eqn. 5.1 must be modified to account for actual displacement and force boundary conditions. Each nodal point of the idealization has five degrees of freedom, and the forces and displacements corresponding to these may be applied in arbitrary combinations at each nodal point. Displacement boundary conditions are easily accounted for by striking out the rows and columns of the degrees of freedom associated with the boundary constraints and by replacing the corresponding diagonal terms with a non-zero value. Of course, if the specified displacement is non-zero, K must be post multiplied by this value and the resulting vector must be subtracted from R before applying the above procedure. It should be emphasized again that three translational degrees of freedom may be specified at each nodal point while only two rotational degrees of freedom, which are contained in the tangent plane at each node, may be specified.

Correspondingly, five force components may be specified at each node-- three linear forces and two moments. These values also may be applied arbitrarily at each node, and this is accomplished by simply adding their contribution into R of Eqn. 5.1. In general, distributed loads may be accounted for by determining the nodal point forces and moments

from consistent load procedures through the use of the assumed displacement functions for each element (see Section 5.3); or alternately, they may include only linear force components computed from simple tributary area considerations. In general, if no geometric discretization error exists, the consistent load procedure will yield superior results for relatively coarse meshes, while the improvement given by the consistent load procedure will diminish rapidly with decreasing mesh size. Due to the geometric idealization in the present analysis, the use of linear forces only based on tributary area considerations has proved to be generally the most desirable means of representing distributed loads.

5.1 Direct Solution of the Equilibrium Equations

The stiffness matrix K , in which the displacement boundary conditions are accounted for, may be characterized in general as:

- 1) symmetric
 - 2) banded
 - 3) positive definite
 - 4) sparsely populated
- (5.2)

Algorithms which utilize either iterative methods [16] or direct methods [17] for the solution of equations with these properties are well known. Earlier applications of the finite element procedure were based predominately on iterative methods in which property 4 was utilized so that the solution could be obtained while working entirely in the high speed core memory. In the more recent years, however, direct solutions based on Gaussian elimination (or special forms of it such as triangular decomposition) have become the preferred solution procedure due to their overall economy.

and ease of applicability. A direct method (triangular decomposition) was used to obtain the results presented herein; therefore, a brief discussion of this method and of the above properties related to it is pertinent.

The fundamental concept of the Gaussian elimination procedure is to perform operations on K to reduce it to triangular form, after which the unknown displacements are found by back substitution procedures. The three most widely used forms of this procedure result in reducing Eqn. 5.1 to the following forms:

$$Ur = \bar{R} \quad (5.3)$$

$$LDL^T r = R \quad (5.4)$$

$$\bar{L}\bar{L}^T r = R \quad (5.5)$$

where U is an upper triangular matrix and while L and \bar{L} are lower triangular matrices and D is a diagonal matrix. To obtain Eqn. 5.3 the coefficients below the diagonal in the i th column are reduced to zero by adding appropriate combinations of the i th row. This procedure begins with column 1 and is continued until the triangular form is achieved. It should be noted that while performing these operations on K that the corresponding operations have to be performed on the load vector R , and the modified load vector \bar{R} in Eqn. 5.3 is used for the back substitution. The procedures used to obtain Expressions 5.4 and 5.5 are referred to as triangular decomposition in which the matrix K is split into upper and lower triangular matrices without performing operations on the vector R , and these two forms are the most widely

used in practical computer algorithms. This is due primarily to two reasons. First, in the decomposed form, Eqns. 5.4 and 5.5 may be used to solve for as many arbitrary load vectors as desired by simply repeating the back substitution. Second, this is the most desirable form for improving the solution, if necessary, because of inaccuracies caused by rounding errors in the solution (see Fox, Ref. [18]). Examination of the computational effort required to perform the solution of large systems of equations by either of the procedures given in Eqns. 5.3, 5.4, and 5.5 has shown that all three procedures involve essentially the same amount of additions, multiplications, etc., while Eqn. 5.5 requires one square root operation for each equation. Although the procedure used in this analysis is that of Eqn. 5.5, usually referred to as Cholesky's method, the special properties in Expression 5.2, which are discussed below, apply equally well to all three procedures.

The first three properties are very significant as related to the direct solution of large systems of equations. Symmetry permits a reduction of approximately one half in the number of calculations, and also reduces the amount of storage required since symmetry is preserved in the solution. The banding property permits one to consider only the coefficients contained within the band width since it is also preserved during the solution. The positive definite property insures stability of the solution [19]; hence, the solution may be obtained without pivoting. These properties thus enable one to obtain a direct solution by keeping only a small portion of the stiffness matrix in high speed memory at any time, while sequentially retrieving and storing additional information by means of relatively slow input-output devices such as tapes and disks.

The portion of the stiffness matrix required to be in core at any time during the solution determines how large the band width can be. The minimum storage required is $m(m + 1)/2$ where "m" is the half band width, and this requires retrieving and storing information in blocks of "m" numbers. For a 32K core, the maximum half band width permitted by practical programs is approximately 180. If larger blocks of information are to be used for input-output, then the band width must be reduced.

A typical mesh (8x12) of triangular elements suitable for analysis of a cylindrical shell, for example, and a schematic diagram of the assembled stiffness matrix are shown in Fig. 5.1. Since each node has five degrees of freedom, the total number of unknowns, n, is 585. The half band width, m, is 50. To obtain the half band width the entire array of elements is scanned and the maximum difference between the numbers of any two nodes associated with a particular triangle is recorded. The half band width is then given by one plus this number multiplied by five.

For comparison purposes, a corresponding mesh (8x12) of quadrilateral elements is shown in Fig. 5.2. As has been mentioned previously, the interior nodal point degrees of freedom of the quadrilateral element do not appear in the equilibrium equations; therefore, the total number of equations for both mesh representations are the same for this case. The half band width, however, given by the mesh of quadrilaterals is 55 compared with 50 for the mesh of triangular elements.

The shaded zones in the stiffness matrices (Figs. 5.1 and 5.2) indicate the maximum horizontal spread of the non-zero coefficients. It is interesting to note that if this mesh were subdivided to 16x24 subdivisions, each shaded area would retain the same width while the half band widths would be increased to 90 and 95 respectively. Unfortunately,

this type of sparseness does not permit a reduction in computational effort. This property is, however, very useful in assembling K and is described in Section 5.2. The number of multiplications required to decompose the structure stiffness matrix is approximately $nm^2/2$. The number of additions are also approximately $nm^2/2$.

Typical times, in seconds, required for the decomposition (including the time required for transfer of information to and from core) and the back substitution for problems which have been run on the IBM 7094 are:

<u>Mesh</u>	<u>M</u>	<u>N</u>	<u>Decomposition</u>	<u>Back Substitution</u>
4x5	30	150	5	3
8x12	50	585	37	18
12x18	70	1235	159	44
16x22	90	1955	340	77
(irregular)	100	2180	430	93

The algorithm used to solve these equations is written in FORTRAN IV, using disk storage for the back substitutions. Of practical importance is the asymptotic time for the decomposition as measured per multiplication (i.e., $m^2n/2$). This value is approximately 40×10^{-6} and compares favorably with the corresponding value of 30×10^{-6} as reported in Ref. [17] for the time required to perform the corresponding operation utilizing MAP as the programming language. The efficient decomposition times for the subject program are attributed to the use of the discrete block structure described in the following section. The discrete block structure permitted the innermost do-loop of the algorithm to be free of integer arithmetic, which is usually required, for example, if a one dimensional array is used to store K , and in addition transfer of information in large blocks proved to be very efficient.

5.2 Practical Aspects of Computer Algorithms for the Finite Element Procedure

The general computer application of the finite element procedure may be subdivided as follows:

- 1) Computation of element stiffness
- 2) Formation of the stiffness matrix of the complete assemblage
- 3) Solution of the equilibrium equations
- 4) Computation of element stresses and moments

As stated earlier, the efficient use of a direct solution procedure for large systems of equations is made possible by storing only part of the stiffness matrix K in high speed core at any given stage during the solution. This causes certain problems which couple steps 1, 2, 3 and which deserve special attention in the computer program. To illustrate this, the subject computer algorithm for solving the equilibrium equations is considered. This algorithm was constructed so that data to and from the external storage devices would be transferred in large blocks of information. To this end, blocks 1 and 2 in Fig. 5.3 reside in core simultaneously and this requires a maximum space of m^2 numbers. The procedure then consists of first decomposing blocks 1 and 2, after which block 1 is output on tape. Block 2 remains in core since it is required in decomposing block 3. After block 3 has been input and decomposed, block 2 is output on tape, while block 3 remains in core. Block 4 is input and the above procedure is continued until all blocks have been treated.

The coupling between the above steps 1, 2, 3, is illustrated in Fig. 5.3, by considering the contribution of a typical element on K .

As shown, this element contributes to blocks 1 and 2 and also to blocks 3 and 4. The significance of this is that in assembling the individual blocks all the contributions of a given element stiffness cannot be accounted for at the same time; and therefore, its remaining contributions must be stored, otherwise the element stiffness will have to be computed again. Neither alternative is desirable since the remaining contributions must be stored in a way so as to have the capability of random access, while recomputing element stiffnesses requires excessive computer times which may be avoided. This problem has previously been overcome by dimensioning an array of $2m^2$ numbers, by permitting a certain number of element stiffnesses to reside in core while forming the individual blocks; and by the use of random access disk files. The present computer program accounts for this problem by taking advantage of the sparseness property of K in that only the non-zero elements are stored while forming the individual blocks. This procedure does not decrease the maximum permissible band width, and all the contributions of a given element may be accounted for at the same time.

The execution of step 4 is not coupled with the first three steps since this requires only the nodal point displacements, the element geometry, material properties and the assumed displacement function which were used for the evaluation of the element stiffness properties.

5.3 Computation of Consistent Loading and Element Stresses and Moments

In the application of the finite element procedure, all forces acting on the shell must be expressed as nodal point forces in the equilibrium equations of the complete assemblage (Eqn. 5.1). As mentioned earlier in this chapter, distributed loadings may be treated by simple

tributary area considerations or they may be determined by consistent load procedures. In the latter procedure the nodal forces are determined by requiring the energy of these forces going through the corresponding nodal displacements to be equivalent to the energy of the distributed loads going through the displacements over the element which result from the nodal point displacements. By using the principle of virtual displacements, this is expressed for planar elements as:

$$R_i^T \delta r_i = \left[\int_A P(x,y) M(x,y) dA \right] \delta r_i \quad (5.6)$$

where:

- R_i is the consistent load vector,
- δr_i is the nodal point system of virtual displacements,
- $P(x,y)$ is the distributed loading,
- $M(x,y)$ are the displacement functions expressed in terms of the nodal point system of virtual displacements.

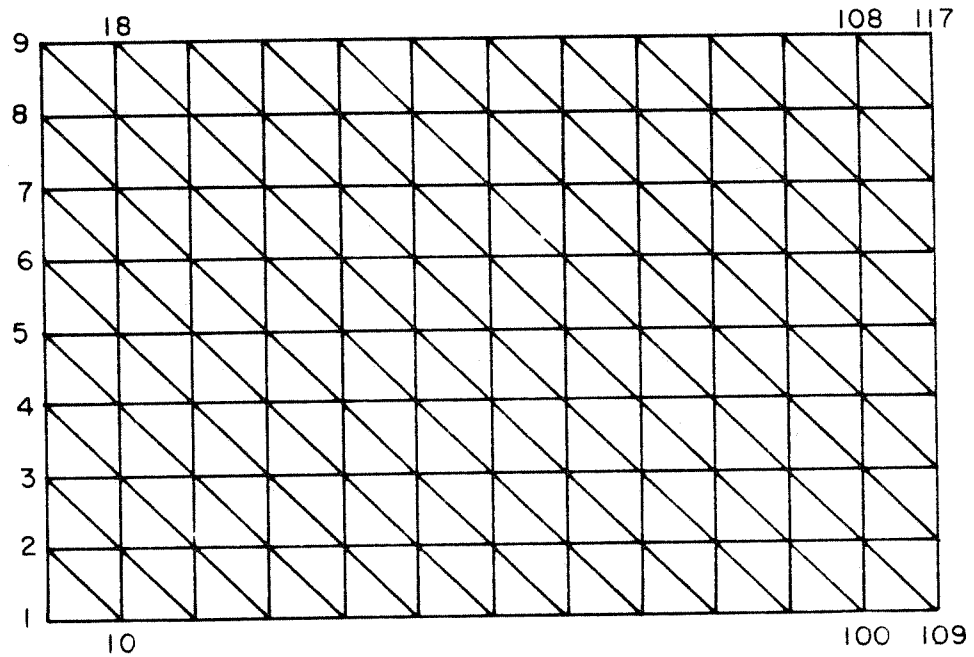
The nodal point system of virtual displacements in Eqn. 5.6 corresponds to the nodal point system of displacements used for the derivation of the element stiffness.

The evaluation of Eqn. 5.6 has been carried out for various plane stress/strain elements in Ref. [12] and has been described for the plate bending element in Ref. [9]. In the present program consistent nodal point loads have been used for the triangular elements only. In general, these element nodal point loads are linear forces resulting from the membrane displacements and the transverse displacements of the plate bending element and nodal point moments resulting from the rotational

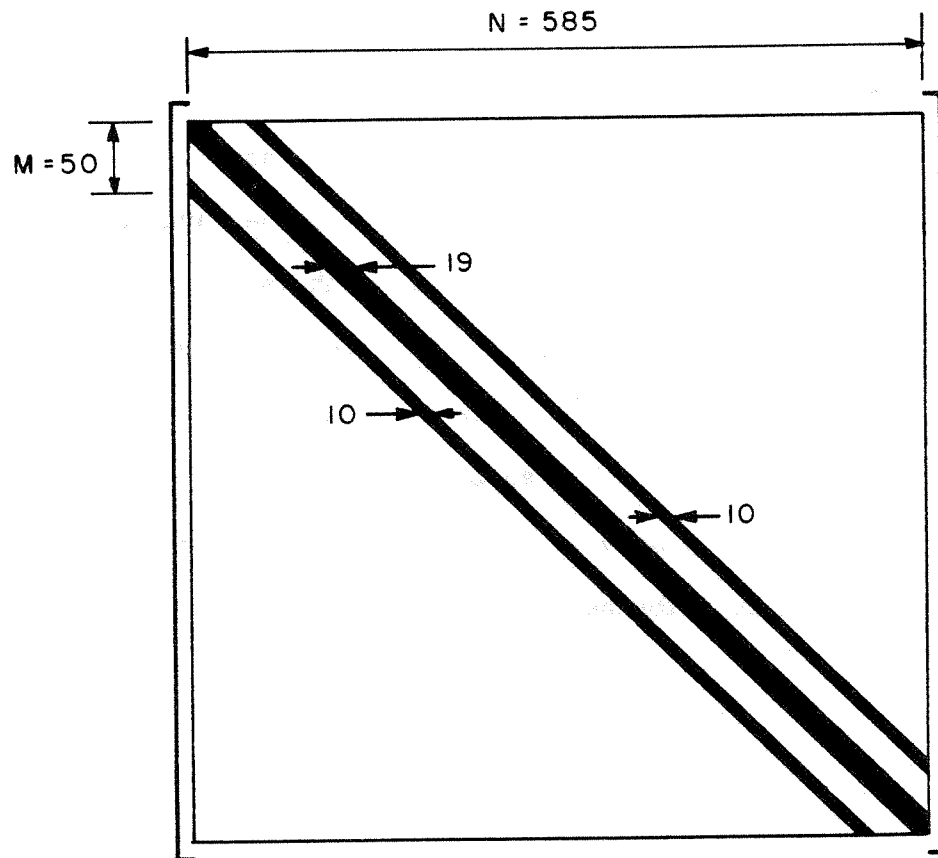
deformation of the plate element. The nodal point loads were first established in element coordinates and then transformed into the base coordinates. The inclusion of nodal point moments for the meshes described in Chapter 6 did not yield significant improvement in the results and in certain cases (for example, the dome supported on rollers, Fig. 6.2) the use of nodal point moments resulted in undesirable perturbations of the displacement patterns in the vicinity of the supported edge. However, the results from all the cases investigated by the use of nodal point loads determined from either consistent load procedures (by using only the linear forces) or tributary area considerations were satisfactory and, in general, only small differences in the results were observed. In all the analyses performed with the quadrilateral element the nodal point loads were linear forces only, which were determined by tributary area considerations and were applied only at the exterior nodes of the quadrilaterals (all the interior nodes were considered to have zero loads).

The solution of the equilibrium equations yields the displacement components of the nodal points of the finite element system. The element stresses and moments are then easily determined from the assumed displacement functions, and this is accomplished by transforming the nodal point displacements into element coordinates and then utilizing expressions of the form of Eqns. 3.26 and 3.32 for the membrane element strains and Eqn. 3.45 for the plate curvatures. Having obtained the element strains and curvatures, the element stresses and moments are obtained from Eqns. 3.7 and 3.20 respectively. It should be noted, however, that the displacement components of the interior points of the quadrilateral must first be recovered and this is accomplished by Eqn. 4.25.

The stress and moment quantities which are of interest in shell analysis are those shown in the lower part of Fig. 5.4. The computation of the element stresses and moments as described in the above paragraph result in these values being referenced to the element coordinates, \bar{x} , \bar{y} , (Fig. 5.4), and it is generally necessary to transform these quantities to a specified coordinate system for ease of interpretation and to obtain average values for nodal point stresses and moments. The procedure used herein is to transform the stresses and moments at each node of each triangle to the surface coordinates defined at these points. This is illustrated for point "i" of a typical triangle in Fig. 5.4 in which the element coordinate \bar{x} is projected onto the ξ_1 - ξ_2 plane defined at point "i." The angle ω is then determined and the element stresses and moments at point "i" are transformed (approximately) to the ξ_1 - ξ_2 plane by using this angle. Since the assumed displacement functions cannot insure local stress equilibrium across the element interfaces, it is desirable to use averaged values in determining nodal point stresses and moments. The adopted procedure in determining the nodal point values is to average the nodal point stresses and moments of all triangles intersecting a given point for the quadrilateral element. This procedure is also utilized for nodal point moments when using a mesh of triangles; however, in this case it is desirable when possible to use the procedure described in Section 2.4 for determining membrane stress components when plane stress bending modes are present.

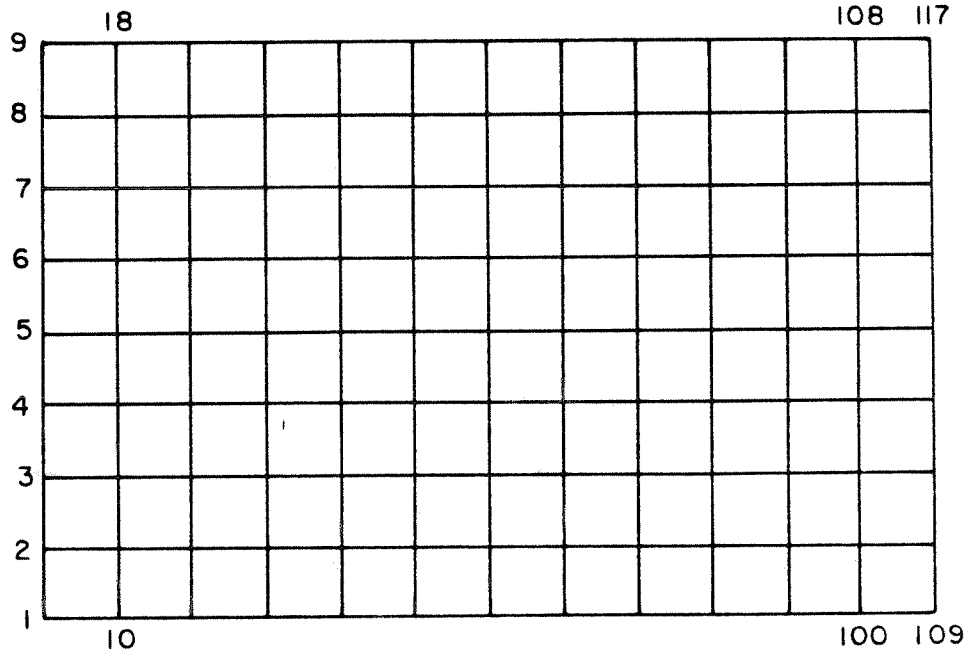


MESH OF TRIANGULAR ELEMENTS

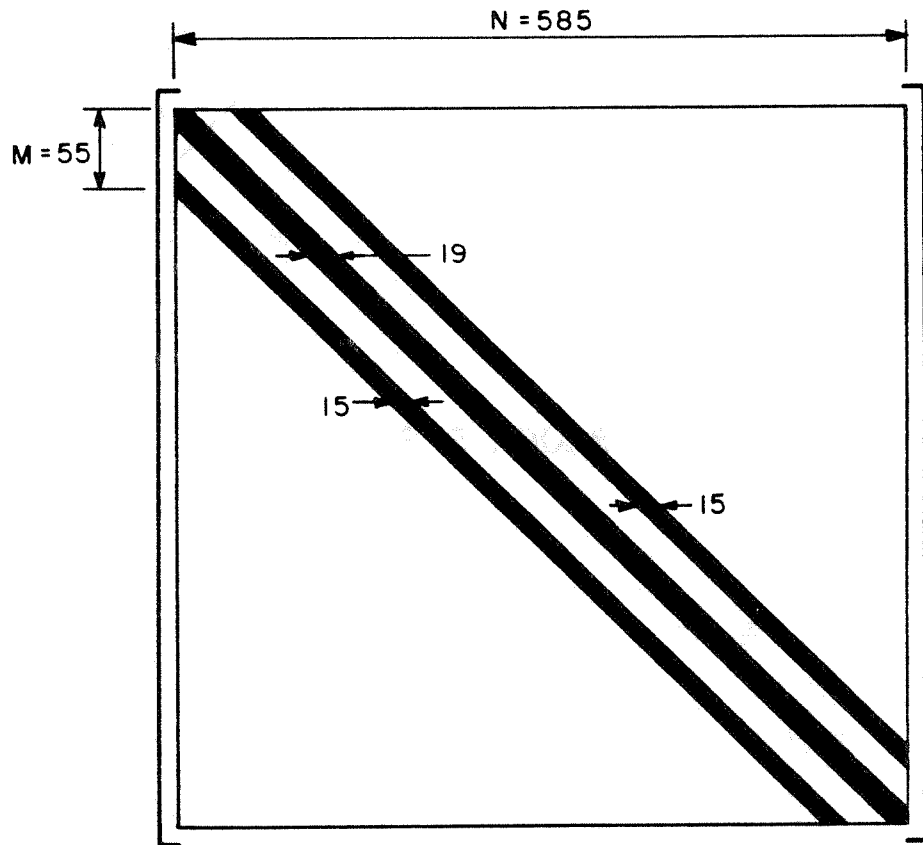


STIFFNESS OF COMPLETE ASSEMBLAGE

FIG. 5.1 TYPICAL SHELL DISCRETIZED WITH TRIANGULAR ELEMENTS



MESH OF QUADRILATERAL ELEMENTS



STIFFNESS OF COMPLETE ASSEMBLAGE

FIG. 5-2 TYPICAL SHELL DISCRETIZED WITH QUADRILATERAL ELEMENTS

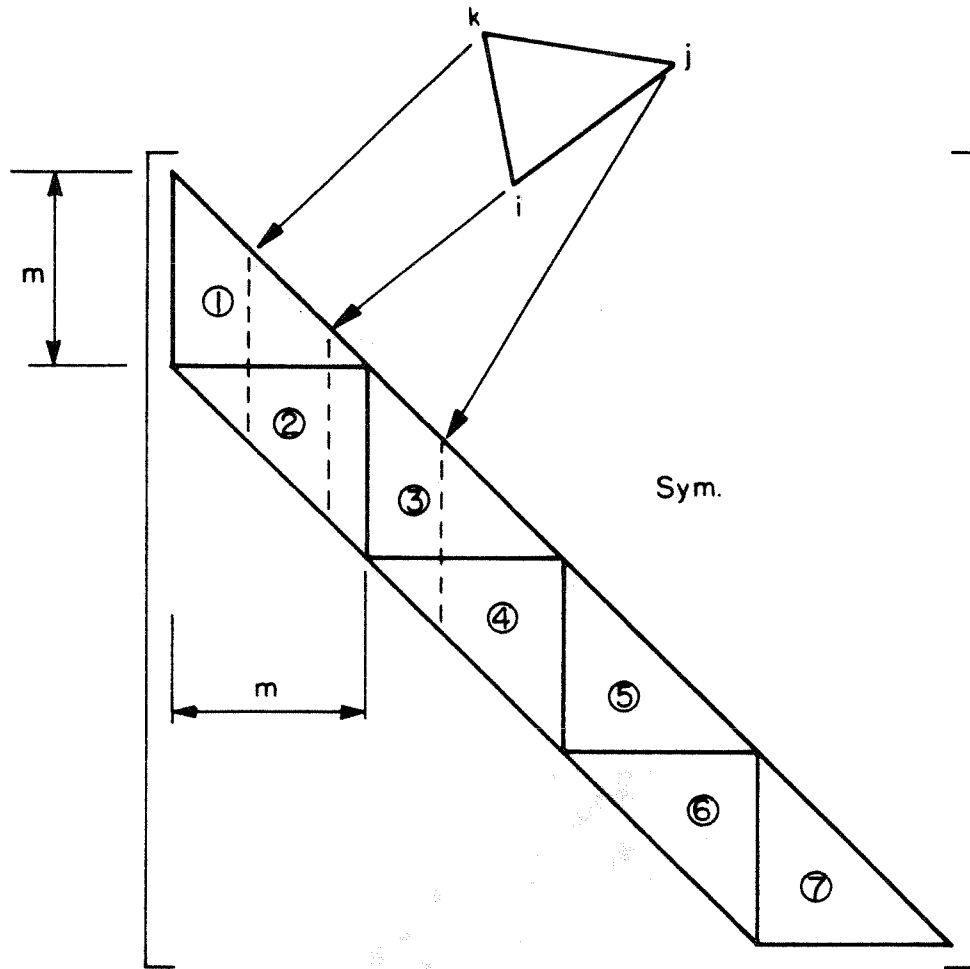
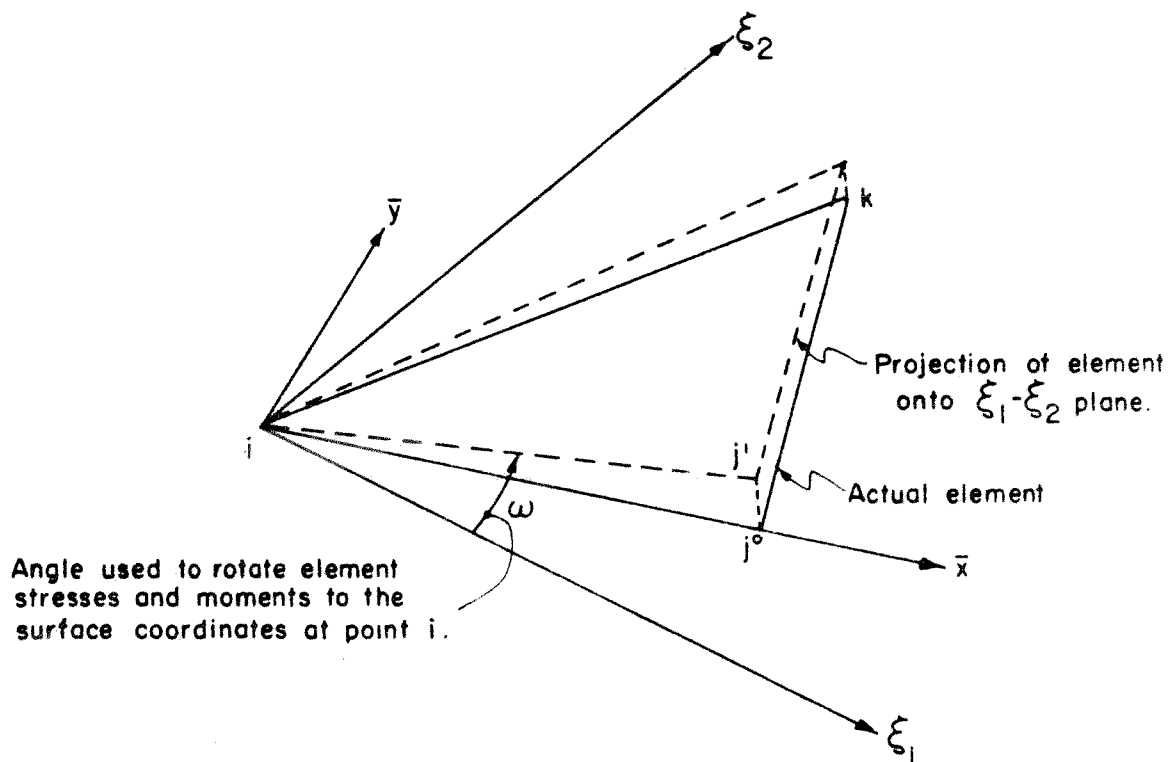


FIG. 5.3 BLOCK STRUCTURE USED FOR DECOMPOSING K .



TRANSFORMATION OF ELEMENT STRESSES AND MOMENTS TO SURFACE COORDINATES.

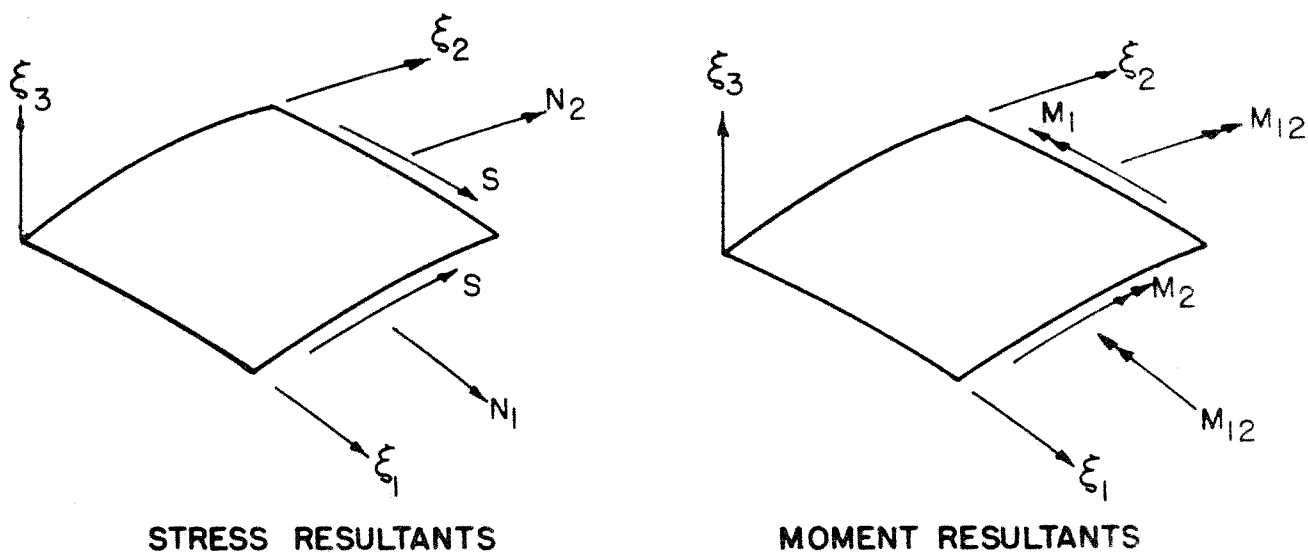


FIG. 5.4 SHELL STRESSES AND MOMENTS

CHAPTER 6. RESULTS OF ANALYSIS

The versatility and the accuracy which can be obtained by this finite element analysis of thin shells is demonstrated by comparing results from this particular analysis with results obtained by using the classical solution procedures (Examples 1, 2, 3, 4, 5, 6) and numerical solutions (Examples 7 and 8) of the equations based on shallow shell theory. The rate of convergence (i.e., improved accuracy with decreasing mesh size) is presented for several cases, since this property may be used to determine the adequacy of the element stiffnesses used in the analysis. Results given by both the quadrilateral and the triangle are compared to establish the relative convergence properties of these two elements. The geometric idealization is considered important in the analysis since it is necessary that the behavior of the idealized shell approach that of the actual shell with decreasing mesh size. Of additional importance is the evaluation of the approximation resulting from the use of the 5 degree of freedom nodal point displacement system.

Obviously all the approximations of the finite element idealization cannot be evaluated separately in a single analysis. It is possible, however, to select particular examples which accentuate one or more of these approximations, and thus a relative evaluation of the individual approximations made in the analysis is possible. Each of the eight examples presented hereafter serve the purpose of demonstrating the effect of one or more of the approximations of the finite element idealization.

The improved membrane stiffness properties of the quadrilateral over the triangle is evident when one considers the cantilever beam (Section 6.1). Because the predominant straining modes in this example are those of

bending (Figs. 2.6.c and 2.7.c), and since the difference in the stiffness properties of the constant strain triangle and the quadrilateral is reflected only in these modes, a direct comparison of these two types of elements is possible. It should be noted that the effects of the geometric idealization and the 5 degrees of freedom are eliminated in this example since the structure is planar.

The spherical dome (Section 6.2), subjected to a state of membrane stresses (Example 2) which are constant everywhere in the shell, is useful in determining the effect of the geometric idealization. This is possible since there is no error resulting from the discretized displacement field since both membrane elements used are able to represent the constant stress state exactly. Moreover, due to the axisymmetric condition the error resulting from the use of the 5 degrees of freedom is annulled because the rotation about the normal is zero in the actual shell. The spherical dome with clamped boundaries (Example 3) is useful in determining the accuracy with which hoop stresses and bending moments with steep gradients may be predicted. Of particular interest in this case is the comparison of the bending moments since the classical solution for this example represents the most accurate bending theory available [20].

The circular cylinders of Section 6.3 (Example 4) are useful in establishing the overall convergence properties of the finite element solution. In this example, it is not possible to isolate the effects of the discretized geometry and the 5 degrees of freedom; however, a direct evaluation of the improved stiffness properties of the quadrilateral element over the triangular element is possible since identical geometric idealizations are obtained with both element types in which the effect of

the 5 degrees of freedom is essentially the same. The results of this analysis are instructive in that the slow convergence given by the constant stress triangular element is offset by the use of the quadrilateral element (due primarily to the improved representation of bending deformation modes). Because these results, with decreasing mesh size, compare favorably with the classical solution, the combined effects of the geometric idealization and the 5 degrees of freedom are seen to result in negligible errors. The purpose of Example 5, a typical interior circular cylinder, is to illustrate that although bending deformation modes are present (see Fig. 6.13), the convergence properties of the constant stress triangle are adequate. This is attributed to the fact that the effect of the gradient of these modes is less severe than those of Example 4 (i.e., for $R = 25'$ and $12.5'$).

The results from the above examples indicate that the combined errors of the geometric idealization and the 5 degrees of freedom disappear with decreasing mesh size. It is of interest to separate these effects, and this can be done by considering the folded plate of Example 6. In this example, no geometric idealization error is present so the discrepancies in the solutions with decreasing mesh size are due to the discretized displacement field and the five degrees of freedom. As expected, the use of the constant stress element results in slow convergence (see Figs. 6.15, 6.16, 6.17) since the individual plates are subjected to bending deformation modes, while the convergence of the quadrilateral is adequate (Figs. 6.15, 6.16, and 6.17). This example shows that the 5 degree of freedom system performed well for a case with large juncture angles between individual elements.

The translational shells of Example 7 point out that slight changes in the longitudinal profile (see Fig. 6.18) cause appreciable changes in the distribution of stress and in the deformation of the three cases of positive, negative, and zero Gaussian curvature. The results of this example indicate that the finite element idealization is adequate in treating problems whose behavior is sensitive to slight changes in the geometry. The conoid of Example 8 represents a structure subjected to a complex state of stress and moment in which the convergence of the triangle and the quadrilateral is about the same.

6.1 Cantilever Beam (Example 1)

This beam is loaded at the free end with vertical shear forces distributed parabolically over the depth resulting in a total vertical force of 40 kips. The geometry, material properties, and the finite element idealizations are shown in Fig. 6.1. The results for the meshes of constant strain triangles and the linear strain triangles were taken from Ref. [12], and the results for the mesh of quadrilaterals were obtained by the subject program.

The tip deflection and the longitudinal stress (σ_x at $x = 12''$, $y = 6''$) are given in Table 2 for the meshes considered. Also shown in Table 2 are the half band width, m , the total number of degrees of freedom, n , and the relative computational effort based on the number of multiplications required to decompose K for each mesh. The two meshes of constant stress triangles (4 and 8 subdivisions over the depth) yield values for the tip deflections which are approximately 15% and 4% in error. The two meshes of quadrilaterals (2 and 4 subdivisions over the depth) give corresponding errors of approximately 6.5% and 1.5%, while the results of the meshes of

linear strain triangles (2 and 4 subdivisions over the depth) are almost exact as related to the tolerances of the errors specified for the other two element types.

The remarkable accuracy given by the linear strain triangle is attributed to the fact that it is able to represent exactly the deformation modes resulting from pure bending while these modes may only be approximated by the quadrilateral because all of its exterior boundaries are constrained to deform linearly. The convergence of the quadrilateral element appears adequate, however, and this element requires much less computational effort in decomposing K than the linear strain triangle for a given number of subdivisions; for example, a mesh of quadrilaterals (8×32) would require about one-third of the computational effort required for mesh C2, Table 2, due to the presence of the mid-side nodes of the linear strain triangle.

6.2 Spherical Dome (Examples 2 and 3)

The second case considered is the spherical dome subjected to an external pressure loading shown in Fig. 6.2. Because of its axial symmetry, it was possible to treat a single segment of the shell in the finite element idealization. Two mesh layouts were considered in which a 30° segment was utilized and the element nodes were located on parallel arcs at meridional angle intervals of 5° and 2.5° respectively. The coarse mesh resulting from the use of 5° intervals is shown in Fig. 6.2.

Two cases were considered for this shell. Example 2 was supported on rollers at the boundary so as to maintain a membrane state of stress, while Example 3 was clamped at the edge. Results for the normal displacement and the hoop stress for Example 2 are shown in Fig. 6.3. These results were obtained by using the coarse mesh (Fig. 6.2). Results were obtained

for this case also by using the fine mesh consisting of 14 arcs over the full 35 degree meridional angle; and the resulting displacement, W , was correct to three significant figures at all nodes, and stresses were well within one per cent of the theoretical values. The meridional moment and hoop stresses determined for the clamped case (Example 3) are shown in Fig. 6.4 and compared with "exact" results for this case taken from Ref. [20]. The slight deviation of the finite element results noted near the clamped edge could have been reduced by refining the mesh in this region. For both examples, a mesh of triangles was used and the nodal point loads consisted of linear forces computed from tributary area considerations. Results from a mesh of combinations of triangles and quadrilaterals (constructed from the subdivisions of the coarse mesh) have been obtained for the membrane case which agreed well with those shown in Fig. 6.3.

6.3 Circular Cylinders with Free Edges (Example 4)

The second form of shell considered is a circular cylinder, loaded by its own dead weight, supported by diaphragms at the ends, and free along the longitudinal edges. Because of its double symmetry only one-quarter of this shell needed to be considered in the analysis, as shown in Fig. 6.5. The end diaphragm was assumed to be infinitely rigid in its own plane and infinitely flexible out of that plane.

Three geometries were used in this analysis which were formed by varying the radius and the maximum subtended angle α , while all other dimensions and material properties were held constant. The three transverse profiles and a typical 4x5 mesh are shown in Fig. 6.5. All of the meshes considered were obtained by dividing the half-span ($L = 25'$) into equal

subdivisions, and by dividing the curved arc ($\eta = 0$ to $\eta = \alpha$) into equal subdivisions.

Results for the vertical displacements (δ_z) across the mid-section for the three geometries are shown in Figs. 6.6, 6.7, 6.8 and are compared to the "exact" results computed by numerical evaluation of the Donnel-Jenkins shell equation [21]. For each case analyses were made by utilizing different mesh sizes in which both triangles and quadrilaterals were used to observe the rate of convergence of the two element types. For a given idealization, the mesh of triangles and quadrilaterals are arranged as shown in Figs. 5.1 and 5.2, so the total number of nodal point degrees of freedom are the same for both element representations. For the cylinder with a radius of 50', the convergence (Fig. 6.6) of the triangular element is reasonably good, while the convergence of the triangle is much poorer for radii of 25' and 12.5' (Figs. 6.7 and 6.8). The corresponding results obtained by the quadrilateral element (Figs. 6.6, 6.7, and 6.8) indicate a marked improvement, and this improvement is accentuated for the latter two geometries. Since identical geometric idealizations are utilized in these analyses, the improved convergence is attributed to the better stiffness properties of the quadrilateral element, primarily in representing bending deformation modes (Fig. 2.6.c). This may be explained in part by considering the longitudinal stress distribution across the central section of the three profiles (Fig. 6.9). In each case, the longitudinal stress has a maximum value at the free edge and diminishes rapidly to zero; therefore, the elements located near the free edge are subjected in part to bending deformation modes.

Comparison of the convergence of the longitudinal stress at the central section as given by the triangle and the quadrilateral is shown in Fig. 6.10. Significant improvement is gained by using the quadrilateral in that the accuracy given by the 8×12 mesh of quadrilaterals is very close to that of a 16×22 mesh of triangles. It should be noted that the longitudinal stresses from the mesh of triangles were determined by considering the longitudinal stresses given by each triangle to be representative of the stress along the side of the triangle which is parallel to the longitudinal axis of the cylinder (see Section 2.4). The stresses from the mesh of quadrilaterals were taken as the average nodal point stresses of all elements intersecting a given nodal point. In addition, three components of bending moments are shown in Fig. 6.11 determined from a 16×22 mesh of triangles.

Of importance in this example is the demonstration of monotonic convergence for both element types as reflected in Fig. 6.6, 6.7, and 6.8, and the considerable improvement in the convergence given by the quadrilateral element. Also as demonstrated by this example, the overly-stiff properties of the constant stress triangle result in deformation patterns which are essentially of the correct form but whose magnitudes differ appreciably from the "exact" values for coarse meshes, and this property is accentuated for the smaller radii (Figs. 6.7 and 6.8). Of additional interest is the convergence of the longitudinal stress components (Fig. 6.10). The upper plot of Fig. 6.10 shows that the convergence of this stress component is similar to the convergence of vertical displacement (Fig. 6.7) with the relative error in the stress component being somewhat greater for coarse meshes. The convergence of the longitudinal stress components is

significantly improved by the use of quadrilaterals (Fig. 6.10). This is due partially to the improved representation of stress given by this element, but primarily to its superior stiffness properties which permit more accurate nodal point displacements for a given idealization.

6.4 Typical Interior Cylinder (Example 5)

This example represents a typical interior unit of a cylindrical roof constructed from a series of repeated cylindrical shells which are considered to be connected monolithically along the longitudinal edges. The longitudinal edges of the typical interior cylinder are assumed to be lines of symmetry in which the rotation about the longitudinal axis and the horizontal displacement are zero. The loading, geometry, material properties (except $\nu = 0.3$ for this case), end support conditions, and the section analyzed are as shown in Fig. 6.5, and the circular profile has a radius of 25' ($\alpha = 40^\circ$). Triangles were used in this analysis and a plot of vertical displacements for two mesh layouts (8x12 and 12x18) is shown in Fig. 6.12. In addition, plots of transverse moment and longitudinal stress given by the 12x18 mesh can be found in Fig. 6.12 and 6.13. The accuracy of these results are considered acceptable. The transverse moment at the longitudinal edge exhibits the greatest error; however, this is due to the steep moment gradient near this edge and may be improved by a local refinement in the mesh.

6.5 North Light Folded Plate Model (Example 6)

The geometry and material properties for this example are shown in Fig. 6.14. The shell is supported on end diaphragms and is loaded by line loads along the fold lines. From considerations of symmetry, one quarter of the shell was used in the analysis, and a typical 6x8 mesh of

quadrilaterals is shown in Fig. 6.14. In utilizing the 5 degree of freedom system for this example, "tangent planes" were constructed at the fold lines (Fig. 6.14) so that the plates from either side would intersect this plane at equal angles, thus constraining the plate bending rotations normal to this plane at the fold lines. The tangent planes of the interior nodes of course are the planes of the individual plates.

Three meshes (3×4 , 6×8 , 12×16) utilizing both triangles and quadrilaterals were used in the analysis and are compared with the "elasticity" method of Ref. [22]. The convergence of the vertical displacements, the longitudinal stresses and the transverse bending moments are shown in Figs. 6.15, 6.16, 6.17. The meshes of triangles result in slow convergence since the individual plates are subjected to longitudinal bending (Fig. 6.16), which accentuate the bending deformation mode (Fig. 2.6.c). Again this case illustrates that the convergence of the longitudinal stresses is similar to that of the nodal point displacements. The overall performance of the 5 degree of freedom nodal point displacement system using the quadrilateral element is very good for this case, and even the 6×8 mesh yields acceptable results. The only departure from the correct form is the transverse bending moment across the interior plate a-e (Fig. 6.17) with the maximum discrepancy occurring at point a (approximately 13% deviation for the 12×16 mesh of quadrilaterals).

6.6 Translational Shells (Example 7)

In this example, three different forms of shells are considered and compared: a parabolic cylinder (PC), an elliptic paraboloid (EP, positive Gaussian curvature), and a hyperbolic paraboloid (HP, negative Gaussian curvature) as shown in Fig. 6.18. Each shell has the same transverse

parabolic profile and is supported at the ends by a diaphragm normal to the shell surface, while the longitudinal edges are free. The loading of each shell is due to its own dead weight.

Certain results of the finite element analyses are presented in Fig. 6.19 using meshes of triangles in comparison with the numerical analysis results presented in Ref. [23]. Uniform rectangular mesh layouts in the horizontal plane were used in the analyses with dimensions as shown on Fig. 6.18. The finite element results for the parabolic cylinder are seen to check well with those given in the reference. The agreement of the longitudinal stresses for the hyperbolic paraboloid also is seen to be excellent, although the vertical displacements and transverse moments for this shell show some slight deviations. This discrepancy is not significant, however, inasmuch as the values are so small.

The greatest discrepancies are found in the case of the elliptic paraboloid, and this analysis was repeated using 4×6 and 8×12 meshes of quadrilaterals. These results are shown in Fig. 6.20. The two meshes yield almost identical results for the vertical displacement and these values are only slightly greater than those of the 12×18 mesh of triangles. The longitudinal stresses given by the 8×12 mesh of quadrilaterals are almost identical to those in Fig. 6.19, while the bending moments are in better agreement with those of Ref. [23]. All of the above discrepancies are not severe, and may be explained in part by the fact that a slightly different structure was considered in Ref. [23]. The shallow shell theory used in that analysis required that the longitudinal profile be assumed in the form of a circular arc while the finite element analysis took account of the true parabolic profile.

6.7 Conoid (Example 8)

The conoidal shell, shown in Fig. 6.21, is supported on all four sides by diaphragms normal to the shell surface, and is subjected to an external pressure load. Only half the shell was treated in the analysis, due to symmetry, using a uniform 12×18 rectangular mesh of triangles (referred to the horizontal plane) and an 8×12 mesh of quadrilaterals.

The normal displacement components and transverse moments computed by the finite element procedure are shown in Fig. 6.22, while two in-plane stress components are shown in Fig. 6.23. Also shown are some results derived from shallow shell theory which were presented in Ref. [24].

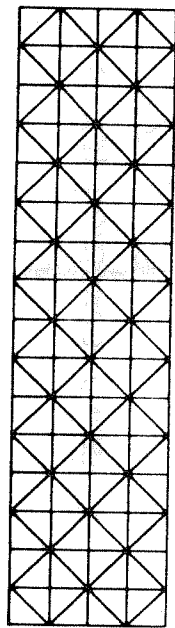
The two finite element analyses show good agreement in the normal displacement component and the stress component. The deviations in the upper plot of Fig. 6.23 are explained by the fact that the stresses from the mesh of triangles were plotted at the mid-point of the sides of the triangles lying along line ($x = D/4$) as explained in Section 2.4. Significant differences in the larger values of the bending moment are apparent and the values given by the mesh of triangles are considered more accurate due to the smaller subdivisions given by the 12×18 mesh.

The general form of the finite element results and those of Ref. [24] are in agreement, but significant differences in magnitude are evident. In this case, it is believed that the finite element results are the more reliable because this shell has a significantly greater rise than would be permitted by shallow shell theory.

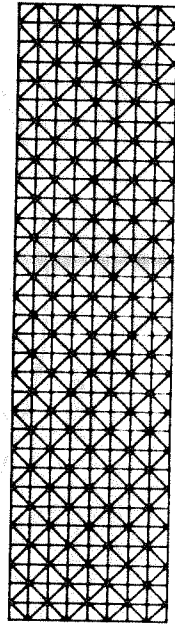
Element	Mesh	m	n	Relative Computational Effort*	Tip Deflection δ_y at $y = 0$	Stress σ_x at $x = 12"$, $y = 6"$
CST	A1	14	170	6.2	0.3056	51.23
	A2	22	594	53.1	0.3419	57.34
QUAD	B1	10	54	1.0	0.3333	55.20
	B2	14	170	6.2	0.3497	58.37
LST	C1	26	170	21.3	0.3551	59.15
	C2	42	594	193.8	0.3557	60.02
Beam Theory (upper bound for δ_y at $y = 0$)					0.3558	60.00

Table 2. Cantilever Beam, Comparison Between CST, QUAD, and LST.

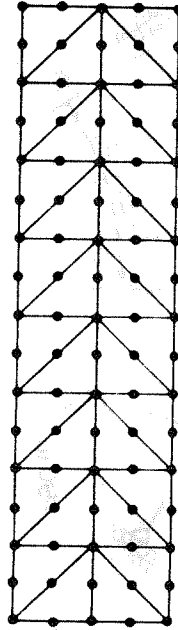
* Based on number of multiplications to decompose K, i.e., $m^2n/2$



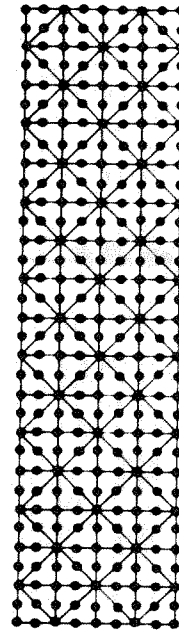
MESH A-1 128 CONSTANT STRAIN TRIANGLES



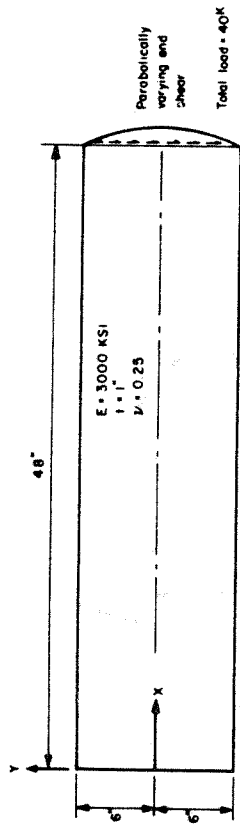
MESH A-2 512 CONSTANT STRAIN TRIANGLES



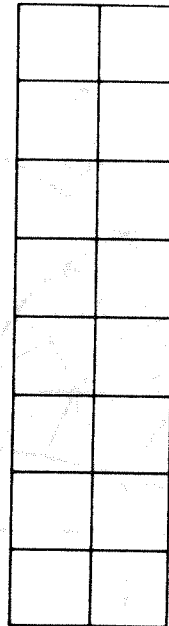
MESH C-1 32 LINEAR STRAIN TRIANGLES



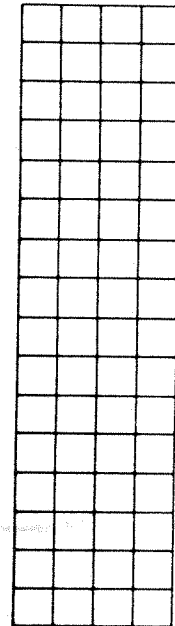
MESH C-2 128 LINEAR STRAIN TRIANGLES



CANTILEVER BEAM LOADED AT FREE END

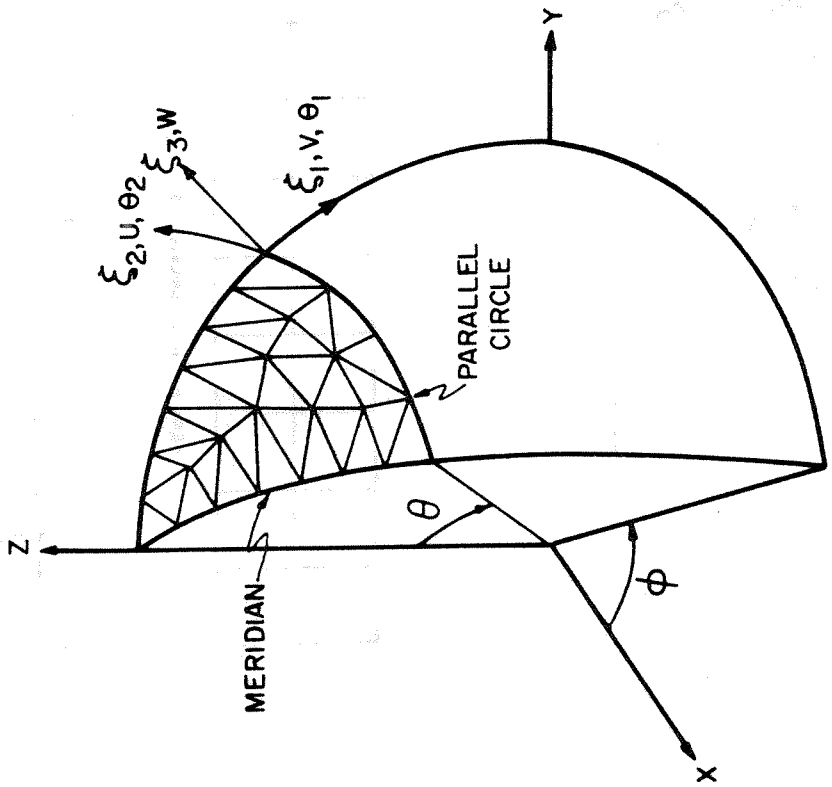


MESH B-1 16 QUADRILATERALS

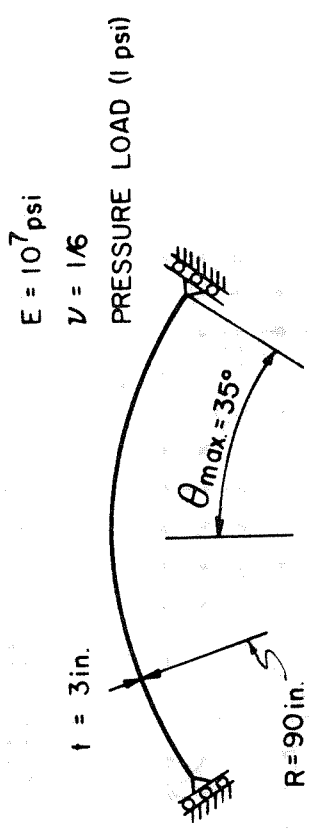


MESH B-2 64 QUADRILATERALS

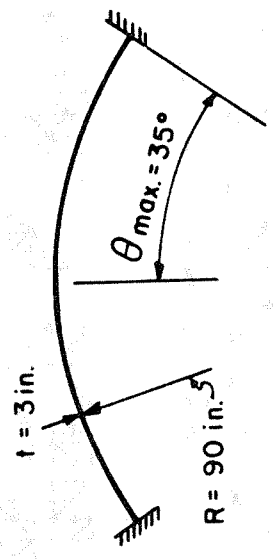
FIG. 6.1 CANTILEVER BEAM AND FINITE ELEMENT IDEALIZATIONS (EXAMPLE 1)



COORDINATE SYSTEM AND COARSE MESH



MEMBRANE CONDITION (EX. 1)



CLAMPED CONDITION (EX. 2)

FIG. 6.2 AXISYMMETRIC SPHERICAL DOME (EX. 1 AND EX. 2)

⊙ FINITE ELEMENT, COARSE MESH

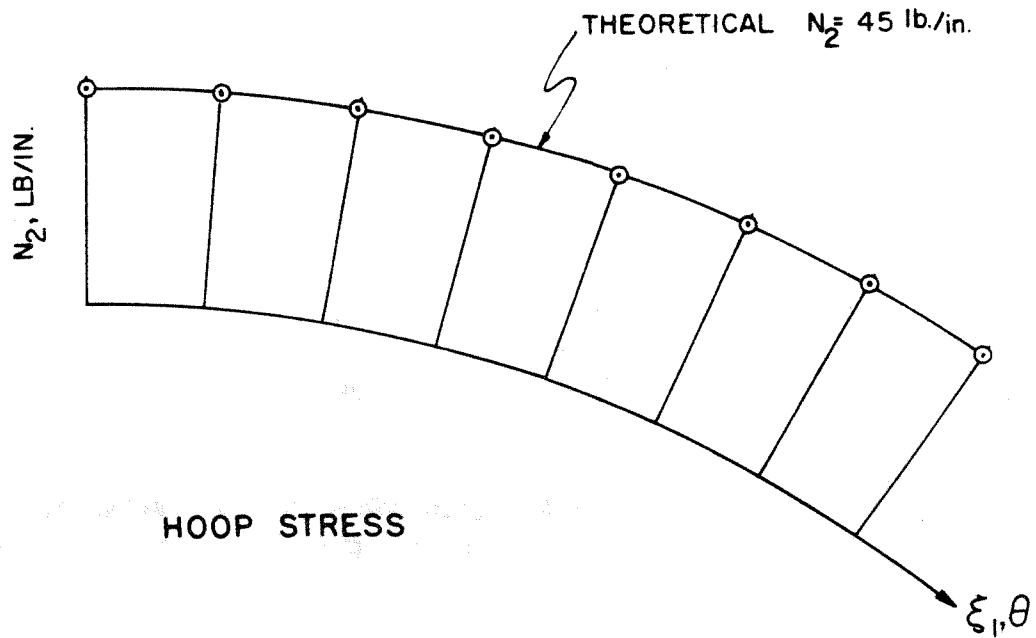
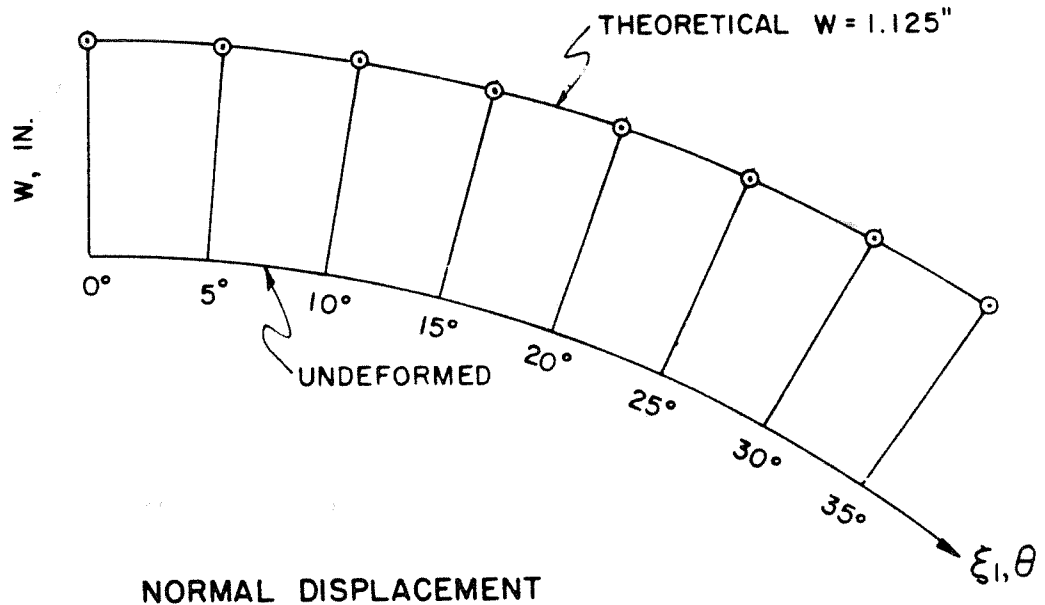


FIG. 6.3 COMPARISON OF DISPLACEMENTS AND STRESSES FOR DOME (EXAMPLE 2)

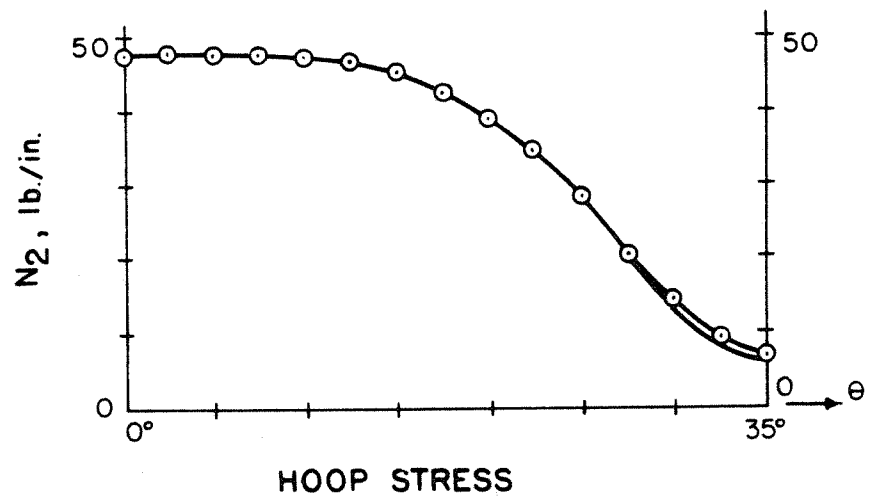
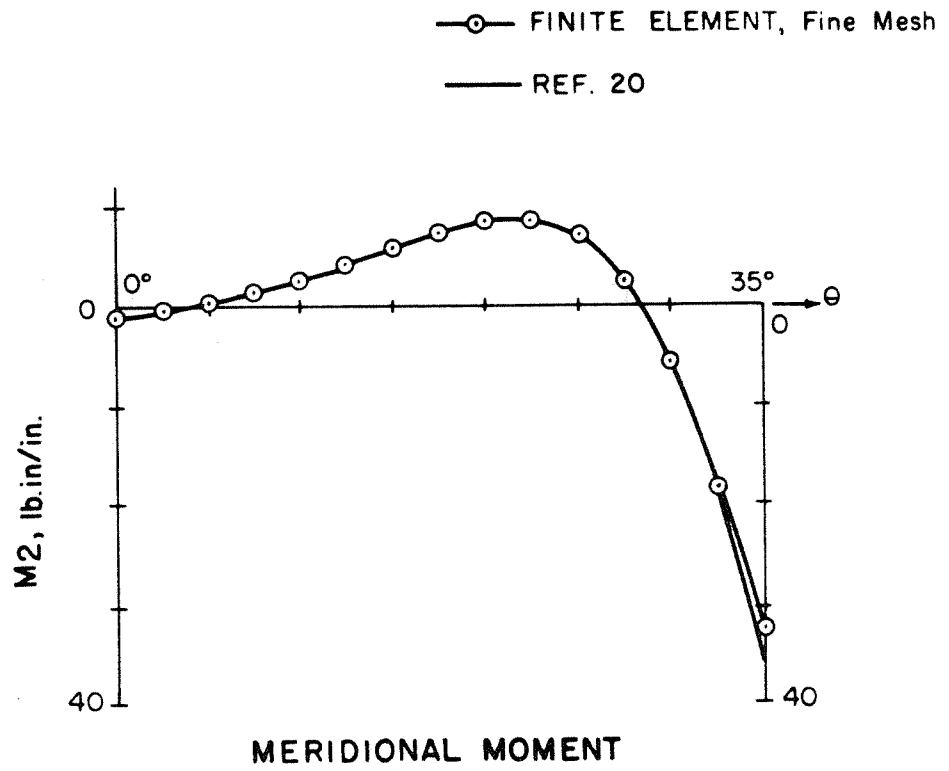
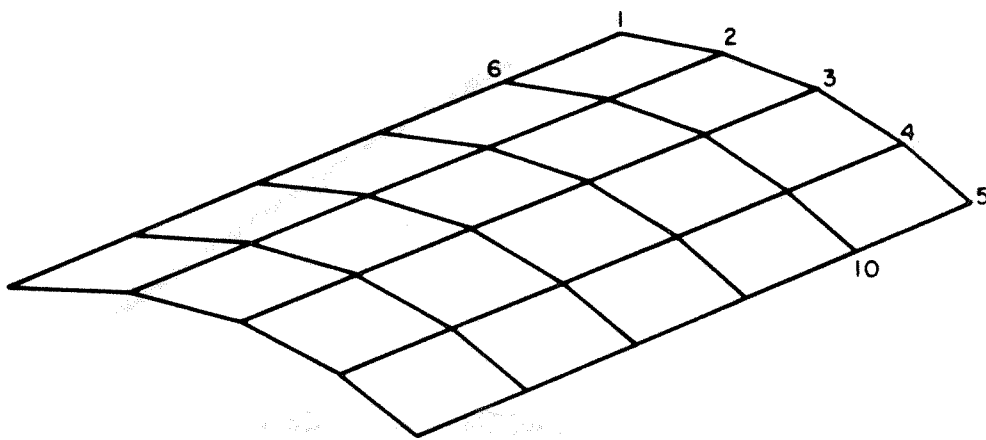
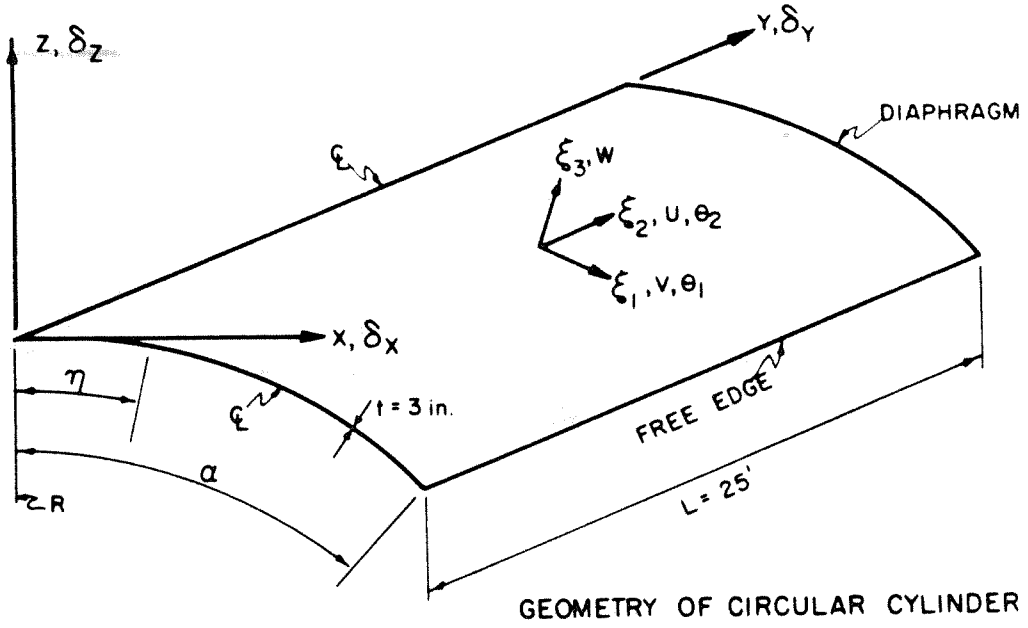
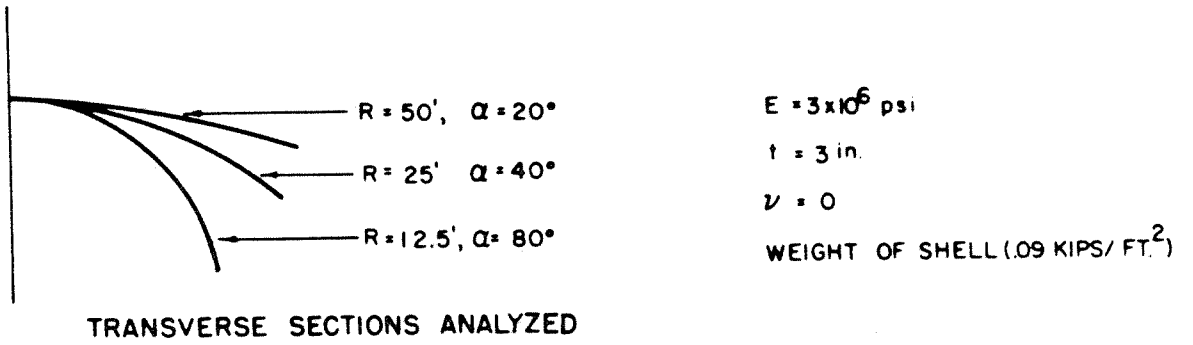


FIG. 6.4 COMPARISON OF MOMENTS AND STRESSES FOR DOME (EXAMPLE 3).



TYPICAL UNIFORM MESH (4x5) OF QUADRILATERALS

FIG. 6.5 GEOMETRY AND MATERIAL PROPERTIES OF CIRCULAR CYLINDERS WITH FREE EDGES (EXAMPLE 4)

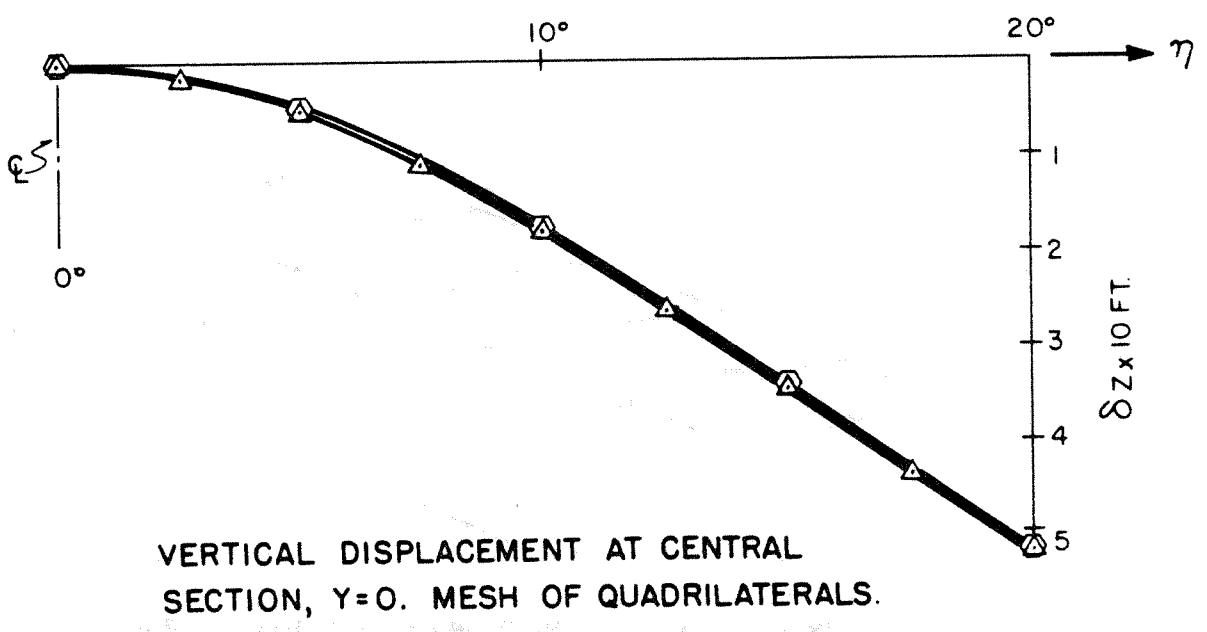
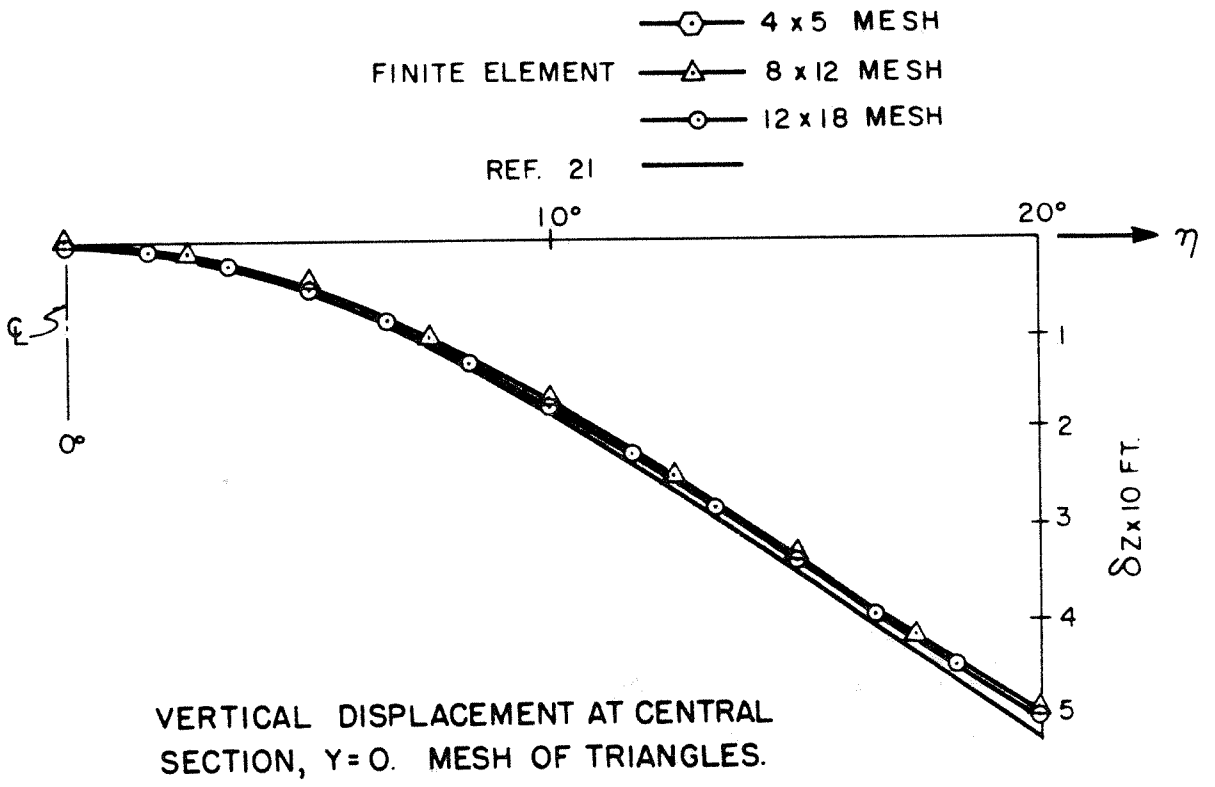


FIG. 6.6 CONVERGENCE OF VERTICAL DISPLACEMENT OF FINITE ELEMENT SOLUTION FOR CIRCULAR CYLINDER WITH RADIUS OF 50 FT. (EXAMPLE 4)

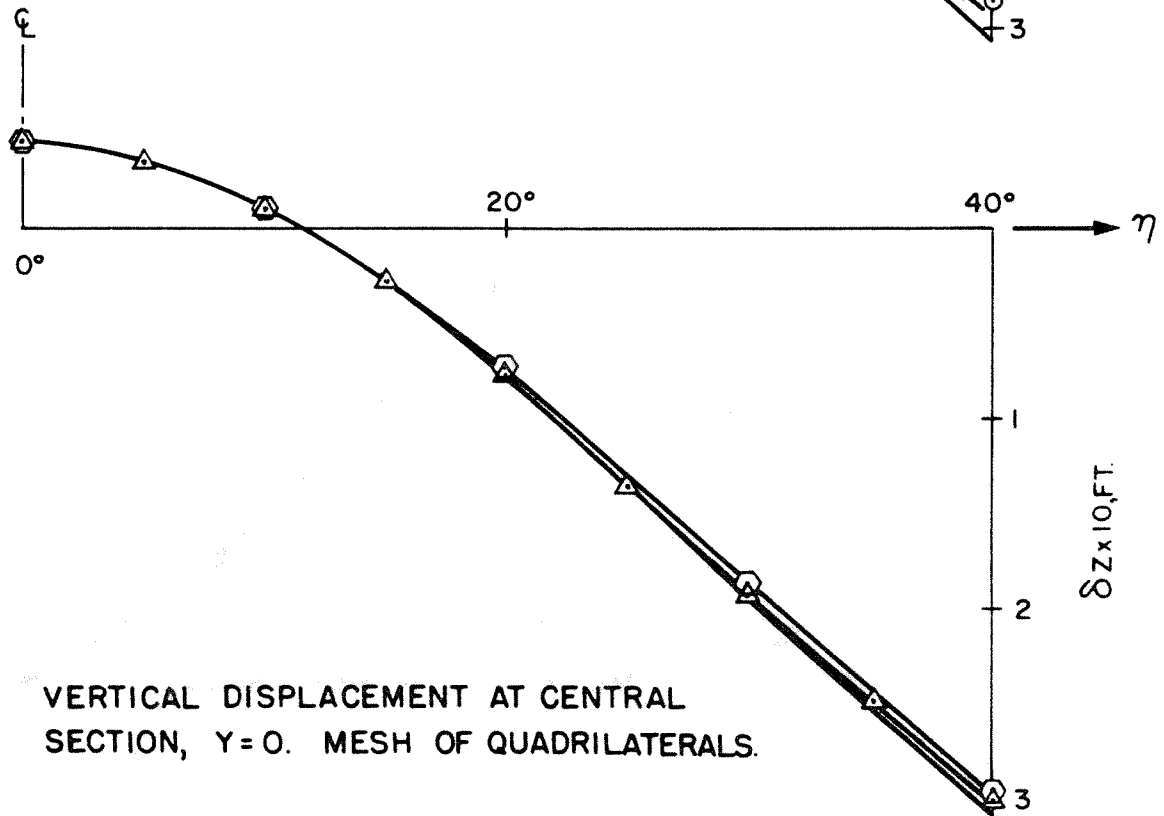
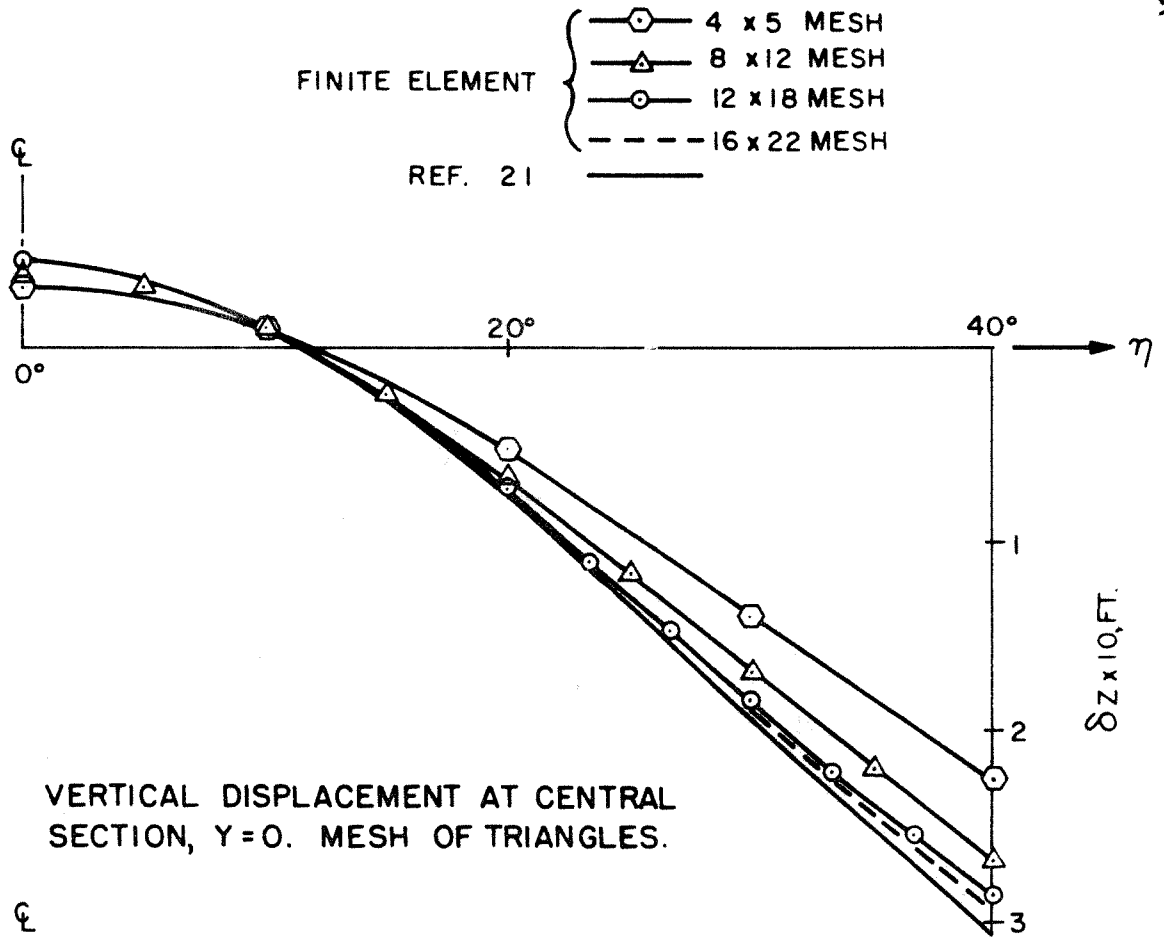


FIG. 6.7 CONVERGENCE OF VERTICAL DISPLACEMENT OF FINITE ELEMENT SOLUTION FOR CIRCULAR CYLINDER WITH RADIUS OF 25 FT. (EXAMPLE 4)

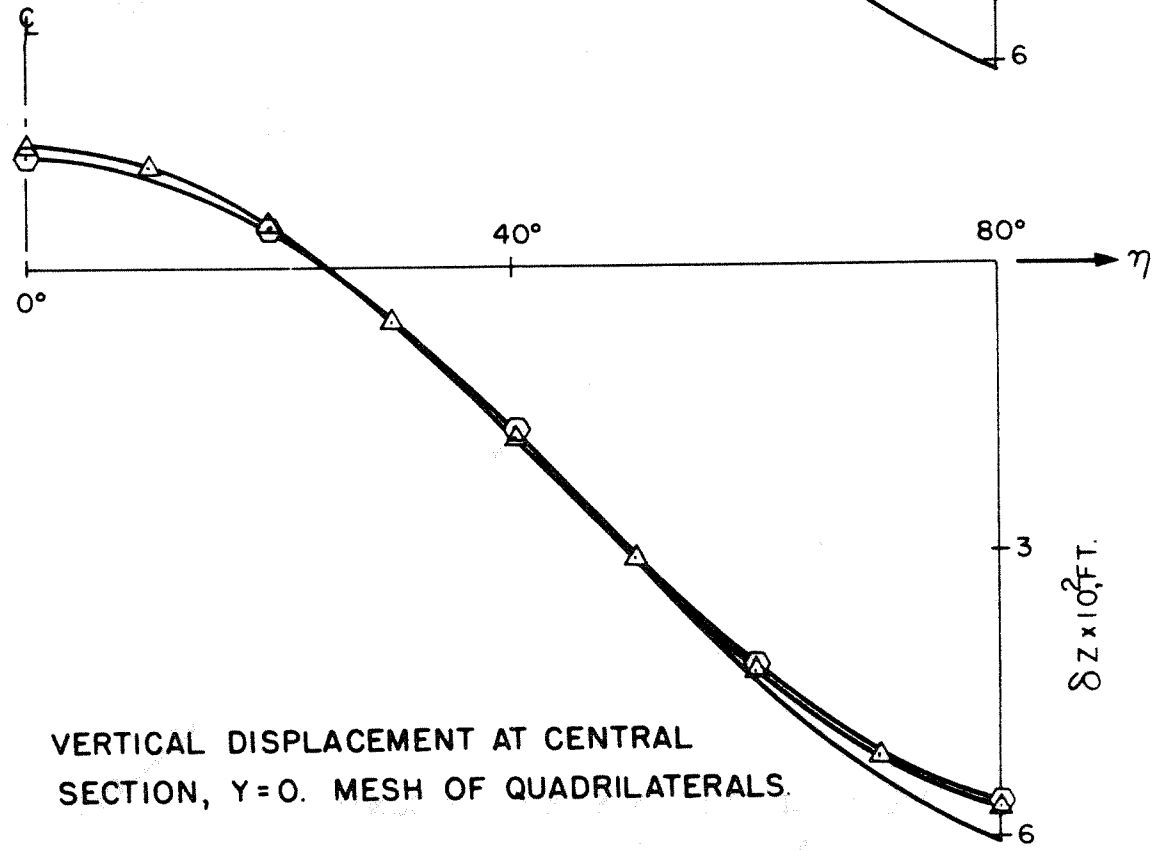
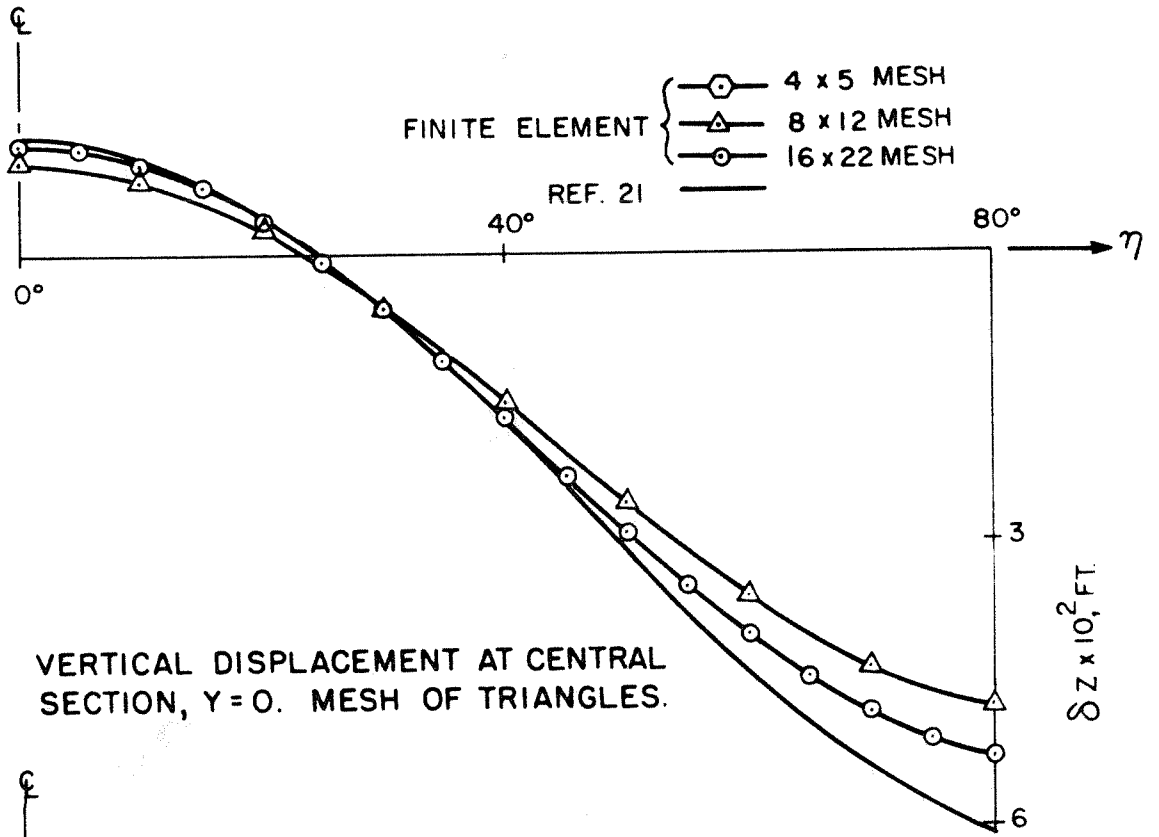


FIG. 6.8 CONVERGENCE OF VERTICAL DISPLACEMENT OF FINITE ELEMENT SOLUTION FOR CIRCULAR CYLINDER WITH RADIUS OF 12.5 FT. (EXAMPLE 4)

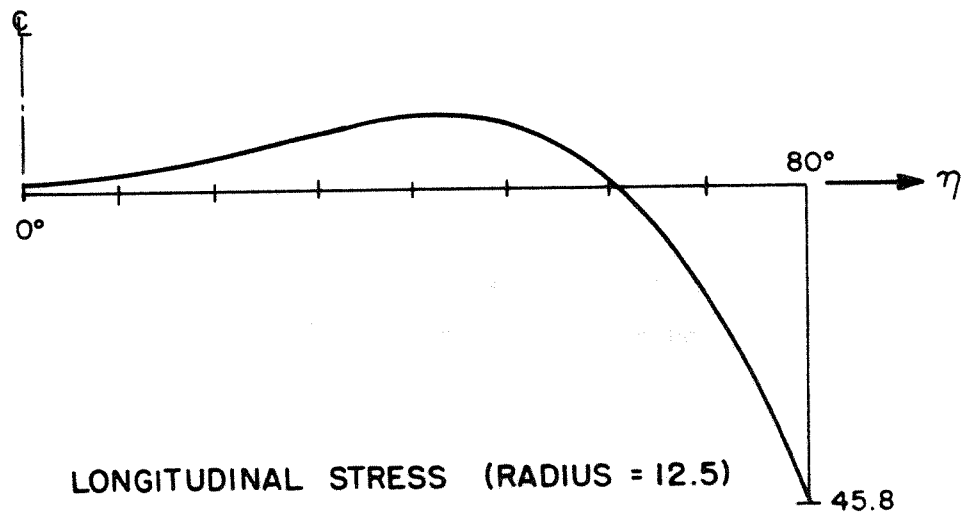
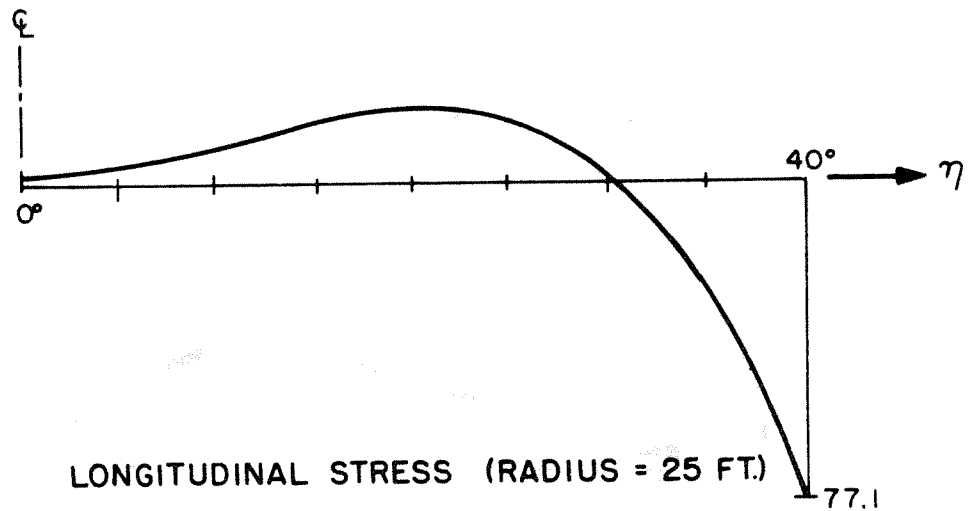
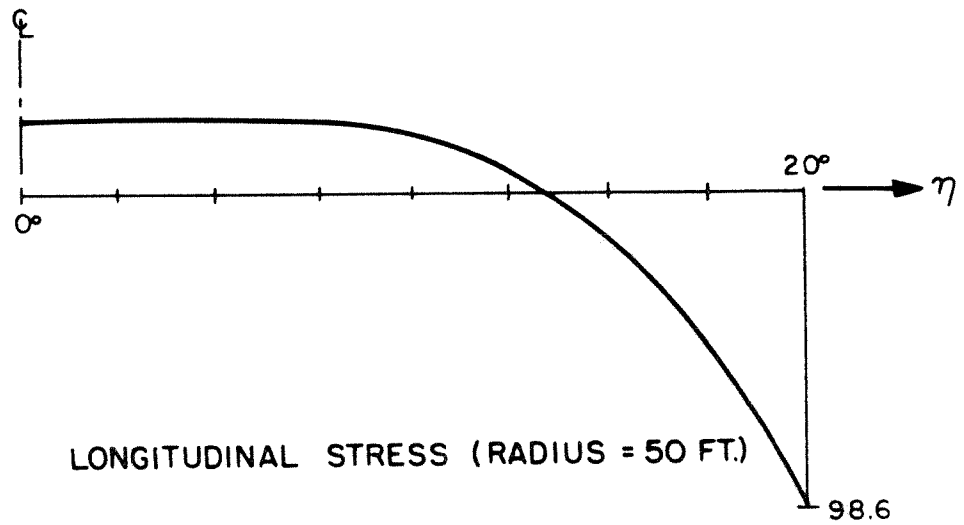


FIG. 6.9 LONGITUDINAL STRESS DISTRIBUTION, N_2 , AT CENTRAL SECTION, $Y=0$, FOR CIRCULAR CYLINDERS WITH RADII OF 50, 25, AND 12.5 FT. (EXAMPLE 4)

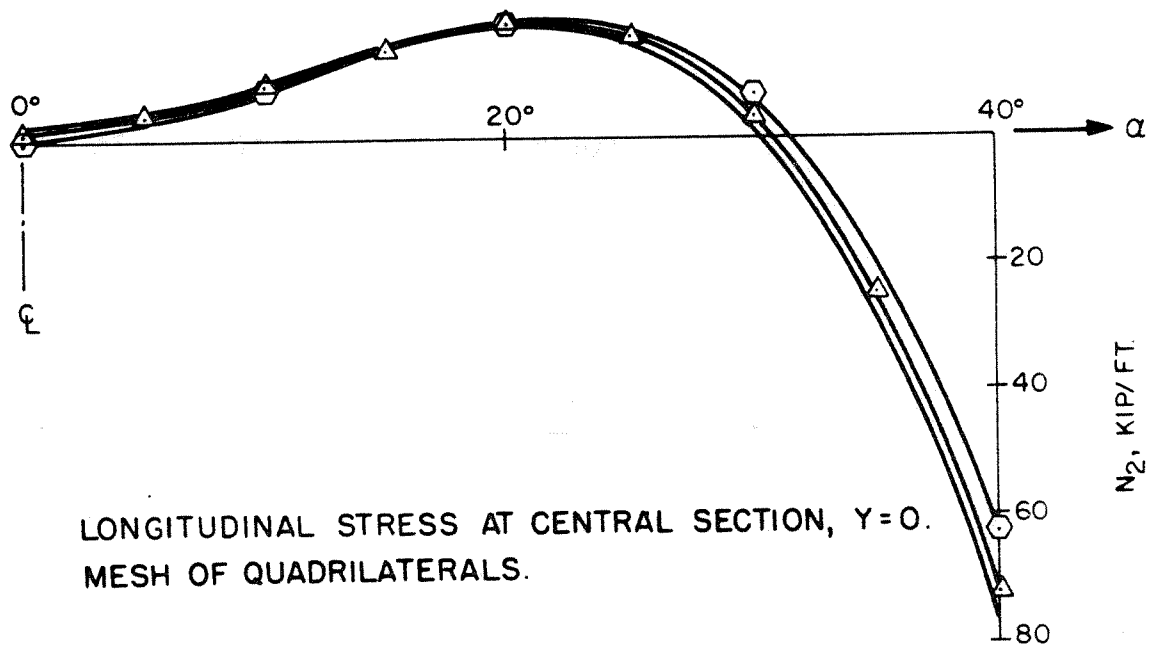
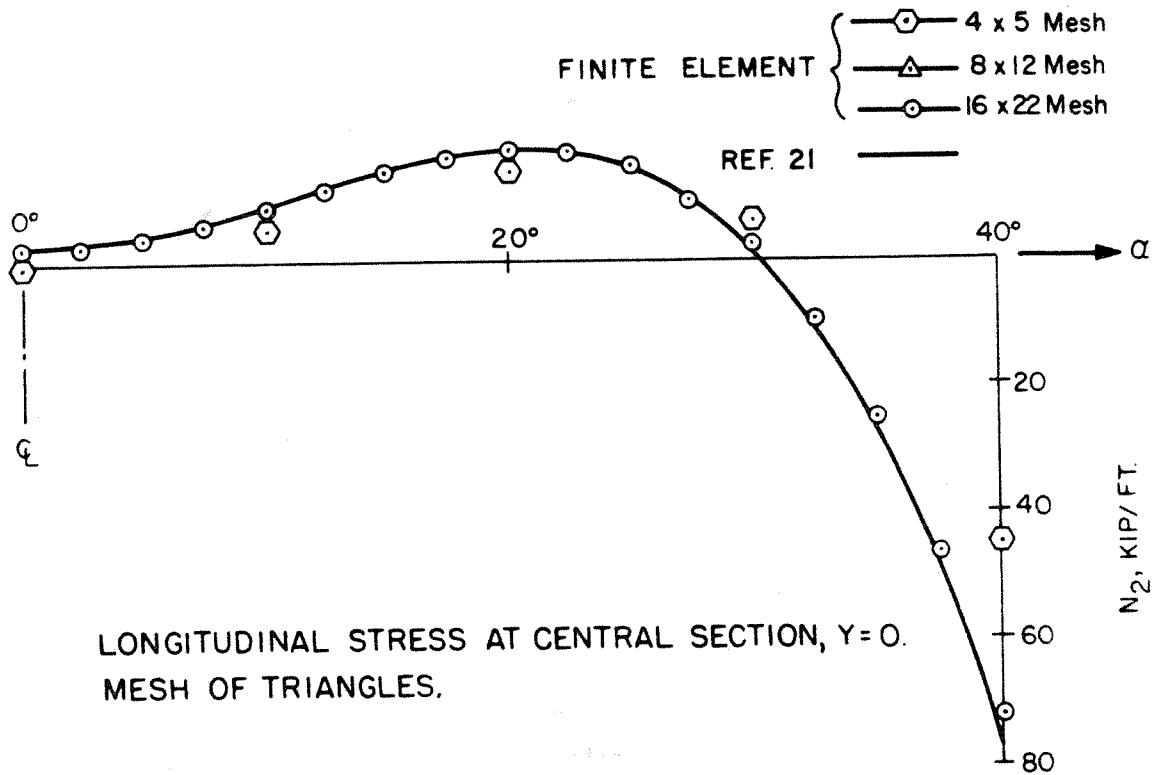
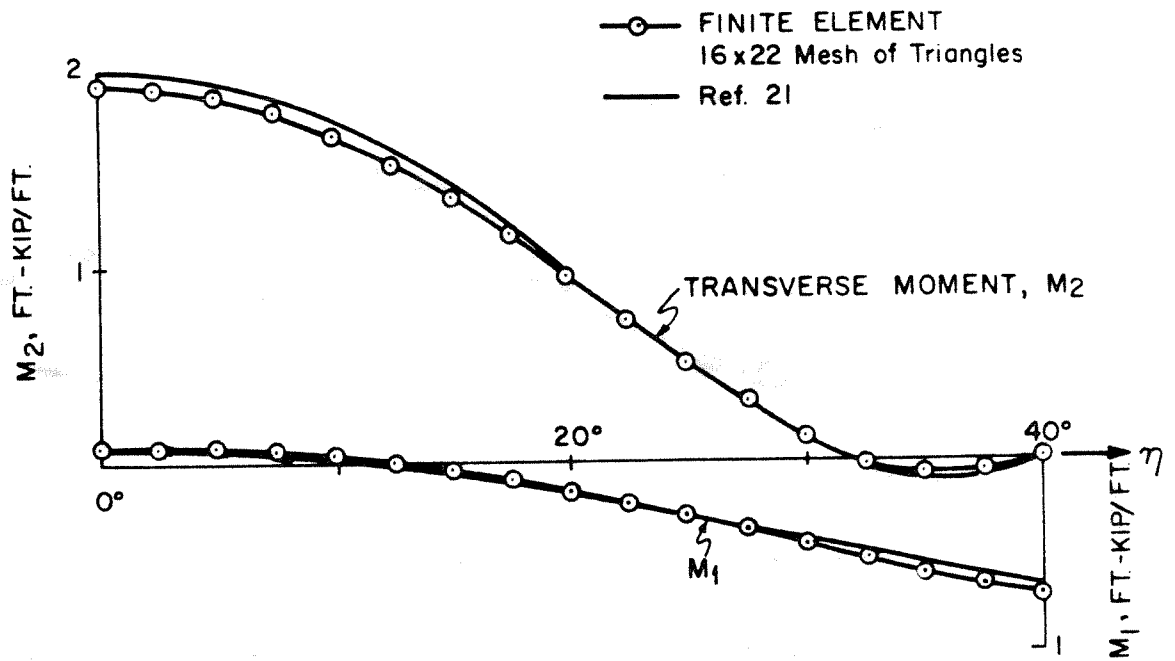
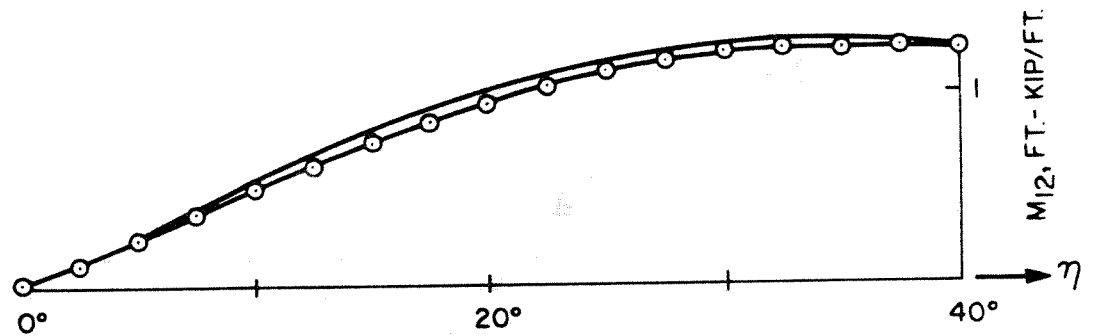


FIG. 6.10 CONVERGENCE OF LONGITUDINAL STRESS OF FINITE ELEMENT SOLUTION FOR CIRCULAR CYLINDER WITH RADIUS OF 25 FT. (EXAMPLE 4)

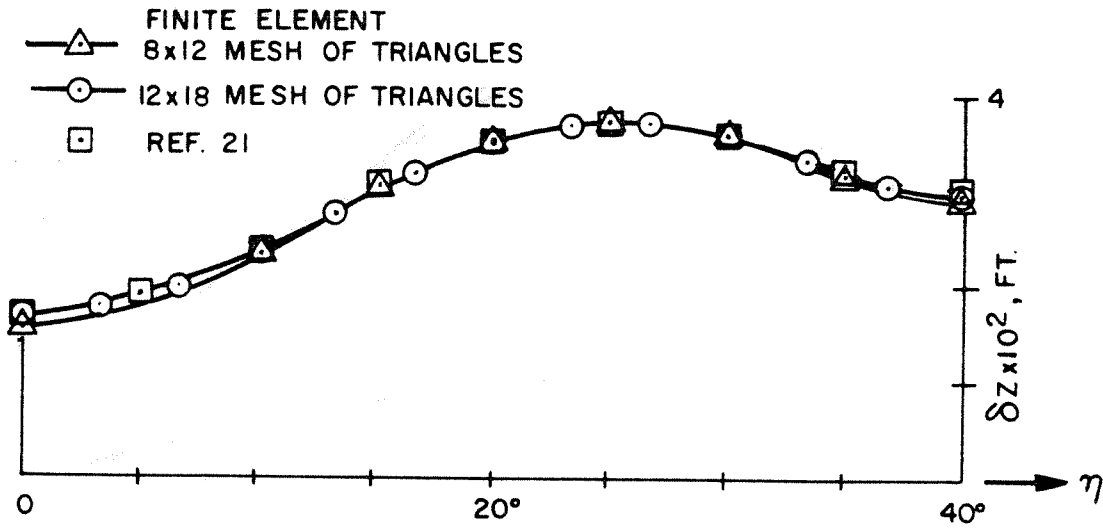


BENDING MOMENTS AT CENTRAL SECTION, $y = 0$

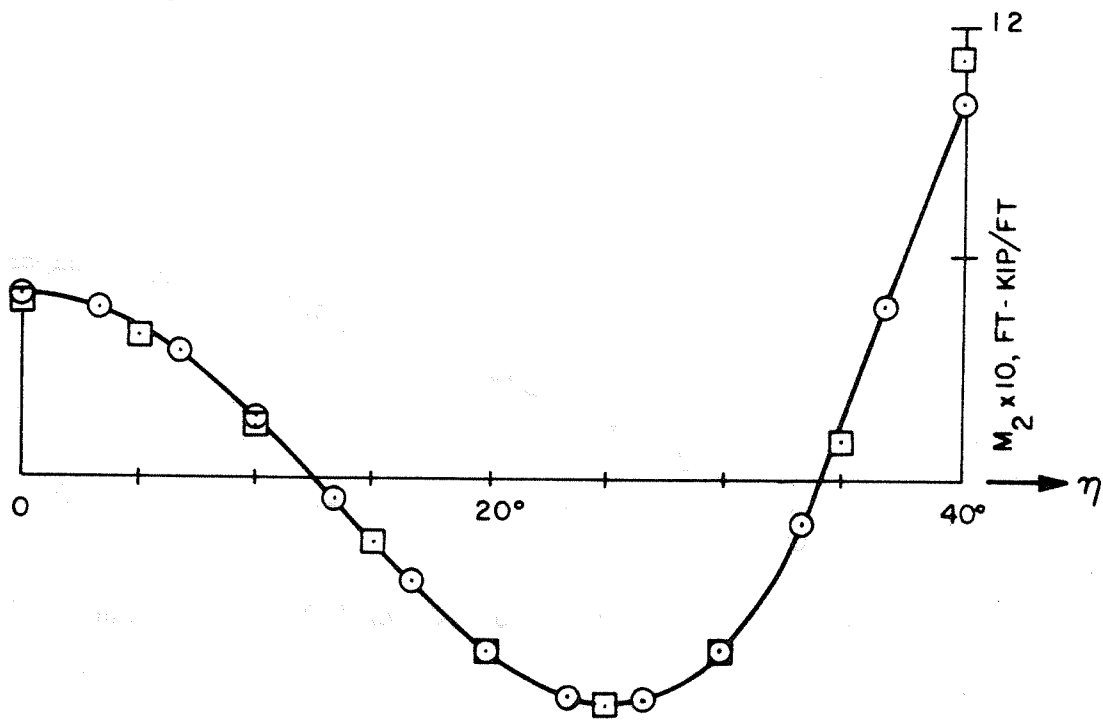


TWISTING MOMENT AT DIAPHRAGM, $y = L$

FIG. 6.11 COMPARISON OF MOMENTS OF CIRCULAR CYLINDER, $R = 25'$ (EXAMPLE 4)

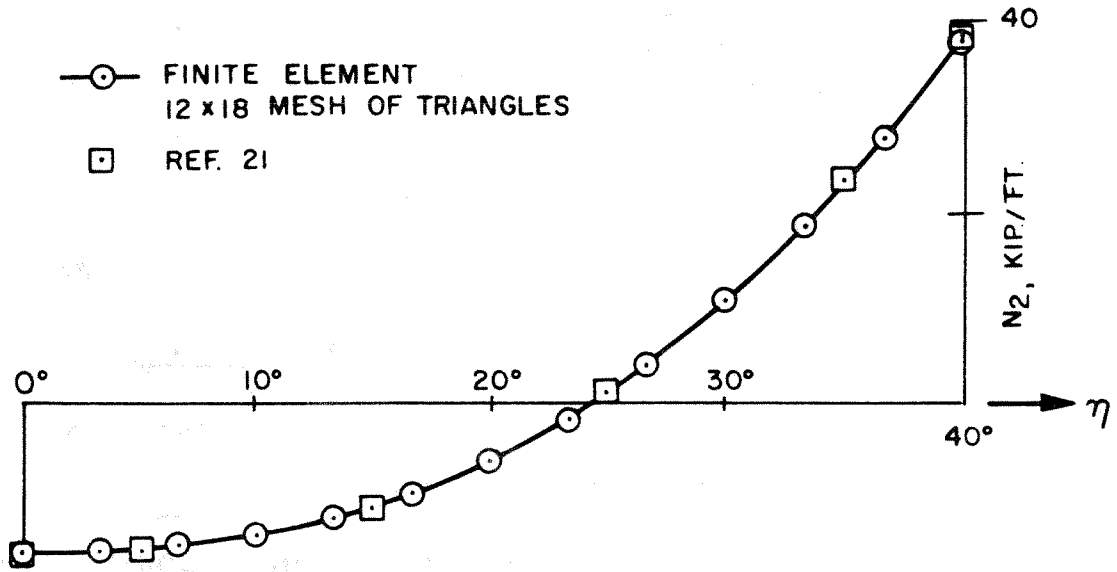


VERTICAL DISPLACEMENT AT CENTRAL SECTION, Y = 0

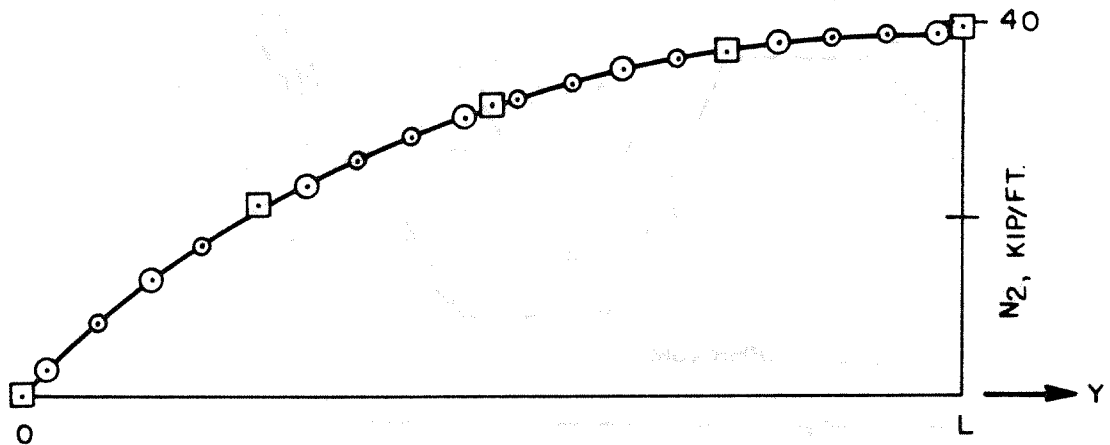


TRANSVERSE MOMENT AT CENTRAL SECTION, Y = 0

FIG. 6.12 COMPARISON OF DISPLACEMENTS AND MOMENTS FOR TYPICAL INTERIOR CYLINDER (EXAMPLE 5)

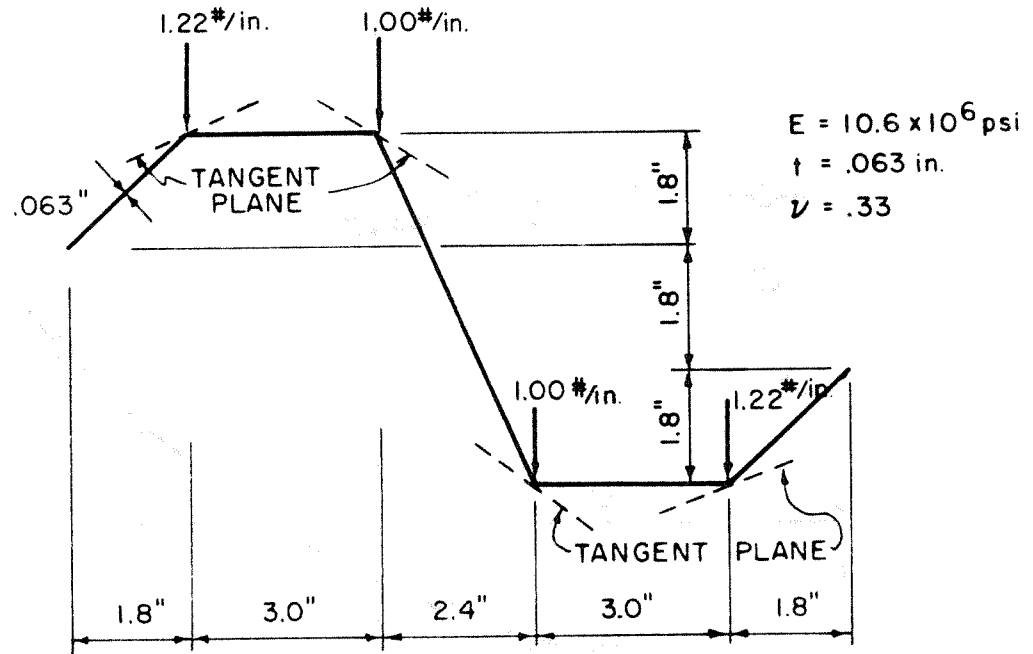


LONGITUDINAL STRESS AT CENTRAL SECTION, Y=0

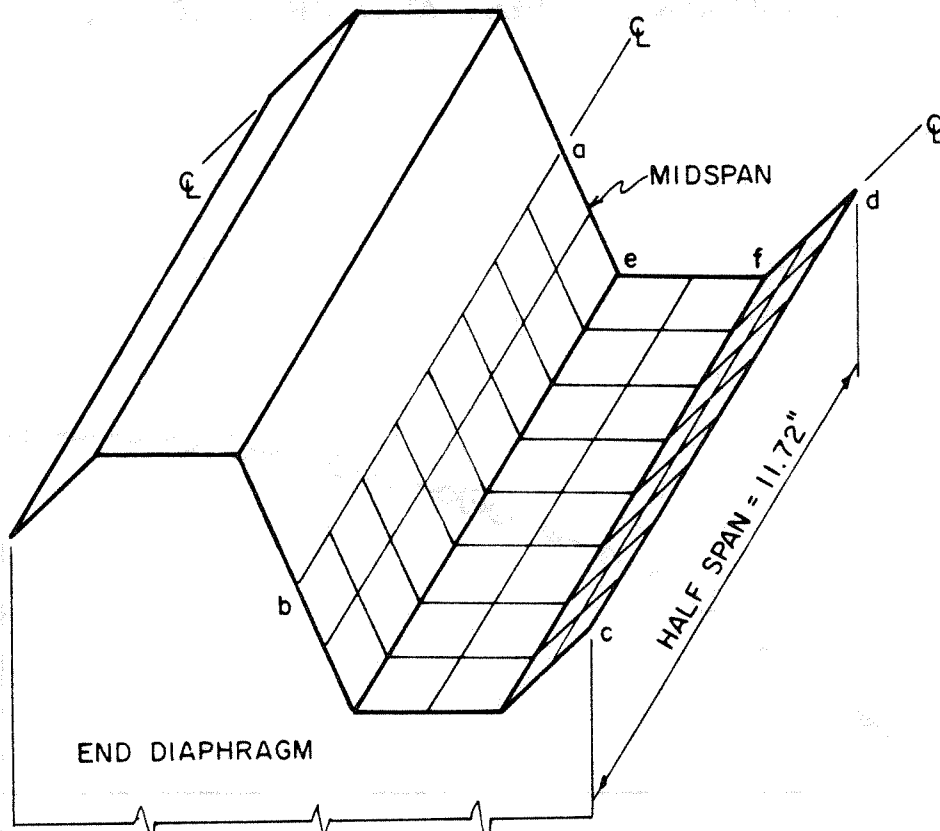


LONGITUDINAL STRESS ALONG INTERSECTING EDGE, $\eta = 40^\circ$

FIG. 6.13 COMPARISON OF STRESS FOR TYPICAL INTERIOR CYLINDER (EXAMPLE 5)



TRANSVERSE CROSS-SECTION AND LOADING OF FOLDED PLATE



SECTION ANALYZED (a,b,c,d) AND TYPICAL 6 x 8 MESH

FIG. 6.14 GEOMETRY AND MATERIAL PROPERTIES OF NORTH LIGHT FOLDED PLATE MODEL. (EXAMPLE 6)

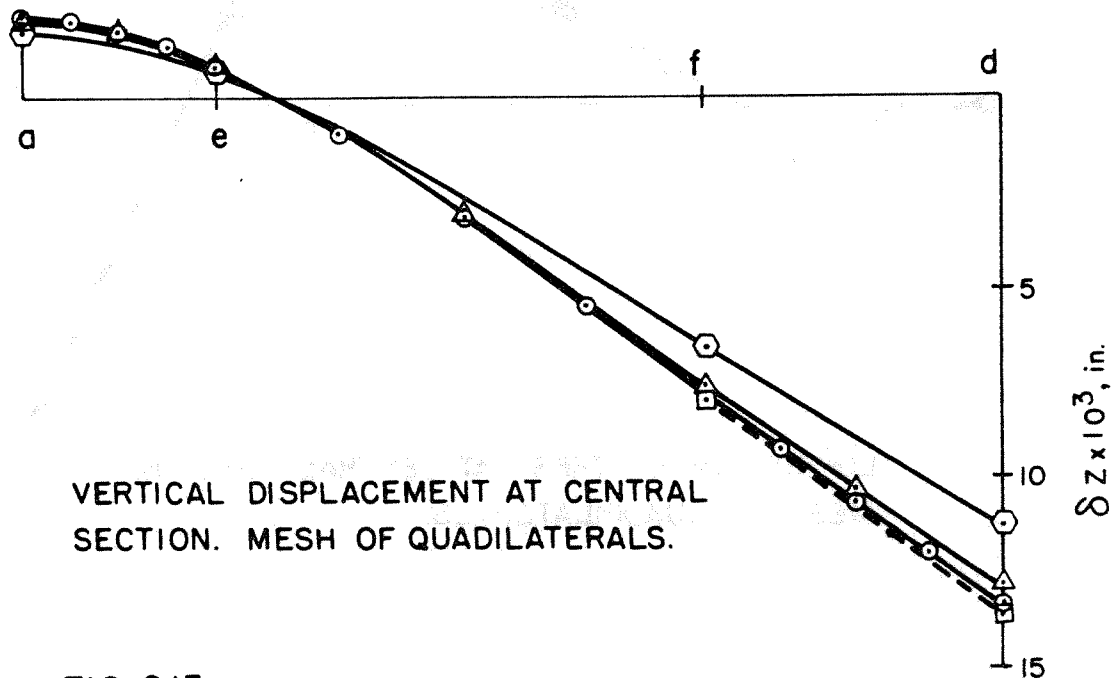
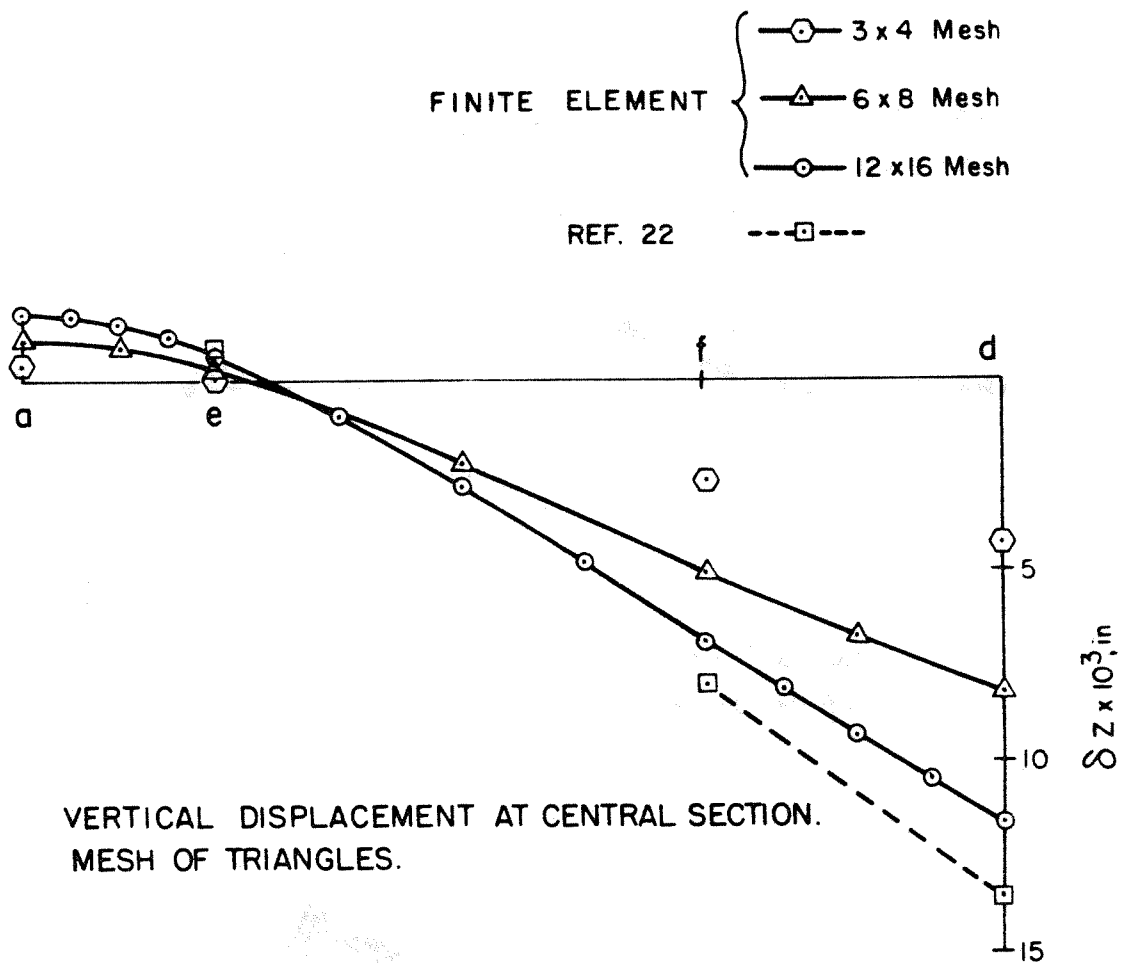


FIG. 6.15
CONVERGENCE OF VERTICAL DISPLACEMENT OF FINITE
ELEMENT SOLUTION FOR NORTH LIGHT FOLDED PLATE
(EXAMPLE 6)

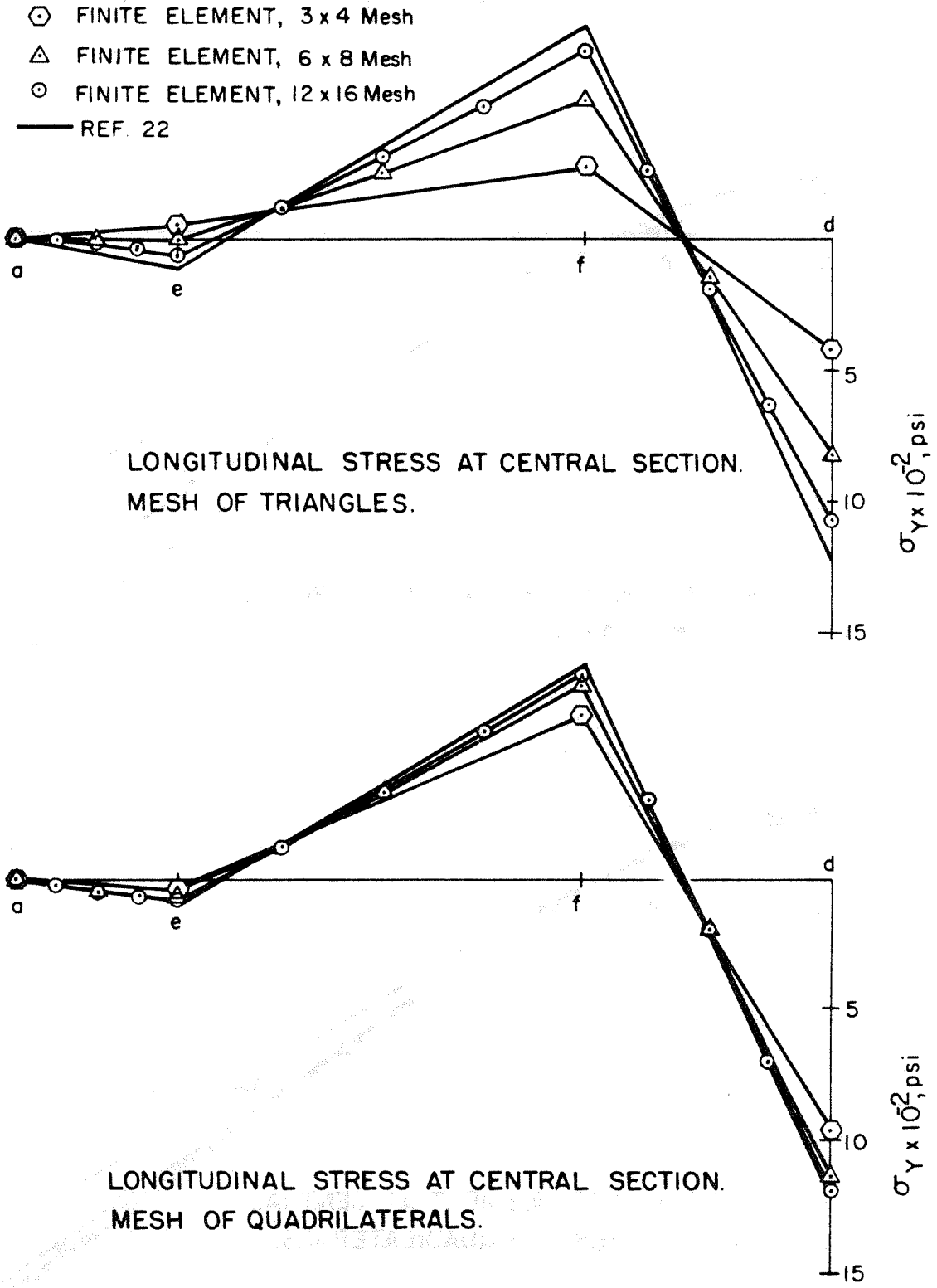
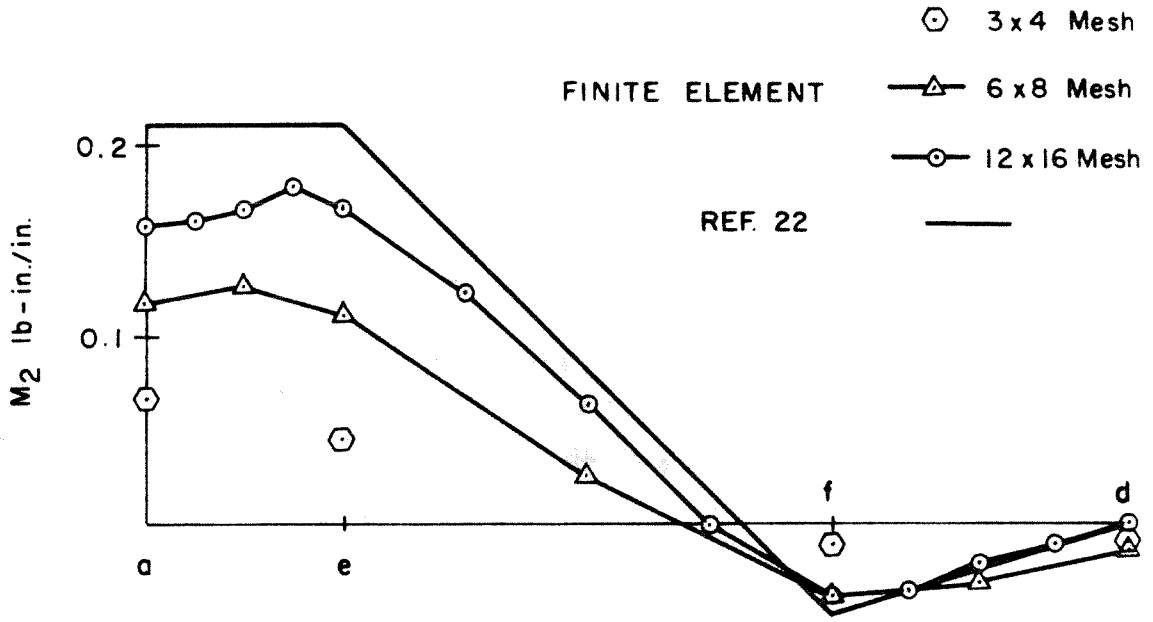
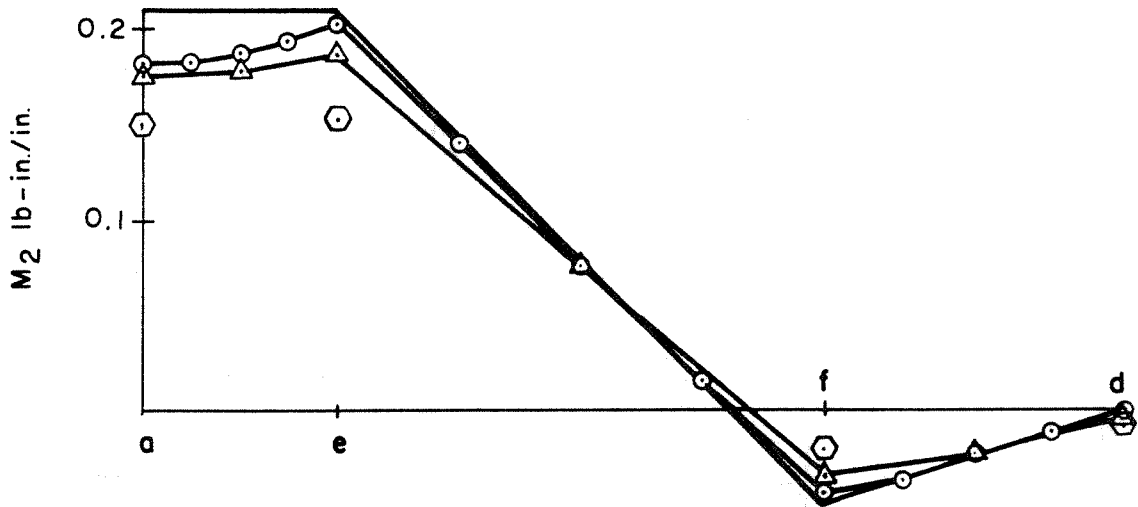


FIG. 6.16 CONVERGENCE OF LONGITUDINAL STRESS OF FINITE ELEMENT SOLUTION FOR NORTH LIGHT FOLDED PLATE (EXAMPLE 6).



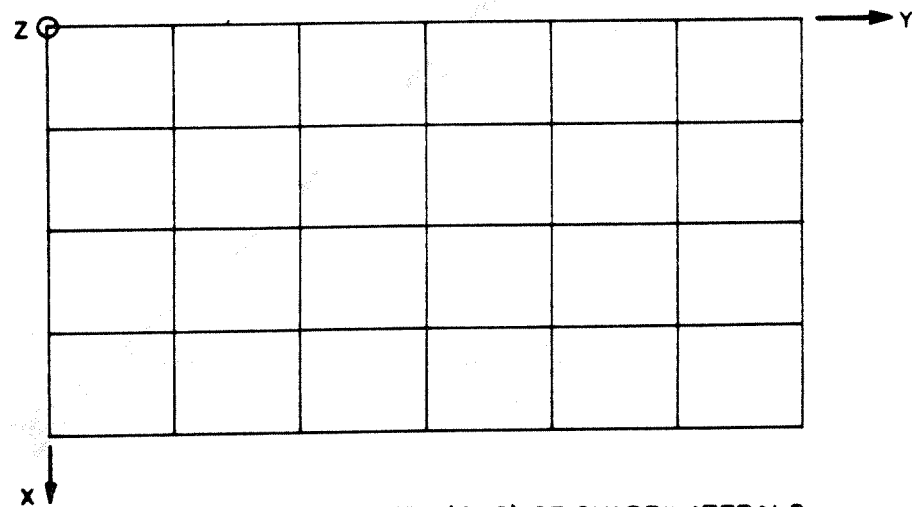
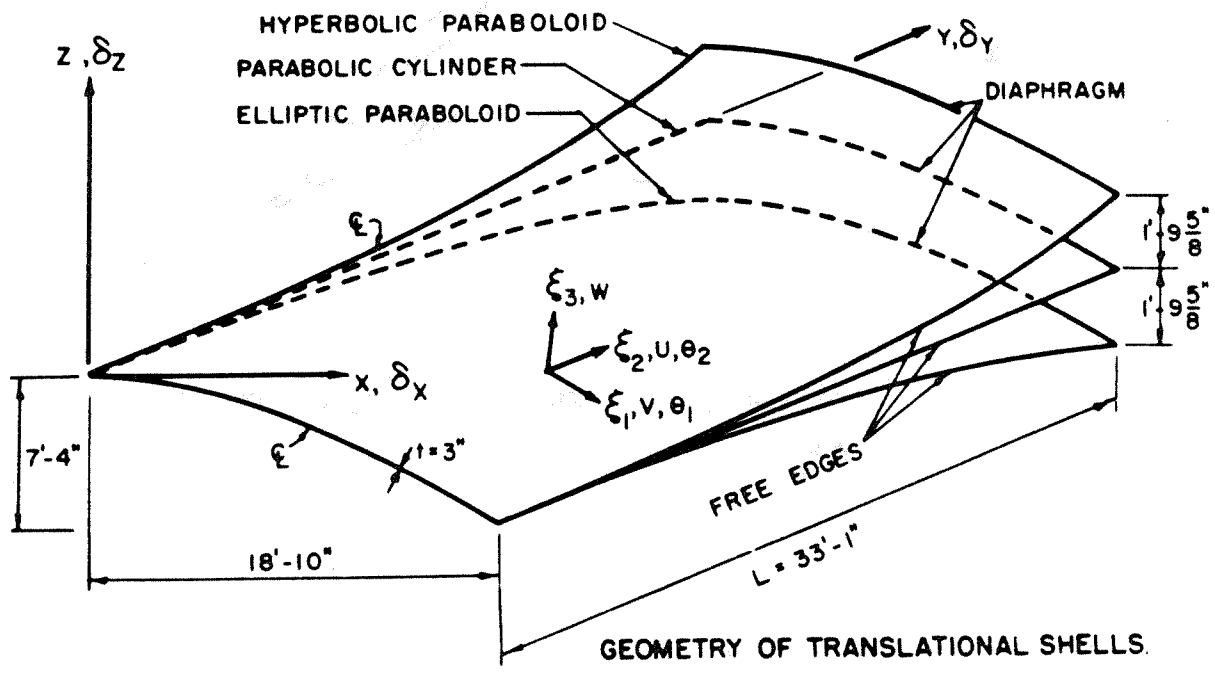
TRANSVERSE BENDING MOMENT AT CENTRAL SECTION.
MESH OF TRIANGLES.



TRANSVERSE BENDING MOMENT AT CENTRAL SECTION.
MESH OF QUADRILATERALS.

FIG. 6.17 CONVERGENCE OF BENDING MOMENT OF
FINITE ELEMENT SOLUTION FOR NORTH
LIGHT FOLDED PLATE

$E = 3 \times 10^6 \text{ psi}$
 $\nu = 0.17$
 WEIGHT OF SHELL (.08 KIPS/FT.²)



TYPICAL UNIFORM MESH (4x6) OF QUADRILATERALS IN HORIZONTAL PLANE.

FIG. 6.18 GEOMETRY AND MATERIAL PROPERTIES OF TRANSLATIONAL SHELLS (EXAMPLE 7)

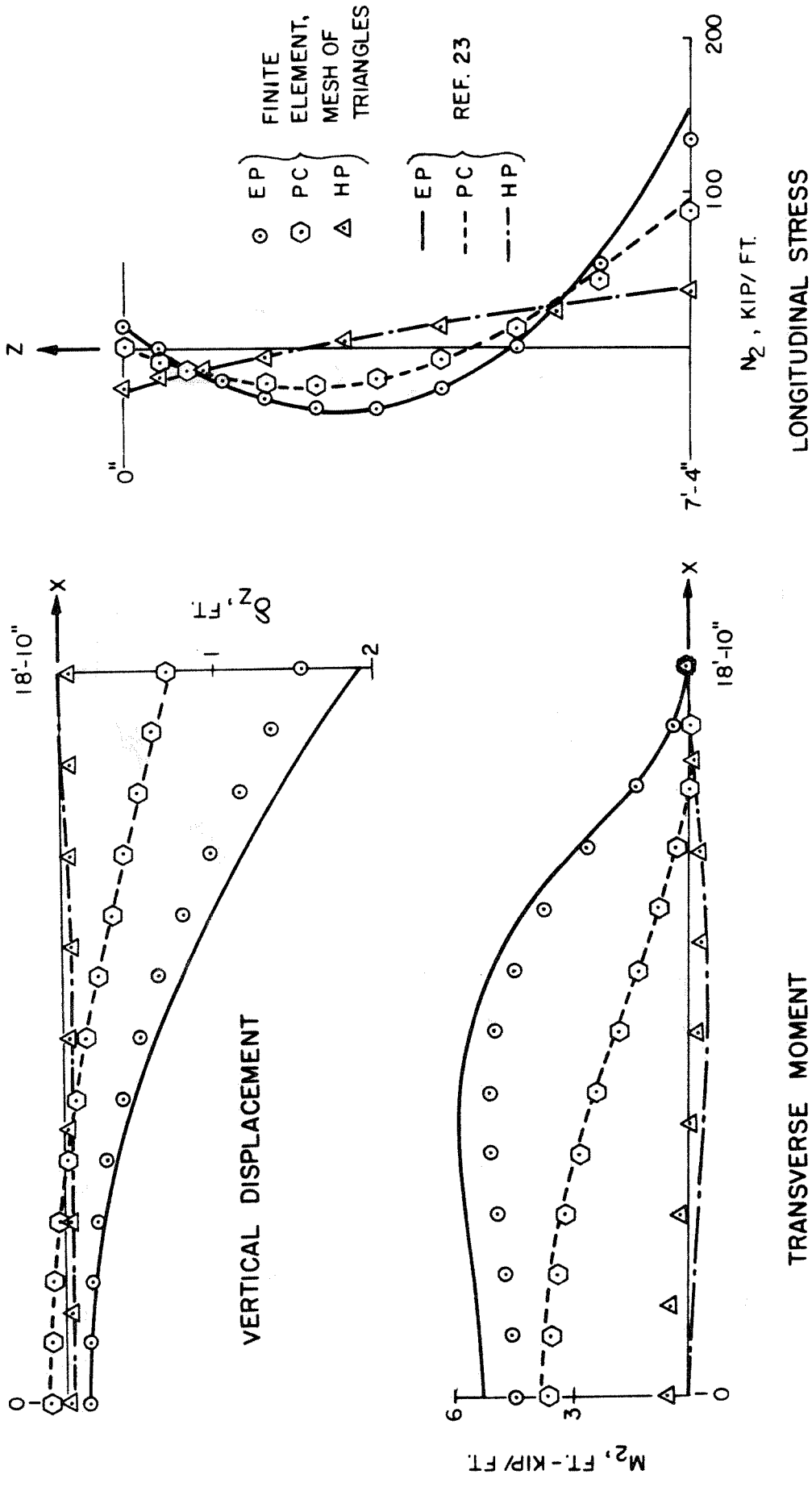
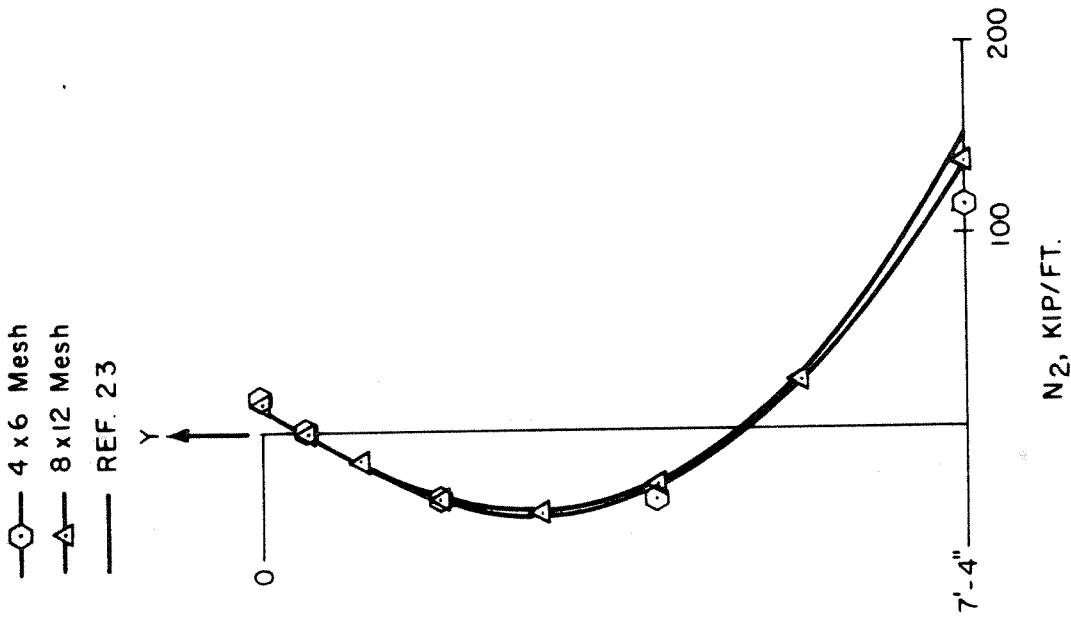
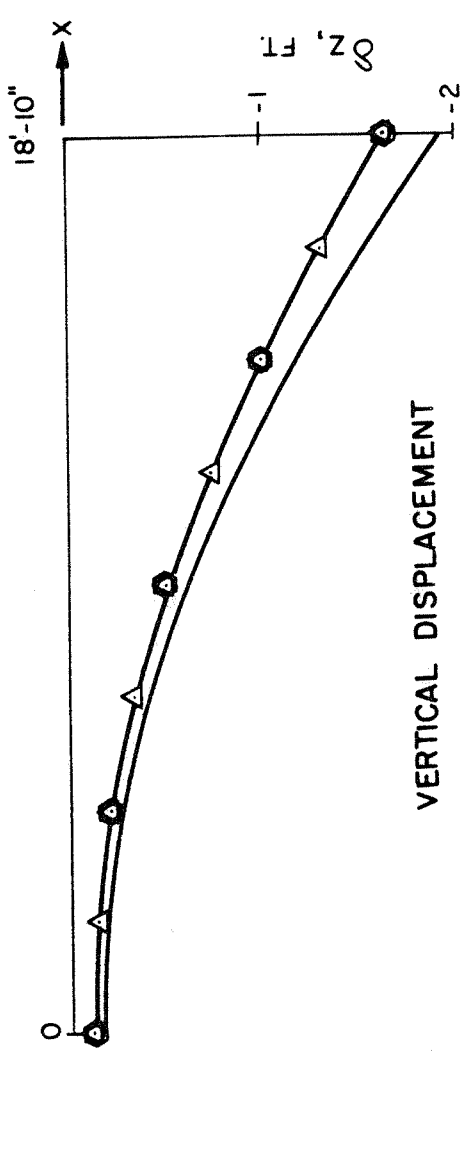


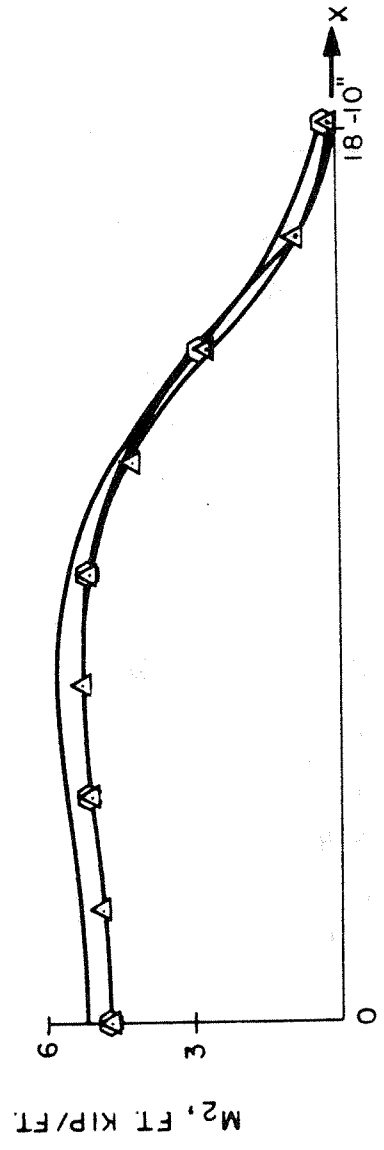
FIG. 6.19 COMPARISON OF RESULTS AT CENTRAL SECTION, $Y=0$, FOR TRANSLATIONAL SHELLS (EXAMPLE 7)



LONGITUDINAL STRESS

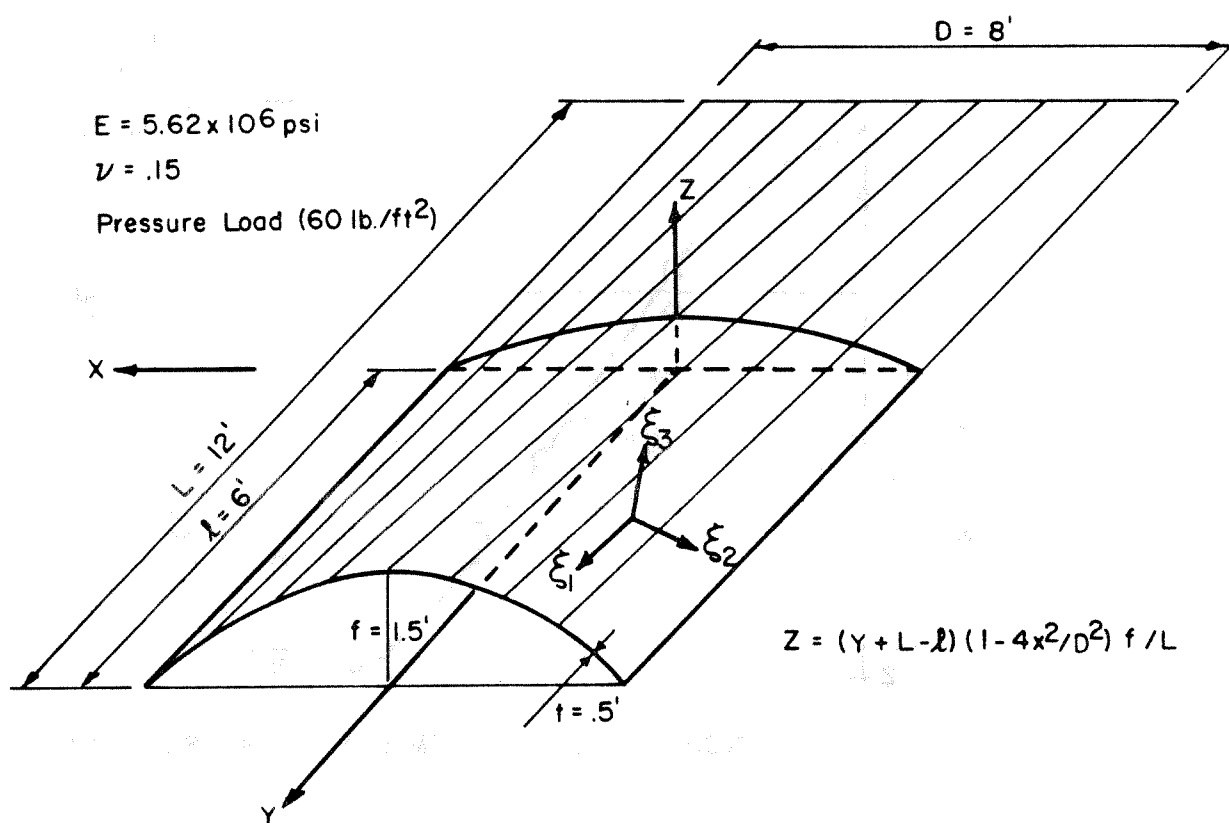


VERTICAL DISPLACEMENT

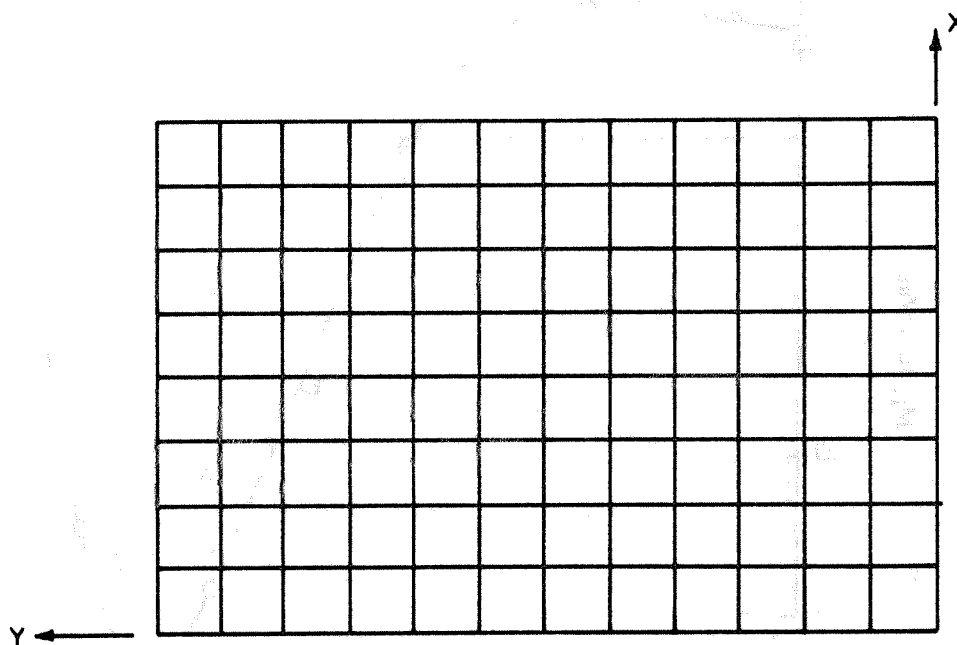


TRANSVERSE MOMENT

FIG. 6.20 COMPARISON OF RESULTS AT CENTRAL SECTION $Y=0$, FOR ELLIPTIC PARABOLOID USING MESH OF QUADRILATERALS. (EXAMPLE 7)

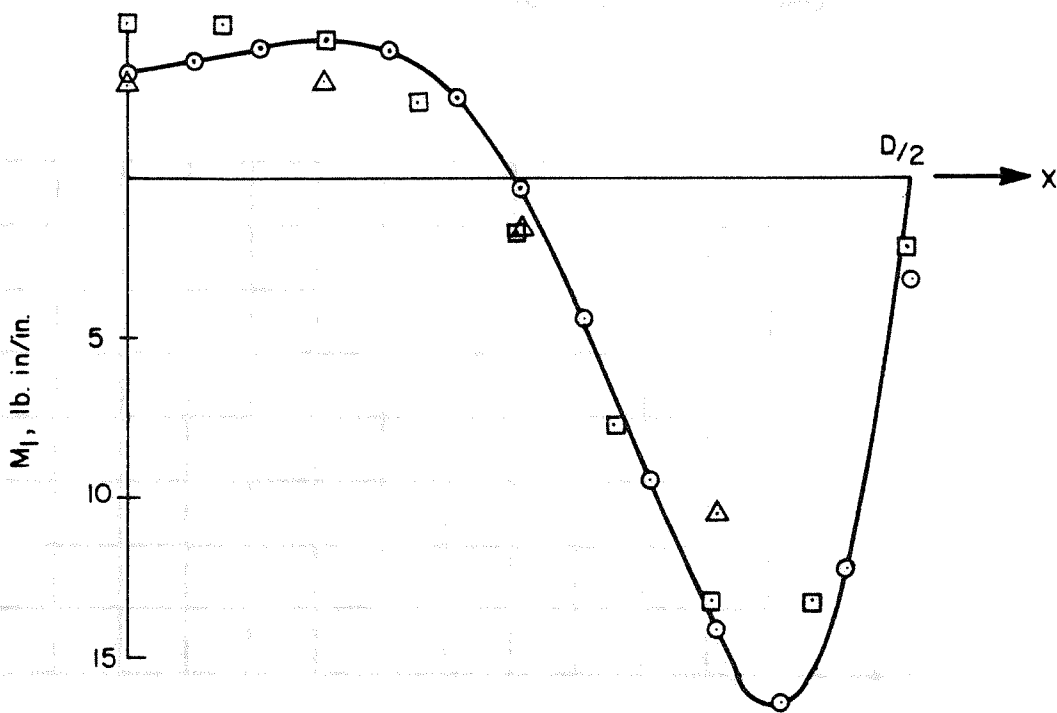
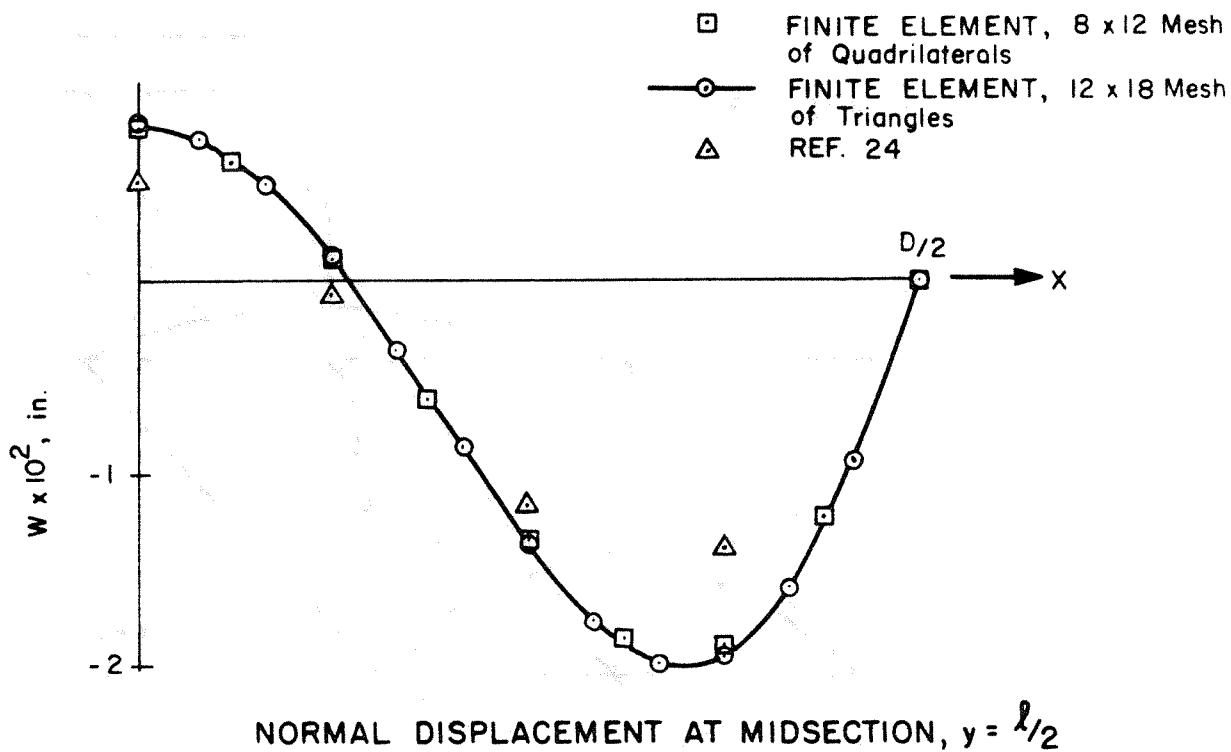


GEOMETRY OF CONOID



TYPICAL UNIFORM MESH (8x12) OF QUADRILATERALS IN HORIZONTAL PLANE

FIG. 6.21 GEOMETRY AND MATERIAL PROPERTIES OF CONOID. (EXAMPLE 8)



MOMENT AT QUARTER SPAN SECTION, $y = l/4$

FIG. 6.22 COMPARISON OF DISPLACEMENTS AND MOMENTS FOR CONOID. (EXAMPLE 8)

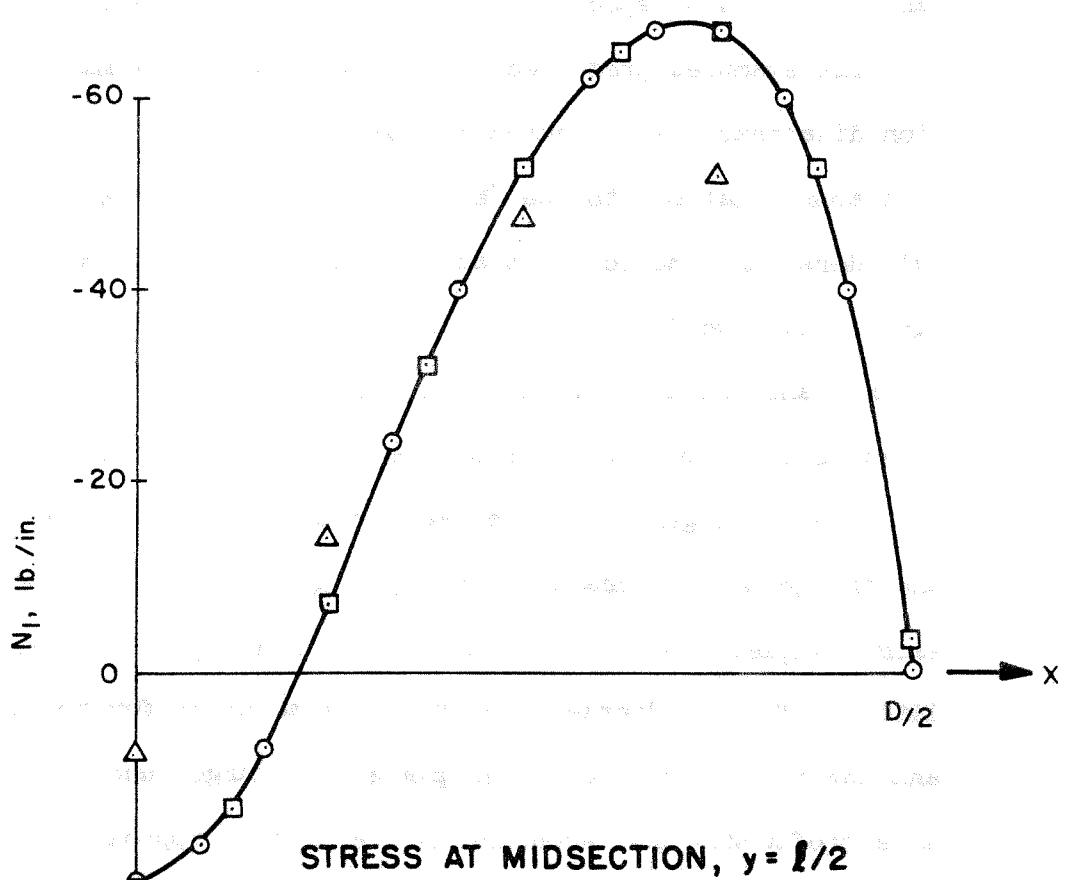
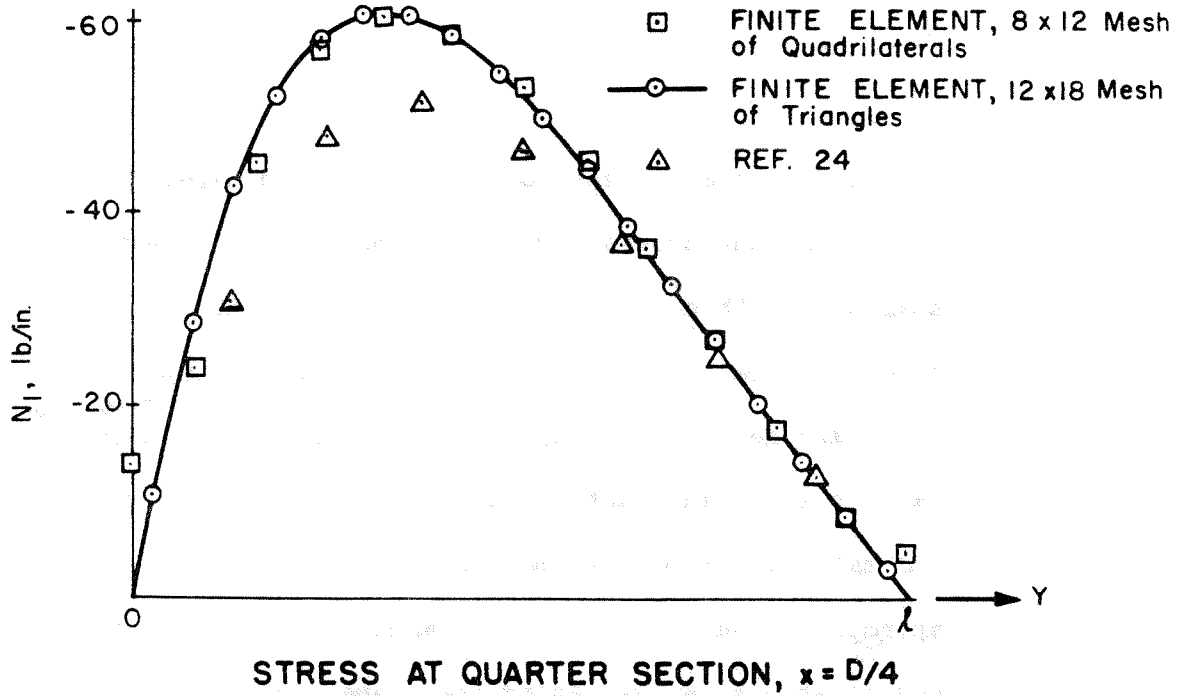


FIG. 6.23 COMPARISON OF STRESSES FOR CONOID. (EXAMPLE 8)

CONCLUSIONS

The finite element solution described herein demonstrates the versatility and the accuracy given by the finite element procedure in the analysis of thin shells. The usual characteristics of the finite element procedure are preserved in this solution in that it is applicable to arbitrary geometries, support conditions, and loadings, which are typically present in practical applications. Shells with variable thickness and material properties may be treated in the analysis by specifying appropriate values for each element in the assemblage; and, with minor modifications in evaluating the element stiffnesses, orthotropic material properties may be considered. In addition, elastic support conditions can be treated by specifying their stiffness properties.

The examples presented showed that the approximations of this solution disappeared with decreasing mesh size, and this solution gave excellent approximations to the "exact" solutions for the dome, the circular cylinders, and the folded plate. In general, the finite element analysis agreed quite well with the "less exact" solution based on shallow shell theory, and the discrepancies in the last example (the conoid) are attributed to the approximations of the shallow shell theory.

The convergence with decreasing mesh size was essentially monotonic and the geometric idealization represented the actual shell adequately in each example. The 5 degree of freedom nodal point system appeared to have little, if any, adverse effects on the solution for smoothly curved shells, and the results of the folded plate with large juncture angles illustrated more profoundly the secondary nature of this approximation. The representation of distributed loadings by either tributary area considerations

or by consistent load procedures, in which only the linear forces were used, was considered adequate for the solution. The most critical approximation in the analysis was the discretized displacement field for the evaluation of the element stiffness properties, and there was a marked improvement in convergence given by the quadrilateral element as compared to the triangular element. This improvement is chiefly attributed to the improved representation of beam-type bending deformation modes of the quadrilateral; however, it should be noted that the plate bending stiffness of the quadrilateral is also superior since four triangular elements are used for the quadrilateral while only two triangles would be used to represent the same region.

Of particular interest in this analysis is the accuracy to which stresses and moments can be predicted. In general it has been demonstrated that with decreasing mesh size, these values approach the accuracy of the nodal point displacements. It should be noted, however, that a given mesh may yield displacements to the desired accuracy while yielding stresses and moments which have not reached the desired accuracy. This behavior may be expected since the solution is based on a displacement model, and usually occurs only in regions subjected to very steep stress and moment gradients. The accuracy of the stresses and moments in these regions may be improved by refining the basic mesh or by local refinement in the regions where these stresses and moments occur.

The potential of this solution procedure is not fully realized in the solutions presented herein since it was desirable to evaluate the procedure by comparison with existing solutions, and in this respect the examples were necessarily limited to relatively simple geometric forms. It is

equally applicable, however, in treating more complex geometries which occur in actual practice, and the 5 degree of freedom nodal point system permits substantial mesh refinement allowing intricacies of geometric detail to be considered in the analysis.

The finite element solution presented herein permits the analysis of shells subjected to static loadings in which the response of the shell is considered to be linear and elastic. This solution may, however, be extended to include the following:

- 1) Dynamic loadings
- 2) Geometric non-linearities
- 3) Material non-linearities

A treatment of dynamic loadings for shells has been presented in Ref. [9] in which a combination of the direct eigenvalue approach and the modified Rayleigh-Ritz technique were utilized in the analysis. A similar treatment of dynamic loadings using the present analysis procedure is also possible. A general procedure for treating geometric and material non-linearities has been developed in Ref. [12]. This development is based on the incremental procedure by utilizing the instantaneous stiffness which consists of the conventional stiffness augmented by the "geometric" or "initial stress" stiffness.

A problem of practical importance in shell analysis is that of stability. Two approaches for treating the stability problem are possible. In the first approach the conventional stiffness (K_c) is referenced to the initial geometry and the geometric stiffness (K_g) is constructed from the stresses resulting from the applied loads (as determined by the conventional

stiffness). This yields the following equation for determining the critical buckling load (λ):

$$[K_c + \lambda K_g] \delta r = 0$$

In the above equation λ is a single parameter characterizing the given static loading and δr are virtual displacements referenced from the initial geometry. Since K_c and K_g are considered constant in the above equation the determination of the critical buckling load λ follows from a classical eigenvalue analysis. The second approach for the stability problem consists of a finite deformation analysis based on the incremental procedure. In this procedure K_c and K_g are no longer constant and they must be evaluated after each step in the analysis by utilizing the deformed geometry. The critical load is determined in this procedure by observing the load-displacement characteristics of the structure. The advantages given by the second approach lie in the fact that the deformed geometry based on observed tests appears to have significant influence on the critical load, and, moreover, material non-linearities may be included in the analysis.

In addition to the above extensions which are possible with the present finite element procedure, the development of doubly curved shell elements which enable a better geometric discretization of the shell is a matter for further research.

REFERENCES

1. M. J. Turner, R. W. Clough, H. C. Martin and L. J. Topp, "Stiffness and Deflection Analysis of Complex Structures", J. Aeron. Sci., Vol. 23, No. 9, 1956.
2. R. W. Clough, "The Finite Element in Plane Stress Analysis", Proceedings, 2nd ASCE Conf. on Electronic Computation, Pittsburgh, Pa., September 1960.
3. R. W. Clough, "The Finite Element Method in Structural Mechanics", Stress Analysis, O. C. Zienkiewicz, G. S. Holister eds., John Wiley & Sons, Ltd., 1965.
4. P. E. Grafton, and D. R. Strome, "Analysis of Axisymmetrical Shells by the Direct Stiffness Method", AIAA J, Vol. 1, 2347, 1963.
5. R. W. Clough and J. L. Tocher, "Analysis of Thin Arch Dams by the Finite Element Method", Theory of Arch Dams, J. R. Rydzewski, ed., Pergamon Press, 1964.
6. O. C. Zienkiewicz and Y. K. Cheung, "Finite Element Method of Analysis for Arch Dam Shells and Comparison with Finite Difference Procedures", Theory of Arch Dams, J. R. Rydzewski, ed., Pergamon Press, 1964.
7. R. W. Clough and C. P. Johnson, "A Finite Element Approximation for the Analysis of Thin Shells", paper submitted to IISS, 1967.
8. R. W. Clough and J. L. Tocher, "Finite Element Stiffness Matrices for the Analysis of Plate Bending", Proceedings, Conference on Matrix Methods in Structural Mechanics, Air Force Institute of Technology, Wright-Patterson Air Force Base, Ohio, October 1965.
9. A. J. Carr, "A Refined Finite Element Analysis of Thin Shell Structures Including Dynamic Loadings", SEL Report, No. 67-9, University of California, Berkeley, 1967.
10. R. W. Clough and O. Greste, "Finite Element Analysis of Tubular Joints: A Report on a Feasibility Study", SEL Report, No. 67-7, University of California, Berkeley, 1967.
11. E. L. Wilson, "Structural Analysis of Axisymmetric Solids", AIAA J, Vol. 3, No. 12, December 1965.
12. C. A. Felippa, "Refined Finite Element Analysis of Linear and Nonlinear Two-Dimensional Structures", SEL Report No. 66-22, University of California, Berkeley, 1966.

13. R. J. Melosh, "Development of the Stiffness Method to Define Bounds on Elastic Behaviour of Structures", Ph. D Dissertation, University of Washington, 1962.
14. R. J. Melosh, "Basis of Derivation of Matrices for the Direct Stiffness Method", AIAA J, Vol. 1, 1631, 1963.
15. B. H. R. Irons and K. J. Draper, "Inadequacy of Nodal Connections in a Stiffness Solution for Plate Bending", AIAA J, Vol. 3, 5, 1965.
16. E. L. Wilson, "Finite Element Analysis of Two-Dimensional Structures", SESM Report, No. 63-2, University of California, Berkeley, 1963.
17. C. W. McCormick and K. J. Hebert, "Solution of Linear Equations with Digital Computers", Calif. Institute of Technology, Pasadena, September 1965.
18. L. Fox, An Introduction of Numerical Linear Algebra, Oxford University Press, 1965.
19. J. H. Wilkinson, Rounding Errors in Algebraic Processes, Prentice-Hall Inc., 1963.
20. S. Timoshenko and S. Woinowsky-Krieger, Theory of Plates and Shells, Engineering Societies Monographs, McGraw-Hill, 1959.
21. A. C. Scordelis and K. S. Lo, "Computer Analysis of Cylindrical Shells", J. Am. Con. Inst., Proceedings, Vol. 61, No. 5, 1964.
22. A. C. Scordelis, E. L. Croy, and I. R. Stubbs, "Experimental and Analytical Study of a Folded Plate", J. of the Structural Division, Proceedings of Am. Society of Civil Engineers, Dec. 1961.
23. A. W. Hedgren, "A Numerical and Experimental Study of Translational Shell Roofs", Ph. D Dissertation, Princeton University, October 1965.
24. H. A. Hadid, "An Analytical and Experimental Investigation into the Bending Theory of Elastic Conoidal Shells", Ph. D Dissertation, University of Southampton, March 1964.